

Journal of

ELECTROANALYTICAL CHEMISTRY

*International Journal Dealing with all Aspects
of Electroanalytical Chemistry,
Including Fundamental Electrochemistry*

EDITORIAL BOARD:

- J. O'M. BOCKRIS (Philadelphia, Pa.)
B. BREYER (Sydney)
G. CHARLOT (Paris)
B. E. CONWAY (Ottawa)
P. DELAHAY (New York)
A. N. FRUMKIN (Moscow)
L. GIERST (Brussels)
M. ISHIBASHI (Kyoto)
W. KEMULA (Warsaw)
H. L. KIES (Delft)
J. J. LINGANE (Cambridge, Mass.)
G. W. C. MILNER (Harwell)
J. E. PAGE (London)
R. PARSONS (Bristol)
C. N. REILLEY (Chapel Hill, N.C.)
G. SEMERANO (Padua)
M. VON STACKELBERG (Bonn)
I. TACHI (Kyoto)
P. ZUMAN (Prague)

E L S E V I E R

GENERAL INFORMATION

See also Suggestions and Instructions to Authors which will be sent free, on request to the Publishers.

Types of contributions

- (a) Original research work not previously published in other periodicals.
- (b) Reviews on recent developments in various fields.
- (c) Short communications.
- (d) Bibliographical notes and book reviews.

Languages

Papers will be published in English, French or German.

Submission of papers

Papers should be sent to one of the following Editors:

Professor J. O'M. BOCKRIS, John Harrison Laboratory of Chemistry,
University of Pennsylvania, Philadelphia 4, Pa. 19104, U.S.A.

Dr. R. H. OTTEWILL, Department of Chemistry, The University, Bristol 8, England.

Dr. R. PARSONS, Department of Chemistry, The University, Bristol 8, England.
Until June 1967: Gates and Crellin Laboratories of Chemistry, California Institute of
Technology, Pasadena, Calif. 91109, U.S.A.

Professor C. N. REILLEY, Department of Chemistry,
University of North Carolina, Chapel Hill, N.C. 27515, U.S.A.

Authors should preferably submit two copies in double-spaced typing on pages of uniform size. Legends for figures should be typed on a separate page. The figures should be in a form suitable for reproduction, drawn in Indian ink on drawing paper or tracing paper, with lettering etc. in thin pencil. The sheets of drawing or tracing paper should preferably be of the same dimensions as those on which the article is typed. Photographs should be submitted as clear black and white prints on glossy paper.

All references should be given at the end of the paper. They should be numbered and the numbers should appear in the text at the appropriate places.

A summary of 50 to 200 words should be included.

Reprints

Fifty reprints will be supplied free of charge. Additional reprints can be ordered at quoted prices. They must be ordered on order forms which are sent together with the proofs.

Publication

The *Journal of Electroanalytical Chemistry* appears monthly and, beginning in 1967, will have four issues per volume and three volumes per year. From January 1967, the journal will be known as the *Journal of Electroanalytical Chemistry and Interfacial Electrochemistry*.

Subscription price: £ 18.18.0 or \$ 52.50 or Dfl. 189.00 per year; £ 6.6.0 or \$ 17.50 or Dfl. 63.00 per volume; plus postage.

Additional cost for copies by air mail available on request.

For advertising rates apply to the publishers.

Subscriptions

Subscriptions should be sent to:

ELSEVIER PUBLISHING COMPANY, P.O. Box 211, Amsterdam, The Netherlands.

ANNOUNCEMENT

The boundaries between what are regarded as electroanalytical chemistry, electrochemistry and colloid chemistry are becoming increasingly diffuse. This has been reflected in the pages of our journal, where many of the papers published are of interest to chemists who consider themselves as falling under any of these three broad divisions.

The linking phenomena are those associated with the electrical double layer, and it is felt that it would be both useful and appropriate to acknowledge these broader interests by extending the scope of the journal to include all phenomena in which the electrical double layer plays an essential role.

These extend from applications in analytical chemistry through the fundamentals of electrode reactions, which are already the staple part of the journal, to studies of the double layer around colloidal particles, the stability of dispersions and electrokinetic phenomena as well as other surface chemical problems such as monolayers and soap films.

Since this broadening of the scope does not involve any change in the basic interests of the journal, the title will be only slightly modified. From January 1967 it will become:

JOURNAL OF ELECTROANALYTICAL CHEMISTRY AND INTERFACIAL ELECTROCHEMISTRY

An International Journal Devoted to All Aspects of Electroanalytical Chemistry, Double Layer Studies, Electrokinetics, Colloid Stability and Electrode Kinetics

Since the aim of a journal must be to publish papers rapidly, it has been decided that three volumes will be published in 1967 instead of the present two. The delay in publication will thereby be reduced to a minimum level.

Dr. R. H. OTTEWILL of the University of Bristol has agreed to join the board of Editors, and will have special responsibility for the papers which fall within his field of interest.

Papers for publication should be sent to one of the following addresses:

Professor J. O'M. BOCKRIS, John Harrison Laboratory of Chemistry, University of Pennsylvania, Philadelphia 4, Pa. 19104, U.S.A.;

Dr. R. H. OTTEWILL, Department of Chemistry, The University, Bristol 8, England;

Dr. R. PARSONS, Department of Chemistry, The University, Bristol 8, England;

Professor C. N. REILLEY, Department of Chemistry, University of North Carolina, Chapel Hill, N.C. 27515, U.S.A.

APPLICATION OF MERCURY-PLATED GRAPHITE ELECTRODES TO VOLTAMMETRY AND CHRONOPOTENTIOMETRY

S. P. PERONE AND K. K. DAVENPORT*

Department of Chemistry, Purdue University, Lafayette, Indiana (U.S.A.)

(Received November 15th, 1965)

The preparation and application of mercury-plated electrodes for electro-analytical studies has received much attention recently¹⁻⁵. These electrodes can be extremely useful, particularly for stripping analysis, where the limited electrode volume results in enhanced stripping signals^{4,5}. However, relatively little quantitative data has been published on the electrochemical behavior of these electrodes.

The primary objectives of the investigation reported here were to develop and apply a mercury-plated electrode, which could be prepared conveniently with reproducible size and planar shape, and to critically evaluate its electrochemical characteristics with regard to reproducibility, stability, and electrolytic response. Comparison of experimental behavior with rigorous theoretical voltammetric and chronopotentiometric relationships, as well as with results obtained at a hanging mercury-drop electrode, formed the basis for evaluation of the electrode characteristics.

The substrate chosen for the preparation of a mercury-film electrode was a wax-impregnated graphite electrode. The exposed graphite surface was circular, planar, highly polished and readily reproducible⁶. A previous study of the anodic stripping voltammetry of Hg(II) at the graphite electrode⁷ was used for selection of plating conditions. The mercury film was formed by controlled-potential deposition from a thiocyanate medium. The mercury-plated electrodes prepared were used in voltammetric and chronopotentiometric studies of typical reversible and irreversible systems. The distorting effect of the limited diffusion layer for amalgam-forming systems was investigated chronopotentiometrically, and results were compared to the appropriate theoretical relationships.

EXPERIMENTAL

Apparatus

The voltammetric instrumentation as used previously was used in this study⁷. This included a Sargent Model FS polarograph and a general-purpose operational amplifier instrument. Modifications of the operational amplifier instrument for chronopotentiometry were made readily according to the suggestions of SCHWARZ AND SHAIN⁸. The electrolytic plating involved a single stabilized amplifier potentiostat identical to that discussed previously^{8,9}. A 3-electrode arrangement was used for all experiments where theoretical correlations were obtained.

* Present address, Department of Chemistry, University of Wisconsin, Madison, Wis. (U.S.A.)

Cells and electrodes

The cells, salt-bridge arrangements, reference electrodes, and counter electrodes used in this study were identical to those used in a previous study⁷. When ethanolic solutions were used, auxiliary electrodes were isolated by ethanolic salt bridges. The cell used for voltammetry and chronopotentiometry was immersed in a water bath controlled at $25.0 \pm 0.1^\circ$ (Sargent Thermonitor water bath, E. H. Sargent & Co., Chicago, Ill.) The ring stand used to mount the cell assembly was supported on a thick pile of folded papers, which reduced vibrations considerably. The cell used for electro-deposition of the mercury was not temperature controlled.

The graphite electrodes were the same as used previously (12-in. spectrographic rods, No. L4309, National Carbon Co., N. Y.). The details of the procedure involved in the wax-impregnation, insulation, and surface polishing have been discussed previously⁶. Electrode surface areas were 0.32 cm^2 .

The mercury-plated electrodes were prepared by electrodeposition with stirring from de-aerated solutions of $1 \cdot 10^{-3} \text{ M Hg(II)}$ in 0.1 M KCNS . The electrolysis potential was $-0.70 \text{ V vs. S.C.E.}$ The thickness of the mercury films on the electrodes varied from $0.5\text{--}10 \mu$ (calculated from measured plating currents and the atomic radius of mercury). The $1.0\text{-}\mu$ plate required about 12 min to form, whereas the $10\text{-}\mu$ plate required about 2 h. The $1.0\text{-}\mu$ plate was used for all except the chronopotentiometric experiments, where the plates were of various sizes.

The physical appearance of these mercury films is that of a dull, gray surface. Close examination with a magnifying glass reveals the tiny droplet nature of the film as described by other workers⁵.

The hanging mercury-drop electrode assembly used has been described previously¹⁰.

Materials and solutions

All chemicals were reagent-grade and were used without further purification. All solutions were prepared in water purified by distillation and passage over a mixed-bed cation-anion exchange resin. Hg(II) solutions were prepared as described previously⁷. Anthraquinone solutions were made up in 60% by volume ethanol solvent with 0.1 M, pH 7.2 phosphate buffer as electrolyte. All sample solutions were de-aerated for at least 15 min by passing high-purity nitrogen through a gas-washing bottle containing the inert electrolyte solution and then through a disperser in the sample cell.

RESULTS AND DISCUSSION

Three fundamentally different systems were investigated with the mercury-plated graphite electrode. These were Cd(II) in KCl, iodate in pH 7.2 phosphate buffer, and anthraquinone in pH 7.2 phosphate buffer-60% ethanol. Cd(II) is reduced reversibly to cadmium amalgam, iodate is irreversibly reduced to iodide and anthraquinone is reversibly reduced to a soluble product. These three systems were selected to demonstrate, respectively, the behavior of an amalgam-forming system at the thin-film electrode; the behavior of an activation-controlled process; and the behavior of a reversible process where the product is soluble in solution.

The three systems were investigated by voltammetry with linearly varying

potential. In addition, the cadmium system was investigated using chronopotentiometry, where the effects of the thin-film electrode on the potential-time behavior could be predicted.

Reproducibility and stability of electrodes

The reproducibility and stability of the mercury-plated graphite electrodes were evaluated extensively before experimental correlations with theory were attempted. Using the technique of voltammetry with linearly varying potential and the anthraquinone system, the mercury-plated electrodes were evaluated for reproducibility by making several completely new electrodes and applying them in sequence to the same solution. Figure 1 shows three typical repetitive traces obtained under these conditions. The reproducibility of electrode preparation is most obvious in the peak

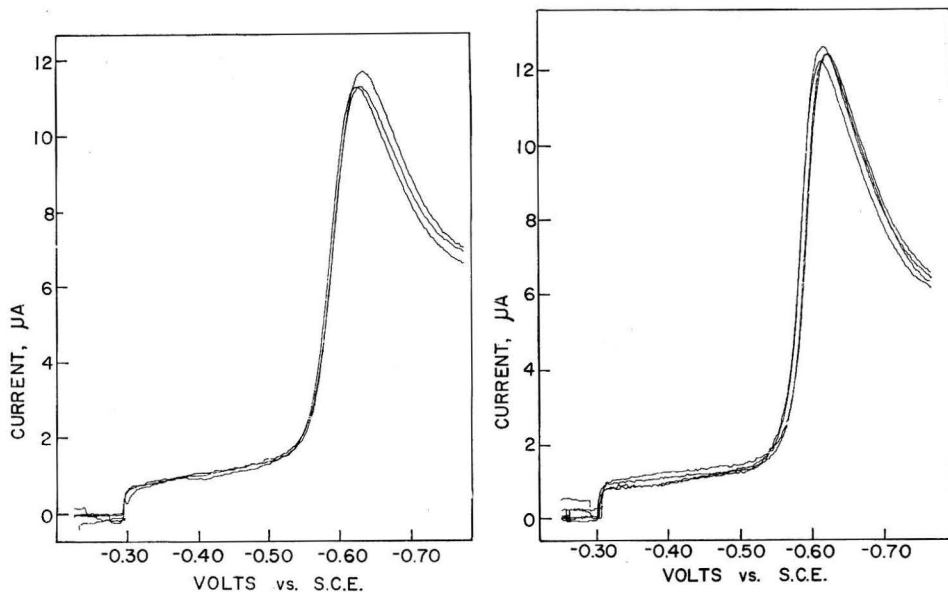


Fig. 1. Reproducibility test using three different mercury-plated graphite electrodes. $1.0 \cdot 10^{-4} M$ anthraquinone; $1.0\text{-}\mu$ electrodes; scan rate, 20.6 mV/sec .

Fig. 2. Reproducibility with a single mercury-plated graphite electrode. $1.0 \cdot 10^{-4} M$ anthraquinone; $1.0\text{-}\mu$ electrode; scan rate, 20.6 mV/sec .

height variation; this was of the order of $\pm(2\text{--}4\%)$. Figure 2 shows typical results of repetitive runs with a single mercury-plated electrode, demonstrating the repeatability obtainable with this electrode. Peak-height reproducibility in this case was $\pm(1\text{--}2\%)$.

The stability of the mercury-plated graphite electrodes is a more difficult problem. Ordinarily, in this work, the electrodes were prepared as needed and transferred externally directly from the plating solution to the sample solution. The only difficulty encountered here was that some traces of oxide apparently formed during the brief transfer period. The presence of oxide was indicated by a small ($0.5 \mu\text{A}$) cathodic peak at $-0.3 \text{ V vs. S.C.E.}$ in the first run with each new electrode.

Thus, a new electrode was "cleaned" of interfering coatings before use by holding the potential at -0.4 V for a few seconds.

It was found that freshly-plated electrodes could be stored overnight in solution without any deterioration or change in characteristics, aside from the necessity of removing accumulated oxide coatings. Longer-term storage in solution appeared to be detrimental to the electrode. Storage in air for longer than a few minutes could not be tolerated.

Voltammetry with linearly varying potential

Reversible deposition—Cd(II). Voltammetric current–voltage curves were obtained with 1.0×10^{-4} M Cd(II) in 0.2 M KCl at the mercury-plated graphite electrode using a potential scan rate of 33.0 mV/sec. These curves were compared to a theoretical curve calculated from the appropriate expression¹¹, see Fig. 3.

The experimental current–voltage curve for the reduction of Cd(II) at the mercury-plated graphite electrode is more drawn-out and is shifted to more cathodic potentials than predicted for unrestricted diffusion into the mercury. Furthermore, the experimental peak current is only 75% of the predicted value. Thus, the curves in Fig. 3 have been normalized in both the current and voltage axes to allow direct comparison.

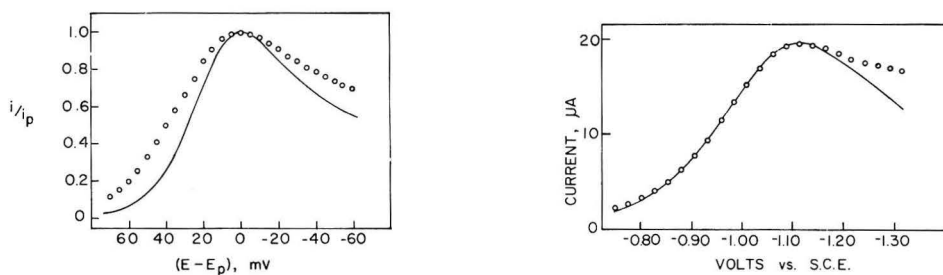


Fig. 3. Current–voltage curves for Cd(II) at the mercury-plated graphite electrode. Line, theoretical; circles, experimental; theoretical peak potential, -0.631 V vs. S.C.E.; experimental peak potential, -0.683 V vs. S.C.E.; theoretical peak current, $9.8 \mu\text{A}$; experimental peak current, $7.3 \mu\text{A}$; scan rate, 33.0 mV/sec; $1.0\text{-}\mu$ electrode.

Fig. 4. Current–voltage curves for iodate at the mercury-plated graphite electrode. Line, theoretical; circles, experimental; $D = 1.00 \cdot 10^{-5}$ cm²/sec; scan rate, 33.0 mV/sec; $1.0\text{-}\mu$ electrode (high currents at end due to beginning of hydrogen evolution).

The distortion and shifting of the experimental curve can be explained qualitatively by considering the effect of limited diffusion of the product away from the electrode surface into the thin mercury film. At any given time after the start of electrolysis, the surface concentration of the reduced form is greater than predicted for semi-infinite linear diffusion. Thus, since this is a Nernstian couple, the peak potential is shifted cathodically, and the drawn-out shape is not surprising. A rigorous theoretical treatment of the diffusion process involved in the voltammetric experiment at a thin-film electrode would be very useful, but the boundary-value problem has not yet been solved rigorously. However, the qualitative observations made above are illustrated more quantitatively below when the chronopotentiometric behavior of Cd(II) is discussed.

Irreversible reduction—iodate. The electroreduction of iodate has been studied extensively as an example of a typical irreversible system^{12,13}. Since the electrochemical behavior of this system depends on heterogeneous kinetic phenomena, its study with the mercury-plated graphite electrode should be a critical test of electrode characteristics.

Current–voltage curves were obtained at the mercury-plated graphite electrode with $1.0 \times 10^{-4} M$ iodate in pH 7.2, 0.1 *M* phosphate buffer, using a scan rate of 33.0 mV/sec. A comparison of the experimental current–voltage behavior with theory¹¹ is shown in Fig. 4. The value of the kinetic parameter, αn_a , that provided the best fit was 0.34. To check this value, identical runs were made on the same solutions with a hanging mercury-drop electrode. A value for αn_a of 0.30 was obtained, which is in reasonable agreement with the data obtained with the mercury-plated electrode. Furthermore, the peak potentials of the curves obtained at both electrodes agreed within 10 mV. The data obtained at both electrodes with the iodate system were consistent with previous studies at the hanging mercury-drop electrode^{13,14}.

Reversible reduction—anthraquinone. Anthraquinone provides an example of a reversible system where the product is soluble in solution. Hence, the problem of limited diffusion of the product should be eliminated, and the distortion observed in the case of Cd(II) should not appear.

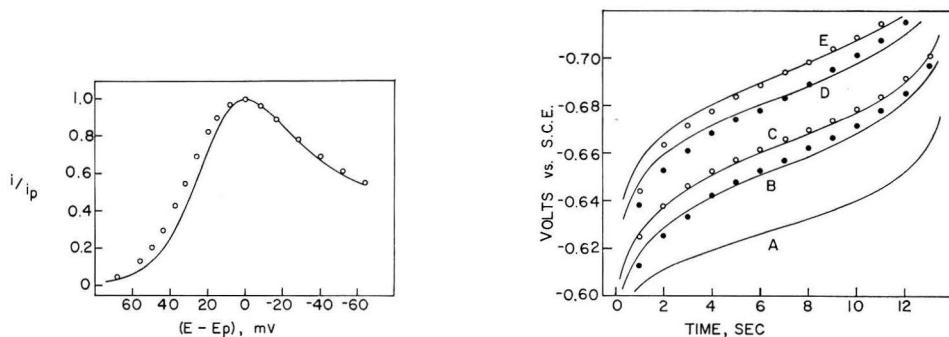


Fig. 5. Current–voltage curves for anthraquinone at the mercury-plated graphite electrode. Line, theoretical; circles, experimental; scan rate, 20.6 mV/sec.; $1.0\text{-}\mu$ electrode; $E_p = -0.62$ V vs. S.C.E.

Fig. 6. Chronopotentiometric curves for Cd(II) at the mercury-plated graphite electrode with varying layer size. Lines, theoretical; circles, experimental. (A), Theoretical curve for semi-infinite linear diffusion (infinitely thick electrode); (B), 10-; (C), 5.0-; (D), 1.0-; (E), 0.5- μ electrode.

Current–voltage curves were obtained with a scan rate of 20.6 mV/sec at both the mercury-plated graphite electrode and the hanging mercury-drop electrode with $1.0 \times 10^{-4} M$ anthraquinone in pH 7.2 phosphate buffer, 60% ethanol. Figure 5 shows the comparison of the current–voltage curve obtained at the mercury-plated electrode with theory¹¹. A normalized plot was made in this case since no diffusion coefficient data were available in this medium. Although the experimental and theoretical curves do not coincide exactly, the agreement of the curve shapes is considerably better than for the reduction of Cd(II). The slight distortion in the experimental curve may be due to the contribution of the non-linear diffusion processes occurring at the electrode edges.

Using a diffusion coefficient estimated from Stokes Law¹⁵ (6.39×10^{-6} cm²/sec) the calculated peak current for anthraquinone is 8.8 μ A. This agrees well with the experimental peak current of 9.5 μ A. Also, the peak potential observed at the mercury-plated electrode falls within 6 mV of the peak potential observed at the hanging mercury-drop electrode.

Chronopotentiometry

Theory. The concentration gradient for the reduced form, substance *R*, in the thin-film electrode can be derived from the following boundary-value problem:

Assume Fick's law governing linear diffusion holds;

$$dC_R/dt = D_R(d^2C_R/dx^2) \quad (1)$$

Initial conditions:

$$t = 0, \quad 0 < x < l, \quad C_R = 0 \quad (2)$$

Boundary conditions:

$$t > 0, \quad i/nFA = F_0 = \text{constant} \quad (3)$$

$$t > 0, \quad x = 0, \quad D_R(dC_R/dx) = 0 \quad (4)$$

$$t > 0, \quad x = l, \quad D_R(dC_R/dx) = F_0 \quad (5)$$

where, *l* = thickness of the electrode film. Other terms have their usual significance¹⁶.

The first boundary condition indicates that a constant current is imposed on the electrolysis cell. The second boundary condition indicates that the diffusion is not semi-infinite, but rather is limited to the thickness of the mercury film. The third boundary condition simply indicates that the imposed current describes the flux of substance *R* at the mercury-solution interface.

The solution to this boundary-value problem has been given by CRANK¹⁷ and can be stated in the form:

$$C_R = F_0 l / D_R \left\{ D_R t / l^2 + (3x^2 - l^2) / 6l^2 - (2/\pi^2) \sum_{n=1}^{\infty} (-1)^n / n^2 [\exp(-D_R n^2 \pi^2 t / l^2)] \cos(n\pi x / l) \right\} \quad (6)$$

for $x = l$, and keeping only the first term in the series,

$$C_R(x = l) = F_0 l / D_R \left\{ D_R t / l^2 + \frac{1}{3} + (2/\pi^2) \exp(-D_R t \pi^2 / l^2) \right\} \quad (7)$$

This relationship does not hold for very small values of *t*, but can be used for *t*-values of the order of a second or greater. For shorter times, an alternative solution has been obtained¹⁸ (Also, as pointed out by DE VRIES AND VAN DALEN¹, eqn. (6) describes the concentration gradient in a thin-film electrode for constant-potential electrodeposition with constant stirring).

Since the time-dependence of the surface concentration of the reactant, substance *O*, is independent of the fate of substance *R* in this uncomplicated constant-current model, the previously derived expression for this dependence¹⁶, along with eqn. (7), can be substituted into the Nernst equation to obtain an expression for the potential-time behavior.

$$E = E_{\frac{1}{2}} + RT/nF \ln [C_o(x=l)/C_R(x=l)] =$$

$$E_{\frac{1}{2}} + RT/nF \ln \left[\frac{C_o^* - 2F_0 t^{\frac{1}{2}}/(\pi D)^{\frac{1}{2}}}{F_0 l/D \left[\frac{1}{3} + Dt/l^2 + (2/\pi^2) \exp(-Dt\pi^2/l^2) \right]} \right] \quad (8)$$

where the usual assumption has been made that $D_o = D_R = D$.

Although the form of eqn. (8) is inconvenient it can be used to calculate potential-time curves for the case where l is known. Also, if Dt/l^2 is greater than about 7, the constant and exponential terms in the expression for $C_R(x=l)$ become insignificant, and eqn. (8) reduces to:

$$E = E_{\frac{1}{2}} + RT/nF \ln \left[\frac{C_o^* - 2F_0 t^{\frac{1}{2}}/(\pi D)^{\frac{1}{2}}}{F_0 t/l} \right] \quad (9)$$

Furthermore, the curves predicted for relatively large electrode films (*ca.* 100 μ) and relatively short transition times (*ca.* 10 sec) are identical to those calculated for a semi-infinite linear diffusion process.

Experimental correlation. Chronopotentiograms were obtained at the mercury-plated graphite electrode with $1.0 \times 10^{-3} M$ Cd(II) in 0.2 M KCl using a constant current of 46.6 μA . The electrode-layer thickness was varied in these experiments, by utilizing 0.5-, 0.7-, 1.0-, 5.0-, and 10- μ -thick mercury films. Experimental and theoretical curves are shown in Fig. 6. The numerical value of $E_{\frac{1}{2}}$ used in the theoretical calculations was obtained by voltammetry with linearly varying potential at the hanging mercury-drop electrode, utilizing the theoretical expressions presented by NICHOLSON AND SHAIN¹¹. The value obtained was $E_{\frac{1}{2}} = -0.617$ V *vs.* S.C.E. Since no diffusion coefficient data were available for the conditions employed here, the theoretical curves were plotted using the apparent diffusion coefficient determined from the transition time. The value obtained was 1.01×10^{-5} cm²/sec. The average experimental transition time for the various electrode thicknesses was 13.8 ± 0.6 sec.

TABLE 1
CHRONOPOTENTIOMETRIC DATA FOR Cd(II) AS A FUNCTION OF ELECTRODE THICKNESS

$l(\mu)$	$E_{\frac{1}{2}}$	$(E_{\frac{1}{2}} - E_{\frac{1}{2}})_{obs.}$	$(E_{\frac{1}{2}} - E_{\frac{1}{2}})_{calcd.}$
0.5	-0.672	-0.055	-0.060
0.7	-0.673	-0.056	-0.056
1.0	-0.665	-0.048	-0.051
5.0	-0.649	-0.032	-0.031
10	-0.642	-0.025	-0.022

The experimental and theoretical curves agree very well. Although the shapes are not identical, the shifts of $E_{\frac{1}{2}}$ with electrode thickness are almost exactly as predicted (see Table 1). Also, since l is the order of 10 μ or less, eqn. (9) can be used, and evaluation of eqn. (9) at $E_{\frac{1}{2}}$ indicates that $E_{\frac{1}{2}}$ is independent of the diffusion coefficient. Thus, the correlation in Table 1 should be independent of any error in D . This agreement is good evidence in support of the theory developed here and demonstrates that theoretical correlations with thin-film electrodes are possible.

ACKNOWLEDGEMENT

This work was supported in part by the National Science Foundation Undergraduate Research Program.

SUMMARY

The preparation and application of mercury-plated graphite electrodes has been discussed. The electrodes were prepared by controlled-potential electrodeposition on the exposed planar surface of a wax-impregnated graphite electrode. The mercury-plated electrodes were evaluated by voltammetric and chronopotentiometric applications to various reversible and irreversible systems. Experimental data were compared to rigorous voltammetric theory. Theory for chronopotentiometric curves at thin-film electrodes with amalgam-forming substances was developed, and experimental correlations with the Cd(II) system were made. In each case correlations were good.

REFERENCES

- 1 W. T. DE VRIES AND E. VAN DALEN, *J. Electroanal. Chem.*, 8 (1964) 366.
- 2 S. A. MOROS, *Anal. Chem.*, 34 (1962) 1584.
- 3 L. RAMALEY, R. L. BRUBAKER AND C. G. ENKE, *Anal. Chem.*, 35 (1963) 1088.
- 4 D. K. ROE AND J. E. A. TONI, *Anal. Chem.*, 37 (1965) 1503.
- 5 W. R. MATSON, D. K. ROE AND D. E. CARRITT, *Anal. Chem.*, 37 (1965) 1594.
- 6 S. P. PERONE, *Anal. Chem.*, 35 (1963) 2091.
- 7 S. P. PERONE AND W. J. KRETLOW, *Anal. Chem.*, 37 (1965) 968.
- 8 W. M. SCHWARZ AND I. SHAIN, *Anal. Chem.*, 35 (1963) 1770.
- 9 G. S. ALBERTS, Ph.D. thesis, University of Wisconsin, Madison, Wis., 1963.
- 10 S. P. PERONE AND T. R. MUELLER, *Anal. Chem.*, 37 (1965) 2.
- 11 R. S. NICHOLSON AND I. SHAIN, *Anal. Chem.*, 36 (1964) 706.
- 12 P. DELAHAY AND J. E. STRASSNER, *J. Am. Chem. Soc.*, 73 (1951) 5219.
- 13 R. D. DE MARS AND I. SHAIN, *J. Am. Chem. Soc.*, 81 (1959) 2654.
- 14 S. P. PERONE AND C. V. EVINS, unpublished results.
- 15 F. DANIELS AND R. A. ALBERTY, *Physical Chemistry*, John Wiley and Sons, N.Y., 1957, p. 505.
- 16 P. DELAHAY, *New Instrumental Methods in Electrochemistry*, Interscience, N. Y., 1954, 2nd ed., p. 179, ff.
- 17 J. CRANK, *The Mathematics of Diffusion*, Oxford University Press, London, 1956, p. 58.
- 18 H. H. MACEY, *Proc. Phys. Soc. London*, 52 (1940) 625.

J. Electroanal. Chem., 12 (1966) 269-276

UTILISATION DE L'IMPEDANCE OPERATIONNELLE POUR LA DETERMINATION DES COEFFICIENTS DE DIFFUSION*†

EUGÈNE LEVART ET EMMANUEL POIRIER D'ANGÉ D'ORSAY

Laboratoire d'Electrolyse du C.N.R.S., Bellevue, Hauts-de-Seine (France)

(Reçu le 11 janvier, 1966)

I. CONSIDÉRATIONS THÉORIQUES

Récemment, l'un de nous¹ a attiré l'attention sur l'intérêt que présente l'utilisation de l'impédance opérationnelle de Laplace pour le traitement des résultats obtenus en régime transitoire. Ce procédé, élaboré en vue de la détermination des paramètres cinétiques d'une réaction d'électrode, permet non seulement d'améliorer la précision pouvant être atteinte par les différentes méthodes impulsives ou périodiques, mais encore d'établir un trait d'union entre elles.

Dans cette communication, nous nous attacherons plus spécialement à l'application de ce procédé à la détermination des coefficients de diffusion des espèces électroactives.

La particularité du procédé proposé est que les deux grandeurs électriques accessibles expérimentalement, c'est-à-dire le courant, I , et la polarisation, V , ne sont pas exploitées directement, mais après avoir été transformées, par l'un des procédés connus²⁻⁴ en polarisation opérationnelle, U , et en courant opérationnel, J , définis respectivement comme suit :

$$U(s) = \int_0^{\infty} V(t) e^{-st} dt \quad (1)$$

$$J(s) = \int_0^{\infty} I(t) e^{-st} dt \quad (2)$$

Dans ces formules, s représente le paramètre opérationnel de Laplace qui a pour dimension l'inverse du temps.

De plus, il est à noter que les deux fonctions $V(t)$ et $I(t)$ peuvent constituer indifféremment le signal perturbateur, l'autre étant alors la réponse correspondante du système électrochimique étudié. Enfin, une caractéristique importante du procédé proposé est que la perturbation imposée peut être de forme quelconque, impulsive ou cyclique.

Considérons le rapport $U(s)/J(s)$: à condition que le signal appliqué soit suffisamment faible pour n'engendrer sur tous les processus élémentaires que des variations linéaires, ce rapport représente l'impédance opérationnelle $Z(s)$ qui est une caracté-

* Communication présentée à la 16e réunion du C.I.T.C.E., Budapest, 1965.

† Les travaux exposés dans cet article constituent une partie de la thèse de Doctorat ès-Sciences physiques de Mr. POIRIER D'ANGÉ D'ORSAY (Paris, 1966).

téristique du système étudié et ne dépend donc pas de la méthode de relaxation utilisée pour l'obtenir.

$Z(s)$ est la résultante des impédances opérationnelles de tous les éléments constitutifs du circuit équivalent au système électrochimique étudié. Celui-ci peut être représenté par la Fig. 1, dans lequel C_d est la capacité de double-couche, R_e la résistance de la cellule et Z_f la composante faradique de l'impédance globale; l'expression de Z_f contient les différents paramètres cinétiques et en particulier les coefficients de diffusion D_{Ox} et D_{Red} . L'expression de l'impédance globale est facile à obtenir:

$$Z(s) = \frac{Z_f(s)}{1 + C_d Z_f(s) \cdot s} + R_e \quad (3)$$

La détermination de la composante faradique $Z_f(s)$ de l'impédance opérationnelle globale permet, ainsi qu'on l'exposera plus loin, de déterminer les valeurs des coefficients de diffusion. Le procédé le plus simple consiste à exploiter la fonction $Z(s)$

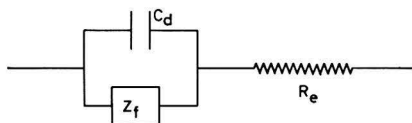


Fig. 1. Circuit représentatif d'un système électrochimique.

dans le domaine des valeurs faibles de s , ce qui permet de rendre négligeable le terme capacitif. L'éqn. (3) se simplifie alors en

$$\lim_{s \rightarrow 0} Z(s) = Z_f(s) + R_e \quad (4)$$

Le calcul de l'expression analytique de Z_f est impossible dans le cas général, mais il est réalisable pour quelques cas types de réaction d'électrode. Il sera supposé pour simplifier que le transport massique est assuré uniquement par diffusion linéaire semi-infinie.

Dans ce cas, les variations des concentrations c_{Ox} et c_{Red} en fonction du temps et de la distance x à partir de l'électrode sont régies par la deuxième loi de Fick:

$$\frac{\partial c_{Ox}}{\partial t} = D_{Ox} \frac{\partial^2 c_{Ox}}{\partial x^2} \quad (5)$$

$$\frac{\partial c_{Red}}{\partial t} = D_{Red} \frac{\partial^2 c_{Red}}{\partial x^2} \quad (6)$$

La solution de ce système d'équations différentielles peut être obtenue grâce à la transformation de Laplace:

$$s\Gamma_{Ox} - c_{Ox}^0 = D_{Ox} \frac{d^2 \Gamma_{Ox}}{dx^2} \quad (7)$$

$$s\Gamma_{Red} - c_{Red}^0 = D_{Red} \frac{d^2 \Gamma_{Red}}{dx^2} \quad (8)$$

où Γ_{Ox} et Γ_{Red} représentent les concentrations transformées et c_{Ox}^0 et c_{Red}^0 les concentrations à l'équilibre; on a donc, compte-tenu de la condition finale:

$$x = \infty: \quad c_{\text{Ox}} = c_{\text{Ox}}^0, \quad c_{\text{Red}} = c_{\text{Red}}^0$$

$$\Gamma_{\text{Ox}} = \alpha \exp\left(-\sqrt{\frac{s}{D_{\text{Ox}}}} x\right) + \frac{c_{\text{Ox}}^0}{s} \quad (9)$$

$$\Gamma_{\text{Red}} = \beta \exp\left(-\sqrt{\frac{s}{D_{\text{Red}}}} x\right) + \frac{c_{\text{Red}}^0}{s} \quad (10)$$

Après avoir explicité les coefficients α et β à l'aide de la première loi de Fick, compte-tenu de l'égalité des flux opposés à l'interface :

$$\frac{I_f}{AzF} = -D_{\text{Ox}} \left(\frac{\partial c_{\text{Ox}}}{\partial x}\right)_{x=0} = D_{\text{Red}} \left(\frac{\partial c_{\text{Red}}}{\partial x}\right)_{x=0}, \quad (11)$$

on obtient pour $x=0$:

$$\Gamma_{\text{Ox}}(x=0) = \frac{J_f(s)}{AzFD_{\text{Ox}}^{\frac{1}{2}}} s^{-\frac{1}{2}} + \frac{c_{\text{Ox}}^0}{s} \quad (12)$$

et

$$\Gamma_{\text{Red}}(x=0) = -\frac{J_f(s)}{AzFD_{\text{Red}}^{\frac{1}{2}}} s^{-\frac{1}{2}} + \frac{c_{\text{Red}}^0}{s}. \quad (13)$$

Dans ces équations, I_f et $J_f(s)$ représentent, respectivement, le courant faradique et son expression transformée, A est la surface de l'électrode, F le Faraday et z le nombre d'électrons échangés dans la réaction d'électrode.

Il est à remarquer que les éqns. (12) et (13) ont été obtenues sans qu'il soit nécessaire de préciser un mode particulier de contrôle pour la réaction d'électrode (diffusion seule ou associée à un processus d'interface). Ceci est dû au fait que nous n'avons pas fait intervenir la tension d'électrode $U(s)$.

Pour obtenir l'expression explicite de Z_f , il est évidemment nécessaire de compléter les formules (12) et (13) par une relation entre $U(s)$ et les paramètres caractéristiques des différentes étapes de la réaction d'électrode.

1. Considérons tout d'abord le cas du contrôle par diffusion seule, la vitesse des processus d'interface et des réactions chimiques associées étant supposée infiniment grande.

On peut alors écrire l'expression suivante pour la surtension de diffusion :

$$\eta = \frac{RT}{zF} \left(\ln \frac{c_{\text{Ox}}}{c_{\text{Red}}} - \ln \frac{c_{\text{Ox}}^0}{c_{\text{Red}}^0} \right) \quad (14)$$

qui, pour de faibles perturbations ($\eta \ll RT/zF$), se simplifie en

$$\eta = \frac{RT}{zF} \left(\frac{c_{\text{Ox}}}{c_{\text{Ox}}^0} - \frac{c_{\text{Red}}}{c_{\text{Red}}^0} \right) \quad (15)$$

dont la transformée est

$$U(s) = \frac{RT}{zF} \left(\frac{\Gamma_{\text{Ox}}}{c_{\text{Ox}}^0} - \frac{\Gamma_{\text{Red}}}{c_{\text{Red}}^0} \right) \quad (16)$$

En remplaçant dans cette dernière équation Γ_{Ox} et Γ_{Red} par les éqns. (12) et (13), on obtient l'expression suivante pour l'impédance opérationnelle :

$$Z_f(s) = \frac{U(s)}{J_f(s)} = \frac{RT}{Az^2 F^2} \left(\frac{I}{c_{Ox^0} D_{Ox^{\frac{1}{2}}}} + \frac{I}{c_{Red^0} D_{Red^{\frac{1}{2}}}} \right) s^{-\frac{1}{2}} = \mu s^{-\frac{1}{2}} \quad (I7)$$

où A représente la surface de l'électrode.

Il en résulte que l'impédance opérationnelle de diffusion est inversement proportionnelle à la racine carrée de s . Il suffit donc de tracer la droite $Z_f(s) = f(s^{-\frac{1}{2}})$. Celle-ci nous donnera μ par sa pente. En prenant deux valeurs différentes de c_{Ox} et c_{Red} , nous pourrions alors obtenir les coefficients de diffusion D_{Ox} et D_{Red} .

2. Dans le cas où la réaction d'électrode est contrôlée non seulement par le transport massique, mais encore par le transfert de charges, pour les surtensions faibles ($\eta \ll RT/zF$), nous avons l'expression connue suivante:

$$\eta = \frac{RT}{zF} \left(\frac{c_{Ox}}{c_{Ox^0}} - \frac{c_{Red}}{c_{Red^0}} + \frac{I_f}{I_0} \right) \quad (I8)$$

dans laquelle I_0 est le courant d'échange.

Après transformation on obtient:

$$U(s) = \frac{RT}{zF} \left(\frac{\Gamma_{Ox}}{c_{Ox^0}} - \frac{\Gamma_{Red}}{c_{Red^0}} + \frac{J_f(s)}{I_0} \right) \quad (I9)$$

Nous avons donc, après avoir remplacé Γ_{Ox} et Γ_{Red} par les éqns. (I2) et (I3), pour l'impédance opérationnelle l'expression suivante:

$$Z_f(s) = \frac{U(s)}{J_f(s)} = \frac{RT}{Az^2 F^2} \left(\frac{I}{c_{Ox^0} D_{Ox^{\frac{1}{2}}}} + \frac{I}{c_{Red} D_{Red^{\frac{1}{2}}}} \right) s^{-\frac{1}{2}} + \frac{RT}{zFI_0} = \mu s^{-\frac{1}{2}} + R_t \quad (20)$$

qui exprime bien l'additivité des impédances de ces deux étapes successives. Remarquons que cette dernière formule pourrait aussi être établie à partir d'une relation $J_f(s) = f[U(s)]$ donnée récemment pour le cas du contrôle mixte considéré⁵. On voit que, pour une réaction d'électrode contrôlée à la fois par la diffusion et le transfert, la pente μ de la droite $Z_f = f(s^{-\frac{1}{2}})$ obtenue permet encore de déterminer les coefficients de diffusion.

3. Quand la réaction étudiée comporte en plus du transfert et de la diffusion une réaction chimique associée, l'obtention de Z_f est plus délicate, sauf dans quelques cas particuliers, tels que celui de l'adsorption spécifique, pour lequel un schéma électrique équivalent peut être proposé⁶. Toutefois, comme pour des basses fréquences les réactions chimiques peuvent être représentées par une résistance pure⁷, une portion rectiligne de pente μ doit encore apparaître sur la courbe $Z_f(s)$ tracée en fonction de $s^{-\frac{1}{2}}$ pour des valeurs de s suffisamment faibles. Bien entendu, cette portion rectiligne sera d'autant plus décalée vers les valeurs faibles de s que la réaction chimique associée sera plus lente. Son expression sera semblable à l'éqn. (20):

$$Z_f(s) = K + \mu s^{-\frac{1}{2}} \quad (2I)$$

avec K représentant une constante qui dépend des paramètres cinétiques du transfert, de la réaction chimique et de la diffusion.

2. PARTIE EXPÉRIMENTALE

De nombreux auteurs ont déjà étudié le comportement électrochimique⁸⁻¹² du système Hg(O)/Hg(I) en milieu d'acide perchlorique. Cependant, plusieurs points n'ont toujours pas été élucidés et en particulier la nature des espèces en présence dans les diverses concentrations d'électrolyte support reste mal définie^{10,11}. Nous avons donc fait appel à des mesures d'impédance opérationnelle pour voir s'il existe une variation du coefficient de diffusion de l'ion mercureux reflétant un changement éventuel des espèces en présence.

La cellule d'électrolyte utilisée, en verre Pyrex, est de forme cylindrique et peut contenir 200 ml de solution. Elle est maintenue à température constante grâce à une double enveloppe dans laquelle circule de l'eau thermostatée. L'électrode étudiée est constituée par une goutte de mercure suspendue à un fil de Pt mercuroisé¹³, placé dans l'axe d'une contre-électrode cylindrique en Pt. Des gouttes de volume reproductible sont obtenues à l'aide d'un dispositif à piston Metrohm; leur surface (3.2 mm²) a été calculée par pesée. Une électrode de comparaison, constituée par une nappe de mercure, est placée au fond de la cellule. Une électrode au calomel, saturée, est reliée à la cellule par un pont électrolytique comportant deux robinets fermés situés de part et d'autre d'une solution intermédiaire (HCl). L'emploi d'une atmosphère inerte ne changeant pas les résultats obtenus, toutes les expériences systématiques ont été effectuées à l'air libre.

Remarquons que les équations établies dans le cas de la diffusion linéaire peuvent être appliquées, sans erreurs appréciables, à une électrode sphérique, à condition que son rayon soit supérieur à 0.5 mm et que la durée de perturbation n'excède pas quelques secondes¹⁴. En effet, l'épaisseur de la zone perturbée reste alors négligeable par rapport au rayon de l'électrode. D'ailleurs, une limitation supplémentaire du domaine d'application de ces équations est provoquée par l'effet de la convection qui devient non négligeable sensiblement en même temps que se manifeste l'effet de sphéricité. Le rayon de l'électrode utilisée étant voisin de 0.5 mm, la durée maximale d'application des impulsions a été limitée dans ces expériences à quelques secondes.

Bien qu'une perturbation de forme quelconque puisse en principe être utilisée, nous avons choisi un signal de forme simple dont la transformée a une expression mathématique connue. Ainsi les opérations de transformation se trouvent limitées aux seules courbes de réponse. Le régime galvanostatique a été adopté non seulement en raison de la simplicité de l'appareillage nécessaire, mais encore parce qu'il permet d'assurer un maximum de précision dans le domaine des valeurs faibles de s où on détermine les coefficients de diffusion.

La technique de transformation utilisée consiste tout d'abord à calculer point par point, pour une valeur de s donnée, à partir d'une courbe de réponse enregistrée, la courbe $V(t) e^{-st}$, puis à intégrer graphiquement la surface délimitée par cette dernière. Cette surface donne une valeur de la fonction $U(s)$ et la valeur correspondante de $Z(s)$ en découle puisque pour un signal galvanostatique: $J(s) = I/s$.

Les impulsions d'intensité constante ont été obtenues à l'aide d'un accumulateur branché en série avec une grande résistance et un relais ultrarapide Clare. Le courant impulsif, imposé entre l'électrode de travail et la contre-électrode, a été limité de façon à ce que la surtension finale, mesurée à l'aide de l'électrode de comparaison, ne dépasse jamais 2 mV.

Des courbes galvanostatiques ont été enregistrées à différentes vitesses de balayage. Pratiquement, il suffit de 6 enregistrements (pris entre 10 msec/cm et 500 msec/cm) par solution électrolytique examinée pour pouvoir exploiter le domaine des valeurs de s allant de 2-100. Quelques courbes de la fonction $V(t) e^{-st}$ sont présentées sur la Fig. 2. On voit que, pour une vitesse de balayage donnée, les valeurs de s choisies ne doivent pas varier plus que du simple au double pour permettre l'annulation pratique de la fonction, tout en assurant l'obtention d'une surface d'intégration suffisamment grande.

La Fig. 3 représente en fonction de la concentration en acide perchlorique (entre 0.1 M et 2 M), les droites $Z = f(s^{-\frac{1}{2}})$ obtenues à 30° pour deux concentrations en sel mercurieux légèrement différentes (6.7 et $10 \cdot 10^{-4} M$). Le fait que ces droites se prolongent jusqu'à des valeurs de s aussi faibles que 2 prouve que l'emploi des équations de diffusion semi-infinie linéaire était justifié pour cette étude.

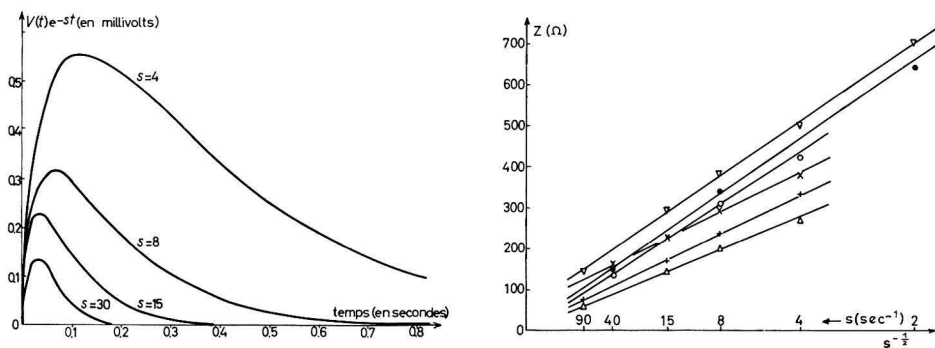


Fig. 2. Exemple montrant des courbes $V e^{-st} = f(t)$ calculées, pour différentes valeurs de s , à partir d'une courbe galvanostatique expérimentale (vitesse de balayage, 100 msec/cm).

Fig. 3. Courbes expérimentales des variations de l'impédance opérationnelle, Z , en fonction de l'opérateur s de Laplace pour une électrode $Hg(O)/Hg(I)$ en milieu $HClO_4$ à 30°. $C_{Hg(I)} = 1 \cdot 10^{-3} M$: (\times), 0.1; (+), 0.5; (Δ), 1 et 2 $M HClO_4$. $C_{Hg(I)} = 6.7 \cdot 10^{-4} M$: (∇), 0.1; (\bullet), 0.5; (\circ), 1 $M HClO_4$.

Il est à remarquer que le calcul du coefficient de diffusion, à partir des valeurs des pentes μ obtenues, est particulièrement simple dans le cas du système étudié ici, puisque dans l'éqn. (20) le terme correspondant à la diffusion de l'espèce réduite est négligeable, étant donné que cette espèce est le constituant unique de la phase métallique (autodiffusion du mercure). Dans ces conditions, D_{Ox} est donc directement calculable par la formule:

$$D_{Ox} = \left(\frac{RT}{Az^2 F^2 C_{Ox}^0 \mu} \right)^2 \quad (22)$$

une seule valeur de μ correspondant à une seule concentration étant nécessaire. L'emploi des deux concentrations en sel mercurieux a permis néanmoins d'améliorer la

précision. En posant $z=2$ dans la formule (22), les valeurs suivantes à 30° ont été obtenues :

HClO_4 0.1 M	$D_{\text{Ox}} = 1.05 \cdot 10^{-5} \text{ cm}^2 \text{ sec}^{-1}$
HClO_4 0.5 M	$D_{\text{Ox}} = 1.08 \cdot 10^{-5} \text{ cm}^2 \text{ sec}^{-1}$
HClO_4 1 M	$D_{\text{Ox}} = 1.25 \cdot 10^{-5} \text{ cm}^2 \text{ sec}^{-1}$
HClO_4 2 M	$D_{\text{Ox}} = 1.21 \cdot 10^{-5} \text{ cm}^2 \text{ sec}^{-1}$

Bien que la dispersion observée dans ces mesures n'ait pas dépassé $\pm 6\%$, compte-tenu de la précision de la technique oscillographique employée ($\pm 3\%$) et de la reproductibilité de la surface des gouttes ($\pm 3\%$), une dispersion voisine de $\pm 10\%$ doit être considérée comme normale pour une série d'expériences effectuées avec la même solution. Dans ces conditions, les variations ($\pm 11\%$) de la valeur de D_{Ox} autour de la valeur moyenne $1.15 \cdot 10^{-5} \text{ cm}^2 \text{ sec}^{-1}$ observées dans les différentes concentrations d'acide perchlorique ne peuvent être considérées comme vraiment significatives. En particulier, il n'est pas possible, à partir de ces résultats, d'affirmer comme IMAI ET DELAHAY¹⁰ qu'il existe une modification chimique de l'espèce diffusante en fonction de la concentration en acide perchlorique.

Les résultats obtenus sont en bon accord avec ceux publiés récemment par SLUYTERS¹¹ qui a trouvé à 25° dans HClO_4 0.1 M et 1 M la même valeur : $0.93 \cdot 10^{-5} \text{ cm}^2 \text{ sec}^{-1}$.

3. CONCLUSIONS

De nombreuses méthodes électrochimiques de détermination des coefficients de diffusion sont connues. Parmi elle citons : mesures du courant limite¹⁵, détermination des pentes des droites $I = f(t^{-1/2})$ en régime potentiostatique¹⁵ et $V = f(t^{1/2})$ en régime galvanostatique⁹, détermination du temps de transition par chronopotentiométrie¹⁶, mesures de l'impédance faradique à l'aide d'un pont alternatif^{17,18}.

Le procédé proposé ici présente certaines analogies avec cette dernière méthode, mais il faut souligner que, d'une part, l'appareillage qu'il nécessite est considérablement plus simple et que, d'autre part, il permet d'isoler plus facilement les différentes étapes à partir du processus global. En effet, la limitation expérimentale du domaine exploitable du côté des fréquences faibles¹⁹ n'existe pas dans le procédé proposé où les valeurs de s peuvent être choisies aussi petites que l'on désire, à la seule condition que le domaine de temps à intégrer permette de conserver le mode de transport massique envisagé. Les expériences montrent que, même dans le cas le plus défavorable, c'est-à-dire celui d'un contrôle par diffusion seule (solutions HClO_4 2 M), cette dernière condition reste encore valable pour des valeurs aussi faibles que 2, ce qui correspond à une fréquence opérationnelle de 0.3 Hz.

La comparaison du procédé proposé avec les autres méthodes impulsionnelles citées permet de constater sa supériorité dans tous les cas où la réaction d'électrode est contrôlée non seulement par diffusion, mais encore par le transfert de charges ou par réaction chimique. La principale raison en est que, restant dans le domaine opérationnel, on n'a pas à recourir aux approximations indispensables pour exploiter en fonction du temps les solutions de l'équation de Fick obtenues dans le cas d'un contrôle mixte.

REMERCIEMENTS

Les auteurs tiennent à remercier Monsieur M. BONNEMAY, Professeur au Conservatoire National des Arts et Métiers, Directeur du Laboratoire d'Electrolyse, pour l'intérêt qu'il a porté à ce travail et les encouragements et les conseils qu'il leur a donnés ainsi que leurs collègues du laboratoire qui ont bien voulu participer aux discussions et échanges d'idées auxquels a donné lieu leur travail. Ils remercient également Monsieur J. C. FARCY pour la collaboration technique qu'il a apportée à l'exécution de la partie expérimentale.

RÉSUMÉ

Des expressions analytiques de l'impédance opérationnelle $Z(s)$, valables pour toutes les méthodes de relaxation, sont proposées pour différents types de réaction d'électrode.

Leur utilisation expérimentale permet de déterminer les paramètres cinétiques et plus particulièrement les coefficients de diffusion des espèces réagissantes.

La partie expérimentale du travail concerne des mesures effectuées en régime galvanostatique impulsif sur le système Hg/Hg₂²⁺, en milieu HClO₄ à 30°. Les résultats, exploités en fonction du paramètre opérationnel s de Laplace, ont permis de constater que le coefficient de diffusion de l'ion mercureux reste sensiblement constant dans un domaine de concentration d'électrolyte support compris entre 0.1 M et 2 M .

Les avantages du procédé proposé sont comparés à ceux des autres méthodes électrochimiques de détermination des coefficients de diffusion.

SUMMARY

Analytical expressions for the operational impedance, Z_s , valid for all relaxation methods, are proposed for various types of electrode reactions.

Used experimentally, they enable kinetic parameters, and, more particularly, diffusion coefficients of reacting species to be determined.

The experimental part of the work is concerned with measurements made under galvanostatic pulse conditions for the Hg/Hg₂²⁺ system in HClO₄ media at 30°. The results, stated in terms of the Laplace operator function, s , have shown that the diffusion coefficient of mercury ion is approximately constant at supporting electrolyte concentrations between 0.1 and 2 M .

The merits of the proposed procedure are compared with those of other electrochemical methods for the determination of diffusion coefficients.

BIBLIOGRAPHIE

- 1 E. POIRIER D'ANGÉ D'ORSAY, *Compt. Rend.*, 260 (1965) 5266.
- 2 M. D. WIJNEN, *Rec. Trav. Chim.*, 79 (1960) 1203.
- 3 W. LORENZ, *Z. Physik. Chem. Leipzig*, 205 (1956) 311.
- 4 D. SCHUMANN, Thèse, Paris, 1964.
- 5 D. M. MOHILNER, Electrochemical Society, Toronto Meeting, May, 1964.
- 6 M. SENDA ET P. DELAHAY, *J. Phys. Chem.*, 65 (1961) 1580.
- 7 K. J. VETTER, *Elektrochemische Kinetik*, Springer, Berlin, 1961, p. 227.

- 8 H. GERISCHER ET K. E. STAUBACH, *Z. Physik. Chem. Frankfurt*, 6 (1956) 118.
- 9 H. MATSUDA, S. OKA ET P. DELAHAY, *J. Am. Chem. Soc.*, 81 (1959) 5077.
- 10 H. IMAI ET P. DELAHAY, *J. Phys. Chem.*, 66 (1962) 1108.
- 11 M. SLUYTERS-REHBACH ET J. H. SLUYTERS, *Rec. Trav. Chim.*, 83 (1964) 217, 968 et 983.
- 12 R. L. BIRKE ET D. K. ROE, *Anal. Chem.*, 37 (1965) 450 et 455.
- 13 H. GERISCHER, *Z. Physik. Chem. Leipzig*, 202 (1953) 302.
- 14 P. DELAHAY, *New Instrumental Methods in Electrochemistry*, Interscience Publishers, London, New York, 1954, p. 62.
- 15 I. M. KOLTHOFF ET J. J. LINGANE, *Polarography*, Interscience Publishers, London, 1952, pp. 18-62.
- 16 J. A. V. BUTLER ET G. ARMSTRONG, *Trans. Faraday Soc.*, 30 (1934) 1173.
- 17 J. H. SLUYTERS, *Rec. Trav. Chim.*, 79 (1960) 1092.
- 18 A. M. BATICLE, 16ème Réunion du C.I.T.C.E., Budapest, 1965.
- 19 K. J. VETTER, *Elektrochemische Kinetik*, Springer, Berlin, 1961, p. 316.

J. Electroanal. Chem., 12 (1966) 277-285

NEW INDICATING SYSTEM: TWIN ELECTRODES, AT ZERO CURRENT

I. PROPOSED MECHANISM*

E. KIROWA-EISNER AND M. ARIEL

Laboratory of Analytical Chemistry, Department of Chemistry, Technion, Israel Institute of Technology, Haifa (Israel)

(Received December 2nd, 1965)

INTRODUCTION

A potentiometric indicating system consisting of twin electrodes at zero current, has been described¹. This system exploits the sharp potential difference peak (PDP) between two identical electrodes at the end-point of an automatic (coulometric or volumetric) titration; the titrant is added at a constant rate with controlled stirring and the potential difference between the electrodes is recorded continuously throughout the titration. The influence of a number of experimental parameters on the PDP has already been investigated¹ and the results (location of the indicating electrodes, direction and intensity of the generating current) combined with the additional information given below, form the basis for the proposed indication mechanism.

EXPERIMENTAL AND RESULTS

The experiments described below were carried out with twin mercury electrodes; the apparatus used has already been described^{1,2,3}; the new indicating system has been applied to acid-base titrations.

Effect of the electrical field on the indicating system

When the titration is carried out coulometrically, an electrical field results from the passage of the generating current through the solution. Since the indicating electrodes are placed at different locations in this field, an initial potential difference, V_0 , will appear between them as soon as the generating current is switched on. The concentration of the titrated species is negligible compared to the concentration of the base electrolyte. Accordingly, the resistance of the solution and, therefore, the initial potential difference, V_0 , will remain constant throughout the titration and the PDP, characterizing the end-point, will be superimposed on it.

The investigation of the effect of the field on the PDP is hampered by the difficulty of isolating any single factor when evaluating its effect on the PDP; variation of one factor is always accompanied by changes in another.

Initial potential difference and cell geometry

The effect of the initial potential difference and the location of the electrodes

* Part of a D.Sc. thesis presented by E.K.E. to the Senate of the Technion.

in the cell, on the height and direction of the PDP was investigated; the results are summarized in Table 1.




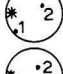

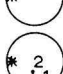
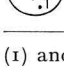
No logical correlation between the initial potential difference and the PDP can be based on these results; the variations of the PDP must be attributed to changes in cell geometry.

Generating current

Changes in the intensity of the generating current result in simultaneous changes of V_0 and the rate of titrant addition. The PDP decreases with decreasing current¹ and since, according to Table 1, V_0 has no effect on the PDP, variations of PDP must be due to the rate of titrant addition.

TABLE 1

EFFECT OF THE INITIAL POTENTIAL DIFFERENCE AND CELL GEOMETRY

Schematic cell plan	Initial potential difference, V_0 (mV)	Height and direction of PDP (mV)
	135	+70
	-130	-70
	-40	+100
	160	+100
	80	+130
	80	-50
	80	0

(1) and (2), two identical electrodes (mercury-coated silver); *, generating electrode; generating current, 20 mA; composition of cell soln.: HNO_3 , $2 \cdot 10^{-4} N$, 5% KNO_3 .

Generating current and cell geometry

Constant values of V_0 may be obtained by the simultaneous adjustment of both the cell geometry and the intensity of the generating current, thus allowing an investigation of the effect of the generating current or cell geometry on the height and direction of the PDP. The results are shown in Table 2.




With the appropriate location of the electrodes within the cell (Table 2), an inverse proportionality between the intensity of the generating current and the height of the PDP is obtained; in these experiments the location of the electrodes is the determining factor.

Volumetric titrations in the presence of an electrical field

An experiment was carried out with constant cell geometry and rate of titrant addition; the intensity and direction of the electrical field were varied. The apparatus employed, shown in Fig. 1, allows an electrical field of desired intensity and direction

TABLE 2

EFFECT OF GENERATING CURRENT AND CELL GEOMETRY

Schematic cell plan	Generating current (mA)	Initial potential difference, V_0 (mV)	PDP, direction and height (mV)
	20	135	70
	17	135	90
	10	135	100

(1) and (2), two identical electrodes (mercury-coated silver); *, generating electrode; composition of cell soln.: HNO_3 (10^{-4} N, approx.), 5% KNO_3 .

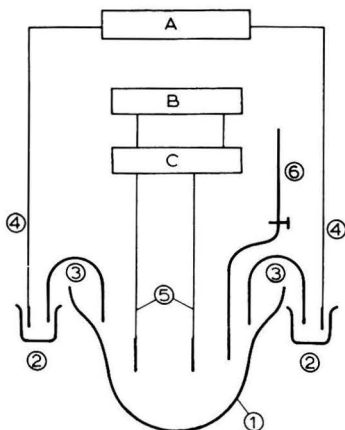


Fig. 1. Titration cell; external electrical field applied does not affect the composition of cell soln. (1), titration cell; (2), auxiliary cell, filled with satd. KNO_3 soln.; (3), salt bridge, filled with satd. KNO_3 soln.; (4), platinum generating electrodes, connected to coulometer; (5), indicating electrodes, twin mercury-coated silver electrodes²; (6), automatic burette; (A), impedance matching unit, differential electrometer according to YARNITSKY³; (B), Polarograph Shimadzu, type RP2 recorder; (C), coulometer Metrohm type E211.

to be set up in the cell, without affecting the composition of the cell solution. The titration is carried out volumetrically. Reversal of the field, achieved by reversing the polarity of the platinum electrodes, or changes in its intensity, achieved by varying the generating current, had no effect on the shape or height of the PDP.

Volumetric titration with automatic recording

The above experiment was repeated with zero current (through the platinum electrodes); this is equivalent to a normal volumetric titration with constant rate of titrant addition and automatic recording. The peak obtained is identical with that obtained in a coulometric titration at the same rate of titrant generation. In this case, as in the case of coulometric titrations, the direction of the PDP is reversed when (a) the indicating electrodes are interchanged; (b) the direction of the titration is reversed (acid or base titration). These experiments show that the electrical field has no effect on the indicating system.

Dynamic causes of the PDP

If the titration is interrupted at various stages, a gradual decay of the potential difference between the indicating electrodes is observed (Fig. 2). When the generating current is switched on, a potential difference appears between the two electrodes (this includes the abrupt appearance of the initial potential difference, V_0). The branches AB in Fig. 2 depict this change. When the current is switched off, the potential difference drops rapidly at first (loss of V_0) and later decays gradually to a stable value (branches BC in Fig. 2). The final potential difference approaches zero and is not dependent on the stage of the titration. The B-points on the potential difference–time curves represent the potential difference at various points of the titration at the moment of this interruption; these are not equilibrium values and are significantly dependent on the extent of the titration. The curve of these maximum potential difference values plotted against progress of titration, is peaked.

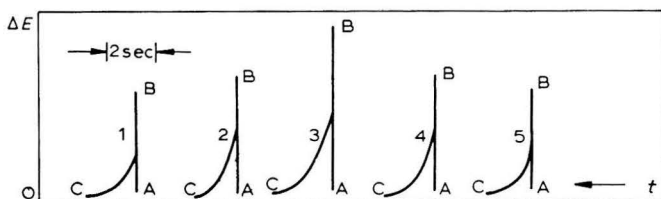


Fig. 2. Coulo–potentiometric titration of acid with interruption of generating current, 1 sec after start. Generating current: 20 mA; composition of cell soln.: $6 \cdot 10^{-5} N$ HNO₃, 10% KNO₃; soln. stirred continuously throughout the recording of potential–time curves. λ , fraction titrated: (1), 1.04; (2), 1.02; (3), 1; (4), 0.98; (5), 0.96.

The appreciable potential difference between the electrodes, and its decay with time, indicate different reaction rates of the two electrodes. This may be attributed to one or more of the following factors: (a) differences in the state of surface area of the electrodes; (b) differences in the rate of titrant supply to the two electrodes and (c) differences in the thickness of the diffusion layers at the two electrodes.

(a) *Differences in the surface area.* Partial oxidation, the formation of intermetallic compounds, precipitates or the adsorption of contaminants from the solution, may all result in differences in the state of the electrode surfaces, causing changes in the exchange current and the transfer coefficients and hence affecting the rate of response of the electrodes. Comparison of the expected behavior of twin electrodes, and experimental titration curves obtained with them, clarifies this point. The expected behavior was based on the following assumptions: (i) electrode (1) has a slower

response rate than electrode (2); (ii) with a solution of constant composition, a potential difference exists between the two electrodes due to the difference in the state of their surface area; (iii) the titration is carried out volumetrically and automatically.

The potential change of each electrode measured against a reference electrode is described by an "S"-shaped curve; the potential difference between the two, when one lags behind the other, is characterized by a peak (PDP) at the end point (Fig. 3).

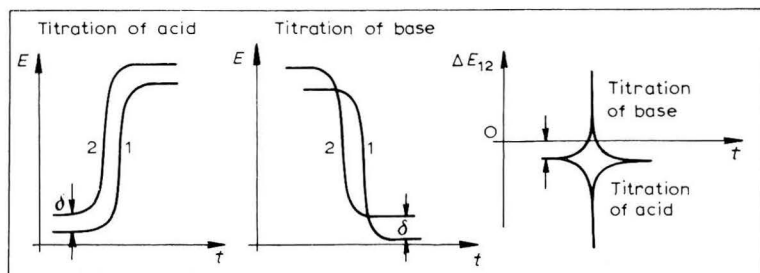


Fig. 3. Expected volumetric acid-base titration curves, with automatic recording for the case of two indicating electrodes having different response rates due to differences in the state of the surface area of the electrodes.

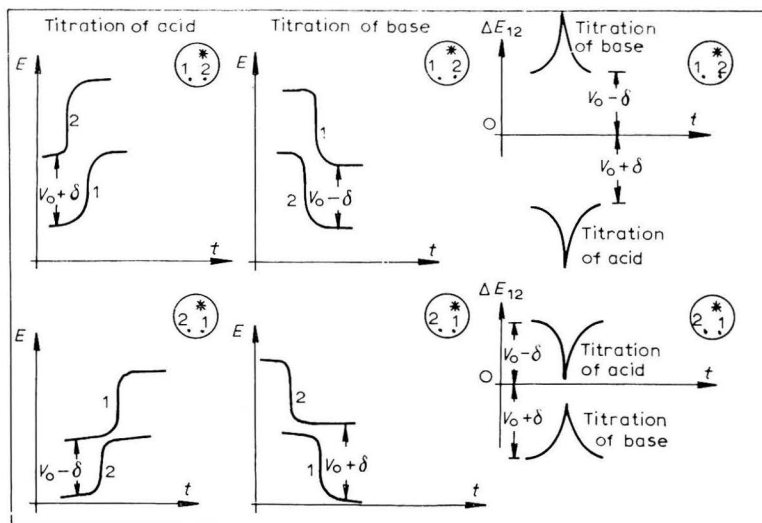


Fig. 4. Expected coulometric acid-base titration curves with automatic recording for the case of two indicating electrodes having different response rates due to differences in the state of the surface area of the electrodes.

When the titration is carried out coulometrically, the initial potential difference, V_0 , is added to the potential difference, δ . This may be positive or negative according to the direction of the generating current and the location of the electrodes, and causes a slight difference between the shapes of the volumetric and coulometric titration curves due to the background on which the PDP appears.

The coulometric titration curves are shown in Fig. 4. If the differences in electrode response are mainly a result of different surfaces, the direction of the PDP must be determined by properties pertaining to the electrodes themselves and not to their location. Previous experiments¹, however, show the location to be the determining factor; the PDP cannot, therefore, be ascribed to inequality in the surface states of the twin electrodes. However, work now in progress⁴ shows that with certain electrodes, surface effects (*e.g.* roughness factor), will be dominant. Experimental volumetric and coulometric titration curves obtained with two glass electrodes resemble the theoretical curves shown in Figs. 3 and 4.

b. Different rate of titrant supply. When stirring is inefficient, the titrant supply will be unequal and the electrode removed from the source of titrant supply will lag behind the one near to it. The expected titration curves (volumetric and coulometric) for this case are shown in Fig. 5.

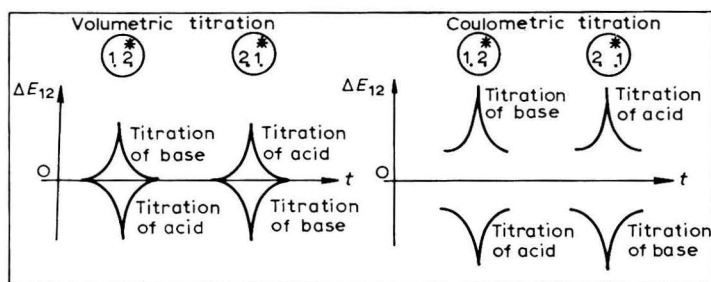


Fig. 5. Expected volumetric and coulometric acid-base titration curves with automatic recording for the case of different rates of titrant supply to the two electrodes.

TABLE 3

EFFECT OF STIRRING RATE

Schematic cell plan	Stirring rate (rev. of magnet bar/sec)	Height of the PDP (mV)
	10	130
	14	110
	19	95
	25	85
	25	80

(1) and (2), two identical mercury-coated silver electrodes; *, generating electrode; generating current: 20 mA; composition of cell soln.: HNO_3 , $6 \cdot 10^{-5} \text{ N}$, 5% KNO_3 ; volume of cell soln.: 60 ml; length of magnet bar: 2.8 cm. In addition to the magnetic stirring, the solution was stirred thoroughly by passing nitrogen gas through a porous glass bubbler.

The following experiments were carried out to determine the extent to which the indicating signal (the PDP) results from this cause:

Stirring. The stirring rate influences the homogeneity of the cell solution during titration. Table 3 shows results obtained with different stirring rates. It can be seen from Table 3 that increased stirring rate results in a decrease in the height of the PDP; however, even at very high stirring rates, a clear peak still appears. The lag in mass transfer, near the equivalent point, required to produce a PDP of 131 mV, may

be calculated*. The experimental PDP of 130 mV (Table 3) is obtained with a stirring rate of 10 rev/sec of the magnet bar; this provides very efficient stirring action and, therefore, cannot be accompanied by such an extensive (5 sec) mass transfer delay.

Reversal of the direction of the magnetic stirring did not affect the direction of the PDP.

Peripheral and central generation. Titrations were carried out with (a) a peripheral generating electrode (a platinum net hugging the cell sides and of cell height) and (b) a wire electrode, centrally placed. When the indicating electrodes remained in fixed positions in the cell, the change from peripheral to central generation did not affect the direction of the PDP.

This experiment proves that the PDP is not the result of solution inhomogeneity. Further exhaustive experiments proved beyond doubt that the PDP is independent of generating electrode location but dependent only on the location of the indicating electrode. Only in extreme cases, when the indicating electrode is placed in the immediate vicinity of the generating electrode (about 2 mm from it), does the stirring fail to overcome the concentration gradient formed, and the nearer electrode leads. Under ordinary experimental conditions, however, this cannot be the factor responsible for the indicating mechanism.

c. Different thickness of diffusion layer. Various regions in the titration cell are stirred at different rates and two electrodes dipping into two such regions will have different diffusion layers. The electrode in the more rapidly stirred region will have a thinner layer than the one dipping in the slower region. As a result the electrodes will have different rates of response to the continually changing composition of the cell solution and the electrode with the thinner diffusion layer will respond more rapidly. According to this concept, the location of the electrodes in the titration cell will determine which leads and which lags; an interchange will result in a reversal of this order and hence a reversal in PDP direction. Two experiments were carried out to prove this to be the determining factor of the twin electrode indicating system.

(i) *Superstirring at one of the indicating electrodes.* When energetic stirring was applied to the region in which one of the indicating electrodes was located, this electrode was always found to lead (Fig. 6). The leading electrode was identified as follows: in the titration of an acid the electrode potential changes towards negative values; the leading electrode will, therefore, be more negative than the other.

(ii) *Vibration of one indicating electrode.* A series of titrations, analogous to those summarized in Fig. 6, was carried out with one of the electrodes directly connected to a vibration stirrer (in place of the stirring rod), thus achieving super-stirring at the vibrating electrode. The results and their conclusions are identical with those shown in Fig. 6.

This investigation suggests the following indication mechanism. In the titration cell with efficient stirring, regions of different liquid velocity arise resulting in different thicknesses of the diffusion layers at the electrodes placed in the solution. This causes the electrodes to respond at different rates to changes in the solution during the titration. The potential change of each electrode (*vs.* reference electrode) is

* The PDP may be calculated for the experimental conditions described in Table 3 (generating current: 20 mA; vol. of cell soln.: 60 ml) and assuming a response lag of 5 sec between the two electrodes. It will be determined by the ΔpH at a single electrode, between the equivalent point and 5 sec earlier or later.

given by an "S"-shaped curve. Owing to small difference in their rates of response, a sharp peak is obtained when their potential difference is recorded throughout the titration.

To ensure quantitative results with this new potentiometric method, the electrode must respond rapidly to changes in the composition of the titrated solution.

In well stirred solutions the thickness of the diffusion layer and, therefore, the

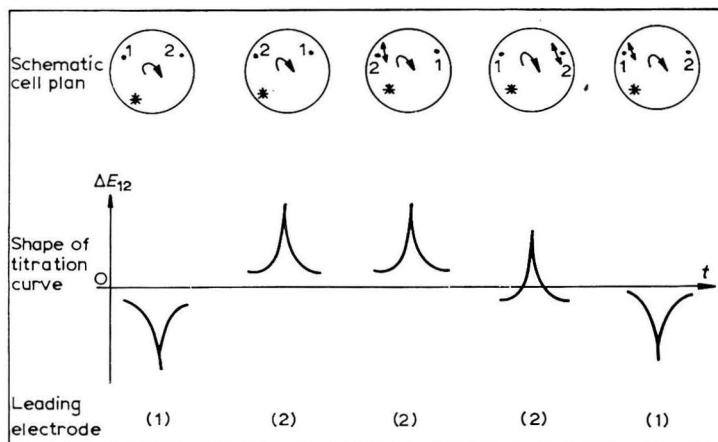


Fig. 6. Effect of super-stirring, at one of the indicating electrodes, on the direction of the PDP. (1) and (2), two identical mercury-coated silver electrodes; (*), generating electrode; generating current: 20 mA; \curvearrowright , magnetic stirring (14 rev/sec of the magnet bar); \leftrightarrow , vibration stirrer (type VR 1, Wissenschaftlich Technische Werkstätten; vibration frequency, 100/sec; vibration amplitude, 2mm); composition of cell soln.: $6 \cdot 10^{-5} N HNO_3$, 10% KNO_3 .

response rate of the electrode, are determined by the roughness factor. Consequently, when mercury electrodes are used for indication, the discrepancy between the equivalent and end points is negligible. Further work on this subject will be reported⁴.

SUMMARY

A mechanism for the new indicating system "twin electrodes, at zero current", is proposed. In the titration cell, even with efficient stirring, regions of different liquid velocity arise, resulting in different thicknesses of the diffusion layers at the electrodes placed in the solution. This causes the electrodes to respond at different rates to changes in the solution during the titration. The potential change of each electrode is given by an "S"-shaped curve. Owing to the small difference in their rates of response, a sharp peak is obtained when their potential difference is recorded throughout the titration.

REFERENCES

- 1 M. ARIEL AND E. KIROWA-EISNER, *J. Electroanal. Chem.*, 10 (1965) 319.
- 2 M. ARIEL AND E. KIROWA-EISNER, *J. Electroanal. Chem.*, in press.
- 3 CH. YARNITSKY, *J. Electroanal. Chem.*, 12 (1966) 265.
- 4 M. ARIEL AND E. KIROWA-EISNER, to be published.

DIFFUSION-LIMITED ADSORPTION AT SPHERICAL ELECTRODES*

SIDNEY L. PHILLIPS

I.B.M. Corp., Box 390, Poughkeepsie, New York 12602 (U.S.A.)

(Received December 2nd, 1965)

INTRODUCTION

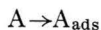
Adsorption at a planar electrode under conditions of diffusion-limited mass transfer has been investigated both theoretically and experimentally by several workers¹⁻⁴. In these studies, the boundary condition normally applied is that the solution concentration of the adsorbable substance is equal to zero at the electrode surface throughout the course of the experiment^{1,4}. Assuming this condition holds, the time at which the faradaic current falls to zero is supposed to coincide with formation of the maximum equilibrium surface coverage of the surfactant⁴. Although this relation between the interfacial concentrations and time was derived for a planar electrode, it has most often been applied to instantaneous current-time data obtained using a dropping-mercury electrode^{1,4,5}.

The equation based on a planar electrode predicts a linear relation between the reciprocal of the bulk concentration of surfactant and the square root of the time at which the faradaic current is zero. The slope of this line is proportional to the ratio of the maximum surface concentration of the surfactant, and the square root of the diffusion coefficient of the adsorbing substance. From the value of this slope alone, it is not possible to calculate separately either the maximum surface coverage or the diffusion coefficient of the surfactant. Thus, in order to calculate both these quantities, either the diffusion coefficient or the equilibrium surface coverage must be determined from a separate experiment⁴.

On the other hand, the form of the theoretical equation relating the maximum surface coverage, bulk concentration, and time at a spherical electrode permits calculation of both bulk diffusion coefficient and equilibrium surface coverage from a series of current-time curves. This is shown in the following derivation.

THEORETICAL

Consider the diffusion-limited adsorption process



The Fick's-Law equation for the diffusional process at a spherical electrode may be written in the form⁶

* Presented in part, Division of Analytical Chemistry, 150th National Meeting of the American Chemical Society, Atlantic City, New Jersey, September 1965.

$$\frac{\partial C_A}{\partial t} = D_A \left[\frac{\partial^2 C_A}{\partial r^2} + \frac{2}{r} \frac{\partial C_A}{\partial r} \right] \tag{1}$$

Here, C_A is the concentration of substance A, t the time, D_A the diffusion coefficient of substance A, and r the radial distance from the center of the spherical electrode. The initial condition

$$t = 0, \quad r \geq r_0: C_A = C_A^0 \tag{2}$$

specifies that at the start of the experiment, the surfactant is homogeneously distributed throughout the solution.

The boundary conditions are similar to those used for the planar electrode case^{2,3}

$$t > 0, \quad r \rightarrow \infty: C_A \rightarrow C_A^0 \tag{3}$$

$$r = r_0: C_A = 0 \tag{4}$$

$$D_A \frac{\partial C_A}{\partial r} = \frac{d\Gamma}{dt} \tag{5}$$

Equation (3) expresses the usual condition of semi-infinite diffusion. In eqn. (4), it is assumed that the surfactant concentration in the volume of solution around the electrode surface is nearly zero until the electrode is almost completely coated. REINMUTH'S calculations indicate that this is a generally valid assumption up to half-coverage in the case of a planar electrode³. In eqn. (5), the adsorption rate is equated to the material flux at the electrode surface.

Equation (1) is readily solved for the initial and boundary conditions using the Laplace transform, and the solution, taking into account eqn. (5), is

$$\Gamma_m = \frac{2C_A^0 \sqrt{D_A t_0}}{\sqrt{\pi}} + \frac{C_A^0 D_A t_0}{r_0} \tag{6}$$

Here, Γ_m is the maximum surface coverage, and t_0 is the time at which this maximum coverage is attained. It is seen that eqn. (6) differs from the plane electrode case by addition of the important second term on the right-hand side. Equation (6) may be rearranged to give

$$\frac{\Gamma}{C_A^0 \sqrt{t_0}} = \frac{2\sqrt{D_A}}{\sqrt{\pi}\Gamma_m} + \frac{D_A \sqrt{t_0}}{r_0 \Gamma_m} \tag{7}$$

It can be seen from eqn. (7), that a plot of $[C_A^0 \sqrt{t_0}]^{-1}$ vs $\sqrt{t_0}$ should give a straight line with a slope equal to $D_A / \Gamma_m r_0$, and an intercept of $2\sqrt{D_A} / \sqrt{\pi} \Gamma_m$. Thus, the slope and intercept yield two equations in two unknowns and may be solved simultaneously for D_A and Γ_m . On the other hand, the comparable equation for a planar electrode yields a straight line that passes through the origin so that only the ratio of the maximum surface concentration and diffusion coefficient can be determined.

In Fig. 1, theoretical plots of the adsorption behavior corresponding to eqns. (1)–(5) are shown for both plane and spherical electrodes. The dimensionless quantities

$$\xi = \Gamma_m / C_A^0 \sqrt{t_0 D_A}, \quad \psi = \sqrt{t_0 D_A} / r_0$$

are plotted for convenience. Using these substitutions, the spherical and planar equations are

$$\text{Sphere: } \sqrt{\pi}\xi = \sqrt{\pi}\psi + 2$$

$$\text{Plane: } \sqrt{\pi}\xi = 2$$

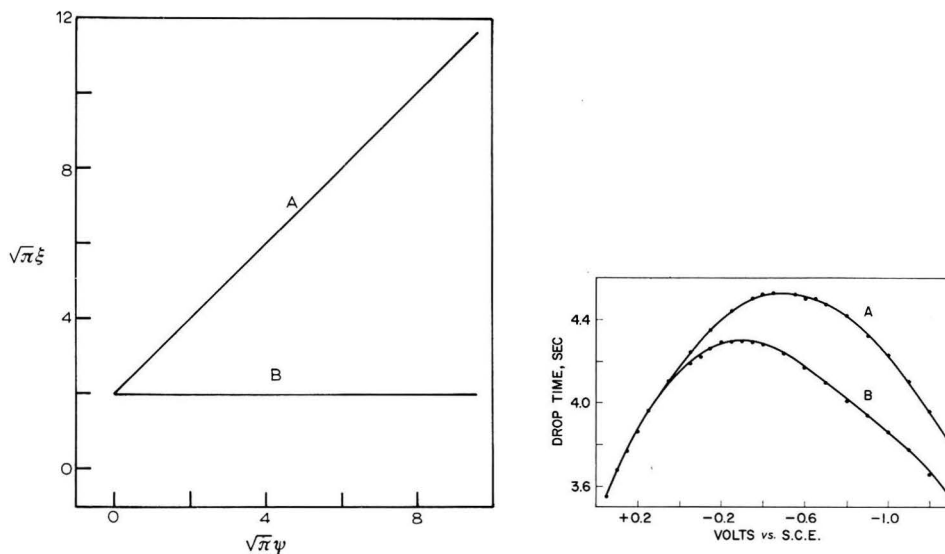


Fig. 1. Theoretical plots of diffusion behavior at spherical (A) and planar (B) electrodes.

Fig. 2. Drop-time vs. applied potential. (A), 0.1 *M* perchloric acid; (B), 0.1 *M* perchloric acid, $5.00 \cdot 10^{-4}$ *M* tetrabutylammonium ion.

EXPERIMENTAL

The potentiostatic method — in which a constant applied potential is maintained at a stationary electrode — was selected for experimental verification of eqn. (7), since this method has several important advantages for investigations involving adsorption behavior. For example, adsorption equilibrium is more likely to be attained than at a dropping-mercury electrode, since the electrode life is invariant with time². In addition, the constant applied potential minimizes the possibility that the kinetics of potential-dependent adsorption processes will change during the course of an experiment.

For experimental purposes, several metal ions in various electrolytes were investigated to determine the degree of inhibition of the electrode reaction by various surfactants. Of these, Cd(II) in 0.1 *M* perchloric acid solution was chosen for further investigation because the reduction step was found to be markedly inhibited by traces of suitable surfactants. Tetrabutylammonium ion was selected for detailed investigation as the adsorbable substance, since it inhibits the electro-reduction of Cd(II), and does not adsorb at potentials appreciably positive of the electrocapillary maximum^{7,8}.

Equipment

The cell used was an 85-ml capacity weighing bottle terminating in a T/S 50/12 joint. A Teflon (trademark, E.I. duPont de Nemours & Co. Inc.) lid was machined to fit snugly over the top of this cell, and the electrodes, nitrogen inlet, dropping-mercury capillary, and Teflon scoop projected through this lid into the cell. The cell design and method used to hang the mercury drops were essentially identical to those discussed by ALBERTS AND SHAIN⁹.

A Wenking potentiostat, Model 6I-R, was used to provide the constant potential. External read-out was accomplished by passing the faradaic current through a decade load resistor, and then recording the resulting voltage drop on either a Sargent Model SR pen-and-ink recorder, or a Leeds and Northrup Type G Speedomax recorder with a chart speed of 20.2 in./min and a 1-sec full-scale pen response time.

Chemicals

All chemicals were reagent-grade. The tetrabutylammonium ion stock solution was prepared by dilution of a standardized solution of tetrabutylammonium hydroxide in methanol (K and K Laboratories). As a satisfactory blank was obtained using the experimental procedure described below in the presence and absence of methanol, the chemicals were not further purified. The water used was twice distilled, the second distillation being made from an alkaline permanganate solution using a borosilicate-glass apparatus.

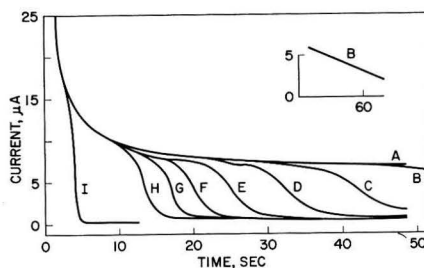
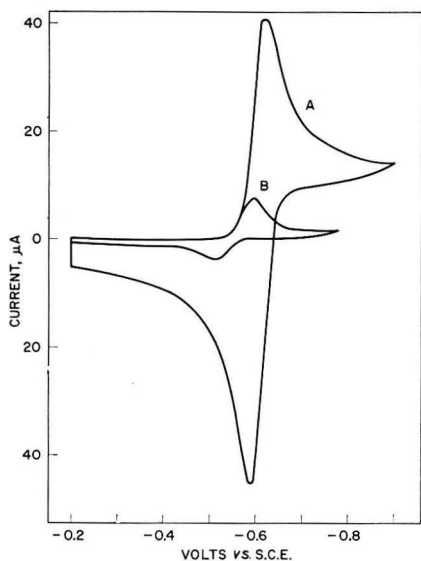


Fig. 3. Cyclic stationary electrode polarograms. (A), $1.64 \cdot 10^{-3} M$ Cd(II), $0.1 M$ perchloric acid; (B), after adding $5.00 \cdot 10^{-4} M$ tetrabutylammonium ion to the soln.

Fig. 4. Diffusion-limited current-time curves. Electrolysis-adsorption potential, $-0.70 V$ vs. S.C.E.; supporting electrolyte, $1.64 \cdot 10^{-3} M$ Cd(II), $0.1 M$ perchloric acid. Tetrabutylammonium ion concn., $\times 10^{-5} M$: (A), 0; (B), 0.80; (C), 1.00; (D), 1.20; (E), 1.40; (F), 1.60; (G), 1.80; (H), 2.00; (I), 4.00.

End-point detection

The time at which the faradaic current fell to zero was determined by linear extrapolation of the falling portion of the current–time curves to the zero current axis.

Procedure

The electro-reducible substance was a $1.64 \times 10^{-3} M$ -solution of Cd(II) in 0.1 *M* perchloric acid solution. A suitable aliquot of a solution of tetrabutylammonium ion in 0.1 *M* perchloric acid was added to the electrolysis cell, and the solution was stirred by nitrogen bubbling. A mercury drop (0.052-cm radius) was then attached to the working electrode while applying the initial potential. The initial and electrolysis-adsorption potentials, +0.25 and $-0.70 V$ vs. S.C.E., respectively, were determined from cyclic stationary electrode polarograms and drop-time *vs.* potential curves such as those shown in Figs. 2 and 3. It can be seen from these figures, that the selected values correspond to the initial and boundary conditions under which eqn. (7) was derived: tetrabutylammonium ion does not adsorb at the initial potential, but does adsorb appreciably at the final potential.

The electrolysis-adsorption potential was applied 30–60 sec after hanging the mercury drop to minimize stirring effects caused by movement of the solution during this step. Current–time curves were then recorded on application of the final potential until the faradaic current fell to a steady-state value significantly less than the initial value. Replicate results were obtained readily by hanging a fresh mercury drop and repeating the procedure. All experimental data were obtained at $25 \pm 0.1^\circ$.

RESULTS AND DISCUSSION

A series of current–time curves was obtained under diffusion-limited conditions, and typical curves are shown in Fig. 4. These show that the current falls towards zero more or less rapidly, depending on the tetrabutylammonium ion concentration. The time at which the current reaches zero, t_0 , was determined for each surfactant concentration by extrapolation of the falling portion of the curves to the zero current axis. With tetrabutylammonium ion concentrations less than $8.00 \times 10^{-6} M$, the faradaic current did not decrease significantly for electrolysis times as long as 90 sec. The experiment was not continued beyond this time because natural convection was found to interfere with the mass transfer step.

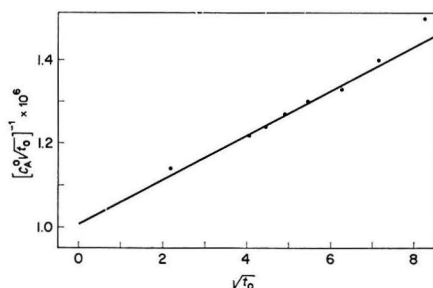


Fig. 5. Bulk surfactant concentration–time relation plotted according to eqn. (7). Data obtained from curves shown in Fig. 4.

A plot of $[C_A^0/t_0]^{-1}$ vs. $\sqrt{t_0}$ is shown in Fig. 5, and, as expected from eqn. (7), a straight line is obtained. The diffusion coefficient and maximum equilibrium surface concentration of tetrabutylammonium ion as determined from the slope and intercept of this line, are $1.0 \cdot 10^{-5}$ cm²/sec, and $3.3 \cdot 10^{-10}$ moles/cm², respectively, in 0.1 M perchloric acid. Since tetrabutylammonium ion is not electroactive in this supporting electrolyte, the calculated diffusion coefficient could not be correlated with that obtained by the usual methods⁶.

SUMMARY

Both the diffusion coefficient and maximum surface concentration of a surfactant may be calculated from potentiostatic current-time curves obtained using spherical electrodes. The theoretically-derived relation between the maximum surface concentration, diffusion coefficient, and time at which maximum surface coverage is attained was tested by adding tetrabutylammonium ion to a solution of Cd(II) in 0.1 M perchloric acid.

REFERENCES

- 1 J. KORYTA, *Collection Czech. Chem. Commun.*, 18 (1953) 206.
- 2 P. DELAHAY AND I. TRACHTENBERG, *J. Am. Chem. Soc.*, 79 (1957) 2355.
- 3 W. H. REINMUTH, *J. Phys. Chem.*, 65 (1961) 473.
- 4 R. W. SCHMID AND C. N. REILLEY, *J. Am. Chem. Soc.*, 80 (1958) 2087.
- 5 J. WEBER, J. KOUTECKY AND J. KORYTA, *Z. Elektrochem.*, 63 (1959) 583.
- 6 I. SHAIN AND K. J. MARTIN, *J. Phys. Chem.*, 65 (1961) 254.
- 7 J. KUTA AND I. SMOLER, *Collection Czech. Chem. Commun.*, 27 (1962) 2349.
- 8 S. L. PHILLIPS, *Anal. Chem.*, to be published.
- 9 G. S. ALBERTS AND I. SHAIN, *ibid.*, 35 (1963) 1859.

CHRONOAMPEROMETRISCHE UNTERSUCHUNG METALLISCHER MONOSCHICHTEN

E. SCHMIDT UND H. R. GYGAX

Institut für anorganische, analytische und physikalische Chemie, Universität Bern (Schweiz)

(Eingegangen am 23. November, 1965)

I. EINFÜHRUNG

Unter einer metallischen Monoschicht wird im folgenden ein Metallfilm an der Phasengrenze Elektrode–Elektrolyt verstanden, der nicht mit dem Elektrodenmaterial identisch ist und dessen elektrochemisches Verhalten den nachstehenden Kriterien entspricht:

1. Die Schicht ist elektrisch neutral in dem Sinne, dass bei ihrem Aufbau durch Adsorption von Kationen Me^{z+} aus der Lösung gleichzeitig die zur Entladung nach



notwendige Ladungsmenge ausgetauscht wird. Ein Einfluss auf die Struktur der Doppelschicht ist nicht auszuschliessen, doch bleiben die damit verbundenen Ladungs- und Kapazitätseffekte klein im Vergleich zu Stromumsatz und Scheinkapazität des Depolarisationsvorgangs (I).

2. Die auf die Reinphase Me bezogene Aktivität a_{Me} des Adsorbats ist eine stetige, monoton steigende Funktion der Flächenkonzentration y (Molmenge Adsorbat pro Einheit der Elektrodenfläche):

$$a_{Me} = \begin{cases} 0 & \text{für } y = 0 \\ 0 \leq f(y) \leq 1 & \text{für } 0 < y < s_y \\ 1 & \text{für } y \geq s_y \end{cases} \quad (Ia)$$

$$da_{Me}/dy = \begin{cases} \geq 0 & \text{für } 0 \leq y \leq s_y \\ 0 & \text{für } y > s_y \end{cases} \quad (Ib)$$

Der mehr oder weniger deutlich hervortretende Sättigungswert s_y , bei dessen Ueberschreitung a_{Me} gegen Eins geht, ist grössenordnungsmässig mit einer monoatomaren Bedeckung (ca. 10^{-9} Mol cm^{-2}) vergleichbar.

3. Ein Transport des Reduktionsproduktes Me ins Elektrodeninnere durch Diffusion unter Ausbildung von Legierungsphasen mit Konzentrationsgradienten senkrecht zur Elektrodenoberfläche findet nicht in messbarem Umfange statt. Diese Bedingung soll als erfüllt gelten, solange die Tiefenausdehnung einer etwaigen Legierungszone zwischen Niederschlag und Unterlage die Abmessungen einer einatomigen Schicht (zweidimensionale bzw. Oberflächenlegierung) nicht übersteigt.

Spezielle, die Schichtstruktur und Sorptionsthermodynamik betreffende Voraussetzungen werden nicht gemacht.

Die Definition erfasst alle gemäss (1) reduktiv entstandenen Metallnieder-schläge bzw. -adsorbate im Nanomolbereich, welche eine bedeckungsabhängige Aktivitätsisotherme besitzen und sich nicht als dreidimensionale Mischphasen endlichen Volumens identifizieren lassen.

Man hat das Auftreten ungesättigter metallischer Monofilme in erster Linie im Zusammenhang mit Potentialmessungen an hochverdünnten radioaktiven Depolarisatoren^{1,2} Me^{z+} diskutiert, in deren Gegenwart vorpolarisierte inerte Messelektroden häufig eine Unterspannung ΔE gegenüber Referenzelektroden der Aktivität $a_{Me}=1$ aufweisen, aus der auf die Existenz eines Oberflächenbelages definierter Aktivität $a_{Me} < 1$ geschlossen wird^{3,4}:

$$\Delta E = E_{\text{gemessen}} - E_{\text{referenz}} = - \frac{RT}{zF} \ln a_{Me} > 0$$

Dagegen ist über analoge Phänomene an arbeitenden Elektroden unter voltammetrischen bzw. chronopotentiometrischen Arbeitsbedingungen vergleichsweise wenig bekannt, trotzdem MILLS UND WILLIS⁵ anhand von Ladekurven schon vor geraumer Zeit zeigen konnten, dass bei der Reduktion verschiedener Metaldepolarisatoren an Gold- und Silberelektroden recht auffällige Unterspannungserscheinungen zu beobachten sind. Spätere quantitative Untersuchungen beschränken sich auf die Systeme Pb-Ag⁶, Tl-Ag⁷ und Tl-Pt⁸ sowie auf einen Versuch von NICHOLSON⁹, die Strom-

TABELLE 1

ZUSAMMENSTELLUNG DER UNTERSUCHTEN KOMBINATIONEN DEPOLARISATORMETALL-UNTERLAGE UND IHRER MISCHUNGSEIGENSCHAFTEN

Depolari-sator Grund-metall	Bi	Pb	Sn	Tl	Cd
Au	V	V	V	O	M/V
Ag	O	O	M	O	M
Cu	—	O	M	O	M/V
Bi	/	M	O	M/V	O
Pb	—	/	—	M	O
Sn	—	—	/	O	O

Die Metalle sind nach steigender Elektronegativität in nicht oder nur schwach komplexierender wässriger Lösung geordnet. (—): Die Unterlage ist für den betr. Depolarisator zu unedel; M: Bildung von Mischkristallen zwischen Depolarisator und Unterlage; V: Bildung von intermetallischen Verbindungen zwischen Depolarisator und Unterlage; O: Verschwindende gegenseitige Mischbarkeit bei Zimmertemperatur.

Die untersuchten Systeme sind doppelt umrandet.

Zeitfunktion der chronoamperometrischen Ablösung von Monoschichten mit linearer Adsorptionsisotherme zu berechnen.

Im Rahmen der vorliegenden Arbeit wird die Abscheidung mehrerer Metalle an Festelektroden chronoamperometrisch auf Monoschichteffekte hin geprüft und in einigen Fällen die zugehörige Aktivitätsisotherme (τ) ermittelt. Die untersuchten Kombinationen Niederschlag-Unterlage wurden nach folgenden Gesichtspunkten ausgewählt (vgl. Tab. 1):

a. Als Depolarisatoren kamen "normale" Metallsysteme gemäss der Klassifikation von PIONTELLI¹⁰ in Betracht, für die am ehesten eine bei Stromdichten um $10 \mu\text{A cm}^{-2}$ polarographisch reversible Bruttoreaktion (τ) zu erwarten ist.

b. Im Abscheidungsgebiet des Depolarisatorions sollte weder die Wasserstoffreduktion noch die anodische Auflösung des Elektrodenmetalls interferieren.

c. Um Komplikationen durch Legierungsbildung auszuschliessen, sollten bei der Versuchstemperatur (25°) keine intermetallischen Verbindungen oder Mischkristalle zwischen Niederschlag und Unterlage beständig sein.

Als Leitelektrolyt diente vor allem eine wässrige Lösung von KCl 0.5 M.

2. MESSMETHODE

Die Durchführung der Versuche erfolgte nach einem chronoamperometrischen* Verfahren unter Verwendung einer Messzelle vom Kammertyp^{6,27}, wobei das polarisierende Spannungssignal von der Form

$$E = {}_aE - \beta t \quad \text{mit } 1.67 \leq |\beta| \leq 3.34 \text{ mV sec}^{-1}, \quad (2)$$

war und von einem potentiostatisierten Schreiberpolarographen (Radiometer PO4 mit Hilfspotentiostaten⁶) geliefert wurde. Der registrierte Stromtransient liess sich auf Grund der vorgegebenen Potential-Zeit-Beziehung (2) je nach Abscisseneichung des Stromschreibers sowohl als Strom-Zeit- wie auch als Strom-Spannungskurve interpretieren.

Die Funktionsweise der (in Fig. 1 schematisch dargestellten) Messanordnung ist dadurch gekennzeichnet, dass für die Elektrodenreaktion (τ) nur eine beschränkte Depolarisatormenge in der Grössenordnung weniger Nanomole zur Verfügung steht, welche in der sogenannten Elektrodenkammer eingeschlossen und gegenüber der restlichen Versuchslösung diffusionsmässig isoliert ist**. Die Kammer hat die Gestalt eines flachen Hohlzylinders variabler Höhe δ mit planparallelen Basisflächen ($0 < \delta < 0.2$ mm, Reproduzierbarkeit der Messung ± 0.001 mm) und wird von der ebenen Messelektrode sowie einem entsprechend geformten Isoliermantel aus Polyvinylchlorid begrenzt. Details der Konstruktion und Handhabung der Messzelle sind an anderer Stelle ausführlich beschrieben worden^{6***}.

Die verwendeten Messelektroden bestanden aus polykristallinen Rundblöcken (Durchmesser 1.0 cm) der in Tab. 1 als Elektrodenmaterialien aufgeführten Metalle, die mit Zuleitungsdrähten versehen und mit Araldit-Giessharz in PVC-Gewinde-

* Zur Nomenklatur elektroanalytischer Methoden vgl. den Literatur¹¹.

** Der Depolarisatortransport durch den in Fig. 1 erkennbaren Leitkanal, der die Elektrolytverbindung zur Gegenelektrode herstellt, bleibt vernachlässigbar klein.

*** Nach einem ähnlichen Dünnschichtverfahren haben ANSON und Mitarbeiter sowie REILLEY und Mitarbeiter chronopotentiometrische Untersuchungen durchgeführt²¹⁻²⁵.

hülsen eingebettet wurden (Fig. 2). Vor dem Einschrauben in die Messkammer wurde die dem Elektrolyten exponierte Vorderseite des Metallblocks auf einer Präzisionsdrehbank unter Stickstoffspülung plangedreht und anschliessend mehrere Minuten lang beim Startpotential des Spannungsdurchlaufs aE (vgl. (2)) vorpolarisiert, um den Auf- bzw. Abbau allfälliger reversibler Sauerstoffadsorbate



zu veranlassen. Von Gold¹⁵ und Silber¹⁶ ist bekannt, dass ihre Oberflächen in neutraler und saurer Lösung innerhalb des untersuchten Potentialintervalls (+0.2 bis -1.0 V/SCE) keine Sauerstoffsorptionsschichten tragen; in allen übrigen Fällen lag der pH-Wert der Messlösung zumindest ausserhalb des Stabilitätsgebietes kompakter Metalloxyde.

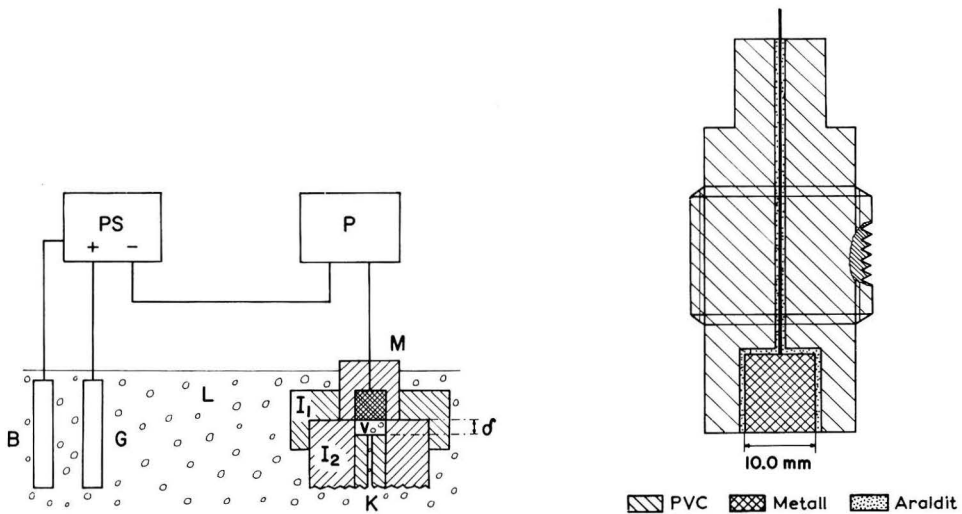


Fig. 1. Schema der Messanordnung. P, Polarograph; PS, Potentiostat; L₁, Oberteil des Isoliermantels; L₂, Unterteil des Isoliermantels; M, Kammerelektrode; G, Gegenelektrode (Ag); B, Bezugelektrode (SCE); K, Leitkanal; V, Elektrodenkammer; L, Depolarisatorlösung.

Fig. 2. Messelektrode.

Die besagte Elektrodenbehandlung führte bei aller Einfachheit zu Stromtransienten befriedigender Reproduzierbarkeit, unabhängig davon, ob die Messungen an frischen Oberflächen oder unter mehrmaliger Benutzung derselben Elektrode ohne mechanische Zwischenbearbeitung vorgenommen wurden. Auf Versuche zur Ermittlung von Rauigkeitsfaktoren wurde verzichtet. Die (makroskopische) Oberfläche der Drehrille schwankte von Metall zu Metall infolge unterschiedlicher Einstell- und Spitzenwinkel des Drehstahls und betrug etwa 110–120% des geometrischen Elektrodenquerschnitts. Bei Probemessungen an chemisch nachpolierten¹⁷ Silberelektroden in KCl-Leitsalzlösung ergab sich eine Verringerung der am Testsystem Pb²⁺-Pb gemessenen Sättigungsbedeckung s_y (vgl. (1)) und damit auch der wirksamen Elektrodenfläche um ca. 25%, ohne dass die Form der Strom-Spannungskurve qualitativ eine Änderung erfuhr¹⁸.

3. DISKUSSION DES MIT MESSELEKTRODEN VOM KAMMERTYP AUFGENOMMENEN STROMTRANSIENTEN METALLISCHER DEPOLARISATOREN

Unter Ausschluss geschwindigkeitsbestimmender chemischer Reaktionsschritte gilt auf Grund der Geometrie des Kammerraums für das Konzentrationsprofil des Depolarisatorions c_{Me} der lineare Diffusionsansatz

$$\frac{\partial c_{Me}}{\partial t} = D \frac{\partial^2 c_{Me}}{\partial x^2} \quad (3)$$

$$\begin{aligned} c_{Me} &= m && \text{für } t = 0 \text{ und } 0 \leq x \leq \delta \\ \partial c_{Me} / \partial x &= 0 && \text{für } x \rightarrow \delta \text{ (impermeable Zylinderbasis)} \\ \partial c_{Me} / \partial x &= i/zFAD && \text{für } x \rightarrow 0 \text{ (Elektrodenoberfläche)} \end{aligned}$$

dessen Auflösung¹² nach c_{Me} den Ausdruck

$$c_{Me} = m - (zFA\delta)^{-1} i(t) * \vartheta_{3(0,tD\delta^{-2})} \equiv {}_0c_{Me} \quad (4)$$

für $x \rightarrow 0$ mit

$$\vartheta_{3(v,x)} = 1 + 2 \sum_{k=1}^{\infty} \exp[-\pi^2 k^2 x] \cos 2\pi kv$$

ergibt^{13,14}. Die Grösse m bezeichnet die konstante Anfangskonzentration von Me^{z+} , D seinen effektiven Diffusionskoeffizienten und A den mit der geometrischen Elektrodenfläche identischen Kammerquerschnitt; reduzierende Ströme erhalten das positive Vorzeichen. Unter dem Symbol $F_{1(t)} * F_{2(t)}$ wird das Faltungsintegral

$$F_{1(t)} * F_{2(t)} \equiv \int_0^t F_{1(t-u)} F_{2(u)} du$$

verstanden.

Gl. (4) erlaubt einerseits die Berechnung von ${}_0c_{Me}$ aus der experimentell ermittelten Strom-Zeitkurve $i(t)$, wobei die numerische Auswertung des Faltungsausdrucks durch die rasche Konvergenz der Thetafunktion

$$\vartheta_{3(0,tD\delta^{-2})} \rightarrow 1 \quad \text{für } t \gg \delta^2/D$$

sehr erleichtert wird. Zum anderen liefert eine Faltung mit der Reihe

$$\alpha \vartheta_{2(0,\alpha t)} = 2\alpha \sum_{k=0}^{\infty} \exp[-\pi^2 \alpha t (k + 0.5)^2]$$

mit $\alpha = D\delta^{-2}$ unter Berücksichtigung der Thetarelation

$$\vartheta_{3(0,t)} * \vartheta_{2(0,t)} = 1$$

(vgl. ref. 12 S. 307) eine Beziehung zwischen ${}_0c_{Me}$ und dem Stromintegral q von der Form

$$zFA(m - {}_0c_{Me}) * D\delta^{-1} \vartheta_{2(0,Dt\delta^{-2})} = i(t) * 1 = \int_0^t i(t) dt \equiv q(t) \quad (5)$$

die sich wegen

$$\lim_{\alpha t \rightarrow \infty} \alpha \vartheta_{2(0,\alpha t)} * 1 = 1 \quad \text{für } \alpha > 0$$

bei hinreichend grossem t zu

$$q(t) \approx mzFA\delta - zFA\alpha c_{Me} * D\delta^{-1}\vartheta_{2(0,Dt\delta^{-2})} \quad \text{für } t \gg \delta^2/D \quad (6)$$

vereinfacht. αc_{Me} hat bei reversibler Elektrodenreaktion (I) im kathodischen Spannungsdurchlauf ($\beta > 0$, vgl. (2)) die Konvergenzeigenschaft

$$\alpha c_{Me} = a_{Me} \exp \frac{zF}{RT}(E - {}_0E) \leq \exp \frac{zF}{RT}(E - {}_0E) \sim \exp[-\beta t] \quad (7)$$

mit $\beta > 0$, so dass der verbleibende Faltungsterm in (6) infolge

$$\lim_{t \rightarrow \infty} \alpha \vartheta_{2(0,\alpha t)} * e^{-\beta t} = 0$$

gegen Null geht und das (reststromkorrigierte) Stromintegral über den gesamten kathodischen Stromtransienten dem Grenzwert $zFAM\delta$ zustrebt:

$$mzFA\delta \equiv q_{cath} \approx q(t) \quad \text{für } t \geq \delta^2/D \text{ und } \beta > 0. \quad (8)$$

Gl. (8) ermöglicht bei Kenntnis der experimentell leicht bestimmbar Grössen m , A und δ eine coulometrische Kontrolle der Ladungsstöchiometrie z der Reaktion (I); der Fehler in q_{cath} bleibt dabei vernachlässigbar klein, d.h. unter 1%, wenn die obere Integrationsgrenze $t \geq \delta^2/D$ so gewählt wird, dass das durch das vorgegebene Elektrodenpotential $E(t)$ (vgl. (2)) bestimmte αc_{Me} in einem Intervall $\langle t - \tau | t \rangle$ mit

$$\tau = 2\delta^2/D$$

(annähernd) verschwindet. Eine Abschätzung unter Verwendung von (5) zeigt nämlich, dass

$$\begin{aligned} & {}_1M_0\alpha \int_0^\tau \vartheta_{2(0,\alpha u)} du + {}_2M_0\alpha \int_\tau^t \vartheta_{2(0,\alpha u)} du \geq (m - \alpha c_{Me}(t)) * \alpha \vartheta_{2(0,\alpha t)} = \\ & = q(t)/zFA\delta \geq {}_1M_u\alpha \int_0^\tau \vartheta_{2(0,\alpha u)} du + {}_2M_u\alpha \int_\tau^t \vartheta_{2(0,\alpha u)} du \end{aligned} \quad (9)$$

wobei ${}_1M_u$, ${}_1M_0$ und ${}_2M_u$, ${}_2M_0$ die Schranken* der Summe ($m - \alpha c_{Me}$) in den Teilintervallen $\langle t - \tau | t \rangle$ bzw. $\langle 0 | t - \tau \rangle$ bezeichnen. Da im kathodischen Spannungsdurchlauf nur αc_{Me} -Werte zwischen 0 und m physikalisch sinnvoll sind (auf die Herleitung werde verzichtet), nehmen wegen $\alpha c_{Me} \rightarrow 0$ in $\langle t - \tau | t \rangle$ die Schranken ${}_jM_t$ die Werte ${}_1M_u = {}_1M_0 = {}_2M_0 = m$ und ${}_2M_u = 0$ an, worauf aus (9) folgt

$$m\alpha \int_0^\tau \vartheta_{2(0,\alpha u)} du \leq q(t)/zFA\delta \leq m\alpha \int_0^t \vartheta_{2(0,\alpha u)} du \leq m\alpha \int_0^\infty \vartheta_{2(0,\alpha u)} du = m$$

oder

$$0.99 m \leq q(t)/zFA\delta \leq m \quad \text{wenn } \tau = 2\delta^2/D.$$

Typische Werte von τ liegen bei ca. 20 sec ($D \approx 10^{-5} \text{ cm}^2 \text{ sec}^{-1}$, $\delta \approx 10^{-2} \text{ cm}$) und sind somit klein gegen den Zeitbedarf t eines vollständigen Polarogrammdurchlaufs ($t \approx 5$ bis 20 min).

Durch (1), (2) und (4) sowie die Bedeckungsbilanz

$$y = y_0 + (zFA)^{-1} \int_0^t i(t) dt \quad \text{mit } y_0 \equiv y(t=0), \quad (10)$$

* αc_{Me} ist beschränkt wegen (7) und stetig, wenn a_{Me} als stetige Funktion von y vorausgesetzt wird.

und eine Bestimmungsgleichung für das Elektrodenpotential

$$E = {}_0E + \frac{RT}{zF} \ln {}_0c_{\text{Me}}/a_{\text{Me}} \quad \text{bei reversibler Reaktion (I),} \quad (11)$$

ist die an der Kammerelektrode gemessene Stromstärke als Funktion von E bzw. t eindeutig festgelegt. Das genannte Gleichungssystem kann in der Regel nicht durch einen geschlossenen Ausdruck nach $i_{(t)}$ aufgelöst werden, doch lassen sich qualitative Aussagen hinsichtlich der Form der Strom-Zeitkurve in Abhängigkeit von einer gegebenen Aktivitätsisotherme (1) herleiten, wenn man die Faltung $i_{(t)} * \vartheta_{3(0,\alpha t)}$ in (4) nach

$$\begin{aligned} i_{(t)} * \vartheta_{3(0,\alpha t)} &= i_{(t)} * \text{I} + 2 i_{(t)} * \sum_{k=1}^{\infty} \exp[-\pi^2 k^2 \alpha t] \\ &\approx i_{(t)} * \text{I} = yzFA \quad \text{wenn } y_0 = 0, \end{aligned} \quad (12)$$

durch das Stromintegral $i_{(t)} * \text{I}$ ersetzt und dabei den Summenterm in (12), der von der Grössenordnung

$$\begin{aligned} 2 |i_{(t)} * \sum_{k=1}^{\infty} \exp[-\pi^2 k^2 \alpha t]| &\leq 2 |i_{(t)}|_{\text{max}} \sum_{k=1}^{\infty} \text{I} * \exp[-\pi^2 k^2 \alpha t] \\ &= \frac{2}{\pi^2 \alpha} |i_{(t)}|_{\text{max}} \sum_{k=1}^{\infty} (\text{I} - \exp[-\pi^2 k^2 \alpha t]) k^{-2} \leq |i_{(t)}|_{\text{max}} / 3\alpha \end{aligned} \quad (13)$$

ist, vernachlässigt*. Der beim Zusammenfassen von (12) mit (1), (2), (4), (10) und (11) erhaltene Ausdruck

$$E = {}_aE - \beta t = {}_0E + \frac{RT}{zF} \ln (m - y\delta^{-1}) - \frac{RT}{zF} \ln a_{\text{Me}} \quad (14)$$

liefert, nach t differenziert, eine Beziehung

$$\frac{zFA dy}{dt} = i_{(y)} = \frac{z^2 F^2 A \beta}{RT} [(m\delta - y)^{-1} + d \ln a_{\text{Me}}/dy]^{-1} \quad (15)$$

für den Strom i , welche den Verlauf des experimentellen Stromtransienten als Funktion der Bedeckung y approximativ wiedergibt.

Nach (15) hat $i_{(y)}$ in erster Näherung folgende Eigenschaften:

a. Der Quotient i/β ist von der Richtung des Spannungsvorschubes unabhängig und besitzt im physikalisch sinnvollen Bedeckungsintervall $0 \leq y \leq m\delta$ Nullstellen bei $y = m\delta$ und $y = 0$ (Die Nullstelle bei $y = 0$ folgt aus $d \ln a_{\text{Me}}/dy \rightarrow \infty$ für $y = 0$, vgl. (1)).

b. Die den Extremstellen des Stroms (Strompeaks und -sattel) zugehörigen Bedeckungswerte y_{max} und y_{min} sind durch die Bedingungen

$$di/\beta dt \sim (m\delta - y)^{-2} + d^2 \ln a_{\text{Me}}/dy^2 = 0 \quad \text{für } 0 < y < m\delta, \quad (16a)$$

* Die Berechtigung für die Ungleichung (13) ergibt sich daraus, dass $i_{(t)}$ innerhalb eines gleichsinnigen (kathodischen oder anodischen) Spannungsdurchlaufs sein Vorzeichen nicht ändert: $i_{(t)}\beta \geq 0$. $|i_{(t)}|_{\text{max}}$ ist der maximale Absolutwert von $i_{(t)}$ in $\langle 0|t \rangle$. Die Vernachlässigung des Summenterms erscheint unbedenklich, solange $|i_{(t)}|_{\text{max}} (3\alpha\delta zFA)^{-1} \ll m$ (vgl. (14)).

und

$$d^2 i/\beta dt^2 \sim -2(m\delta - y)^{-3} + d^3 \ln a_{Me}/dy^3 \quad \left| \begin{array}{l} > 0: \text{Minimum von } i/\beta \\ < 0: \text{Maximum von } i/\beta \end{array} \right. \quad (16b)$$

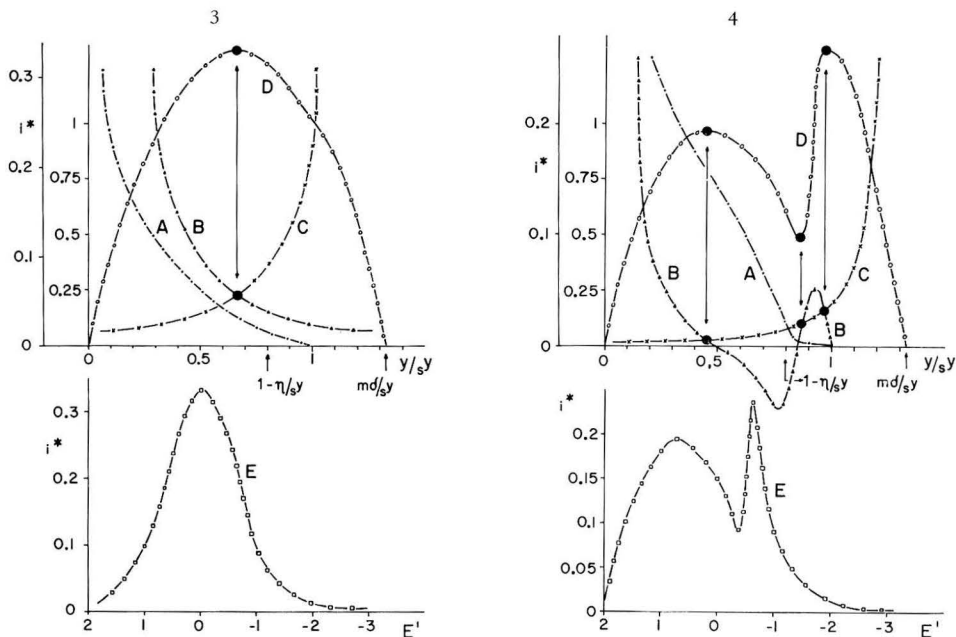


Fig. 3. Theoretische $i_{(y/sy)}$ bzw. $i_{(E)}$ -Kurven von Monoschichten des Einzelpeaktyps gemäss Gl. (14-19). $sy = 3.0 \cdot 10^{-9}$ mole cm^{-2} ; $m\delta = 4.0 \cdot 10^{-9}$ mole cm^{-2} .

A, $-\lg a = -\lg C y/sy$, $C = 1.1$ (vgl. (19)).

B, $-d^2 \lg a/d(y/sy)^2 = 1/(y/sy)^2$; (vgl. (16a) und (17)).

C, $-h_{(y/sy)} = \left(\frac{m\delta}{sy} - \frac{y}{sy}\right)^{-2}$ (vgl. (16a) und (17)).

D, $i^* = \frac{RT}{sy^2 F^2 A\beta} i = \left(\frac{1}{m\delta/sy - y/sy} + \frac{1}{y/sy}\right)^{-1}$ (vgl. (15)).

E, $i^* = f(E')$ mit $E' = \frac{zF}{RT}(E - E_0 - \frac{RT}{zF} \lg(sy/\delta)) = \lg\left(\frac{m\delta/sy - y/sy}{a}\right)$ (vgl. (14)).

Die Kalibrierung der Ordinate rechts gilt für die Kurve A im Masstab 1:1, für die Kurven B und C im Masstab 1:10.

Fig. 4. Theoretische $i_{(y/sy)}$ bzw. $i_{(E)}$ -Kurven von Monoschichten des Vorstufentyps gemäss Gl. (14-18). $sy, m\delta, C$ und E wie in Fig. 3.

A, $-\lg a = -\lg B \frac{y/sy}{1-y/sy}$, $B = 0.20$ (vgl. (18)).

B, $-\frac{d^2 \lg a}{d(y/sy)^2} = \frac{1}{(1-y/sy)^2} - \frac{1}{(y/sy)^2}$; (vgl. (16a) und (17)).

D, $i^* = \frac{RT}{sy^2 F^2 A\beta} i = \left(\frac{1}{m\delta/sy - y/sy} + \frac{1}{y/sy(1-y/sy)}\right)^{-1}$ (vgl. (15)).

Die Kalibrierung der Ordinate rechts gilt für die Kurve A im Masstab 1:1, für die Kurven B und C im Masstab 1:50.

definiert und entsprechen den Schnittpunkten der Hyperbel

$$h_{(y)} = -(m\delta - y)^{-2} \quad (17)$$

mit der zweiten Ableitung $d^2 \ln a_{Me}/dy^2$. Die Zeit- bzw. Potentialkoordinaten der Extremstellen ergeben sich durch Einsetzen von y_{min} bzw. y_{max} in Gl. (14).

Zur Illustration werden in Fig. 3 und 4 die nach Gl. (14–16) unter der Annahme $m\delta > s_y$ berechneten $i_{(y/s_y)}$ bzw. $i_{(E)}$ -Kurven von Monoschichten mit den Isothermen

$$a_{Me(y)} = \begin{cases} By(s_y - y)^{-1} & \text{für } 0 \leq y < s_y - \eta \quad 0 < \eta \leq s_y, \quad B < \eta/(s_y - \eta) \\ g_{1(y)} & \text{für } s_y - \eta \leq y < s_y \quad (\text{Langmuir-Adsorbat}) \\ \mathbf{I} & \text{für } y \geq s_y \end{cases} \quad (18)$$

und

$$a_{Me(y)} = \begin{cases} Cy & \text{für } 0 \leq y < s_y - \eta \quad 0 < \eta \leq s_y, \quad C < (s_y - \eta)^{-1} \\ g_{2(y)} & \text{für } s_y - \eta \leq y < s_y \\ \mathbf{I} & \text{für } y \geq s_y \end{cases} \quad (19)$$

dargestellt. Die den Uebergang von der Monoschicht- zur Sättigungsbedeckung vermittelnden Funktionen $g_{1(y)}$ und $g_{2(y)}$ sollen die in (15) und (16) vorausgesetzte ($n > 2$) fache stetige Differenzierbarkeit von $\ln a_{Me}$ im gesamten Bedeckungsbereich, also auch in der Umgebung von s_y , gewährleisten

In Übereinstimmung mit den Schnitteigenschaften von $d^2 \ln a_{Me}/dy^2$ und $h_{(y)}$ (vgl. (17)) durchläuft i/β im Langmuir-Fall (18) zwei deutlich getrennte Maxima, von denen das im anodischeren Teil der Potentialachse gelegene der Bildung bzw. Auflösung des Monoschichtadsorbats zugeordnet wird ("Vorstufe"), während im Bereich des potentialmässig negativeren "Hauptpeaks" hauptsächlich der Umsatz der gesättigten Bedeckung ($y \geq s_y$, $\ln a_{Me} = 0$) stattfindet. Das Stromminimum liegt beim Wendepunkt von $g_{2(y)}$ in $\langle s_y - \eta | s_y \rangle$.

Der zum linearen Ansatz (19) gehörende i/β -Transient weist demgegenüber nur ein einziges Maximum mit der y -Koordinate

$$y_{max} \left| \begin{array}{l} = \frac{1}{2} m\delta \quad \text{für } m\delta \leq 2(s_y - \eta) \quad \text{mit } \eta \leq s_y \text{ auf,} \\ \approx s_y \quad \text{für } m\delta > 2(s_y - \eta) \end{array} \right. \quad (20)$$

da (16a) in diesem Fall, sofern innerhalb des Isothermenteilstückes $g_{2(y)}$ kein Wendepunkt auftritt, nur die Lösung (20) besitzt und somit nicht mehr als eine Extremstelle in $0 < y < m\delta$ zulässt. Derartige Strom-Zeitkurven mit einem Einzelpeak sind im übrigen charakteristisch für alle Aktivitätsfunktionen mit monoton zunehmender zweiter Ableitung $d^2 \ln a_{Me}/dy^2$.

4. ERGEBNISSE

Bei der chronoamperometrischen Prüfung der in Tab. 1 genannten Systeme wurden in Analogie zu den Ansätzen (18) und (19) entweder Strom-Spannungskurven vom Vorstufentyp mit Vor- und Hauptpeak oder Transienten mit Einzelmaximum gefunden. Repräsentative Beispiele von anodisch-kathodischen Abscheidendurchläufen sowie unmittelbar anschliessend an der gleichen Messelektrode aufgenommenen anodic stripping-Kurven sind in den Fig. 5–7 zusammengestellt, die Potentialdaten der Strompeaks aller untersuchten Depolarisatoren (Leitelektrolyt: KCl oder NH_4ClO_4 0.5 M) finden sich in Tab. 2. Die angegebenen Spannungswerte bezeichnen Unter-

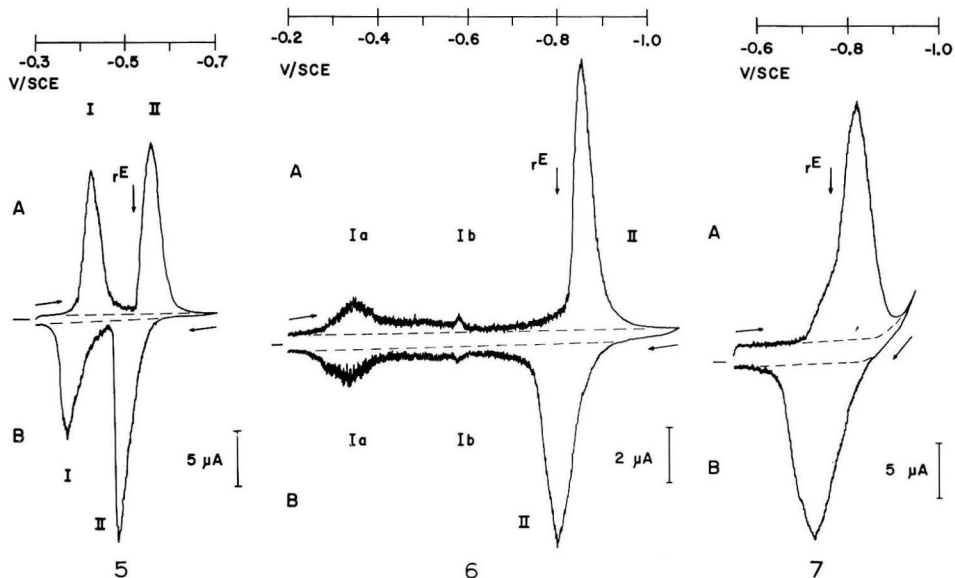


Fig. 5. Strom-Spannungskurve der Depolarisatorabscheidung bzw. Auflösung im System Pb-Cu (Vorstufentyp, Nr. 3 Tab. 2).

A, Potentialvorschub in kathodischer Richtung (Abscheidekurve). B, Potentialvorschub in anodischer Richtung (anodic stripping-Kurve). I, Pb-Vorstufe, II: Pb-Hauptstufe. (---), Grundstrom. rE , Ruhepotential einer reinen Pb-Elektrode. Depolarisator, $3,75 \cdot 10^{-4} M Pb(NO_3)_2$. Leitsalz, $0,5 M KCl$, pH = 5. Elektrodenmetall, Cu. Elektrodenfläche, $A = 0,785 cm^2$. Kammerhöhe, $\delta = 1,0 \cdot 10^{-2} cm$. Durchlaufgeschw., $\beta = 0,1 V min^{-1}$. Widerstand im Leitkanal, $R_K = 1000 \Omega$.

Bei den angegebenen Potentialen wurde die Ohm'sche Spannungskorrektur nicht berücksichtigt.

Fig. 6. Strom-Spannungskurve der Depolarisatorabscheidung bzw. Auflösung im System Tl-Au (Vorstufentyp, Nr. 5 Tab. 2).

Ia, Ib, Tl-Vorstufen an Au; II, Tl-Hauptstufe. rE , Ruhepotential einer reinen Tl-Elektrode. Depolarisator, $4,38 \cdot 10^{-4} M TlCl$. Elektrodenmetall, Au. Weitere Angaben wie in Fig. 5.

Fig. 7. Strom-Spannungskurve der Depolarisatorabscheidung bzw. Auflösung im System Tl-Sn (Einzelpunkttyp, Nr. 8 Tab. 2).

rE , Ruhepotential einer reinen Tl-Elektrode. Depolarisator, $4,38 \cdot 10^{-4} M Tl_2SO_4$. Leitsalz, $0,5 M NH_4ClO_4-HClO_4$, pH = 2. Elektrodenmetall, Sn. Kammerhöhe, $\delta = 1,50 \cdot 10^{-2} cm$. Widerstand im Leitkanal, $R_K = 1050 \Omega$. Weitere Angaben wie in Fig. 5.

spannungen gegenüber dem Ruhepotential

$$rE = {}_0E + \frac{RT}{zF} \ln m \tag{21}$$

einer gesättigt bedeckten Elektrode ($a_{Me} = 1$) im betreffenden Elektrolyten.

Die Kurvenform ist, vom Stromvorzeichen abgesehen, besonders innerhalb der Vorstufenregion im anodischen und kathodischen Durchlauf weitgehend die gleiche (vgl. S. 302). Bei den Kurven vom Vorstufentyp besteht ein Zusammenhang zwischen der Peakform bzw. -höhe und den Dimensionen der Elektrodenkammer dergestalt, dass sich das Stromintegral der Hauptpeaks mit abnehmender Depolarisatordichte $m\delta$ kontinuierlich verringert und nach Unterschreiten eines kritischen Schwellenwertes völlig verschwindet (Fig. 8). Ein solches Verhalten entspricht der

TABELLE 2
PEAKSTRUKTUR DER CHRONOAMPEROGRAMME SÄMMLICHER DEFOLARISATORSYSTEME

Nr.	Depolarisator	Unterlage	Leitelektrolyt (0,5 M)	pH	Kurrenttyp	Durchlauf	Peakpotentiale gegen rE (mV)		Bemerkungen	
							Vorstufen			Hauptstufe oder Einzelpeak
							Ia	Ib		
1	Bi^{3+}	Ag	$HClO_4$	0,5	Vorstufe	cath.	80 ± 5	—	—	
						anod.	105 ± 5	—	—	
2	Pb^{2+}	Ag	KCl	4,5	Vorstufe	cath.	100 ± 5	—	—	
						anod.	115 ± 5	—	—	
3	Pb^{2+}	Cu	KCl	4,5	Vorstufe	cath.	102 ± 5	—	vgl. Fig. 5	
						anod.	130 ± 5	—	—	
4	Sn^{2+}	Bi	NH_4ClO_4 — $HClO_4$	1	Einzelpeak	cath.	—	—	—	
						anod.	15 ± 5	—	—	
5	Tl^+	Au	KCl	5	Vorstufe	cath.	450 ± 10	220 ± 5	vgl. Fig. 6	
						anod.	460 ± 10	220 ± 10	—	
6	Tl^+	Ag	KCl	5	Vorstufe	cath.	165 ± 5	0 ± 5	vgl. Fig. 10	
						anod.	185 ± 10	10 ± 5	—	
7	Tl^+	Cu	KCl	5	Vorstufe	cath.	185 ± 5	15 ± 5	vgl. Fig. 8	
						anod.	200 ± 10	30 ± 15	—	
8	Tl^+	Sn	NH_4ClO_4 — $HClO_4$	2	Einzelpeak	cath.	—	—	vgl. Fig. 7	
						anod.	10 ± 5	—	—	
9	Cd^{2+}	Bi	NH_4ClO_4 — $HClO_4$	2,5	Einzelpeak	cath.	—	—	—	
						anod.	10 ± 5	—	—	
10	Cd^{2+}	Pb	NH_4ClO_4 — $HClO_4$	3	Einzelpeak	cath.	—	—	—	
						anod.	—40 ± 5	—	—	
11	Cd^{2+}	Sn	NH_4ClO_4 — $HClO_4$	2	Einzelpeak	cath.	—	—	vgl. Fig. 9	
						anod.	—40 ± 5	—	—	
							10 ± 5	—	—	

nach Gl. (16a) zu erwartenden Aenderung von Zahl und Abscissenlage der Schnittpunkte von $d^2 \ln a_{Me}/dy^2$ mit $h(y)$ beim Verschieben der Hyperbelasymptote $y = m\delta$ längs der Bedeckungsachse.

Wie aus Tab. 3 hervorgeht, beträgt die im Potentialgebiet $E \lesssim rE$, also ausserhalb des Stabilitätsbereichs von Depolarisatorniederschlägen der Aktivität $a_{Me} = 1$ kathodisch umgesetzte Depolarisatormenge bei allen Systemen etwa $2-3 \cdot 10^{-6}$ mmol

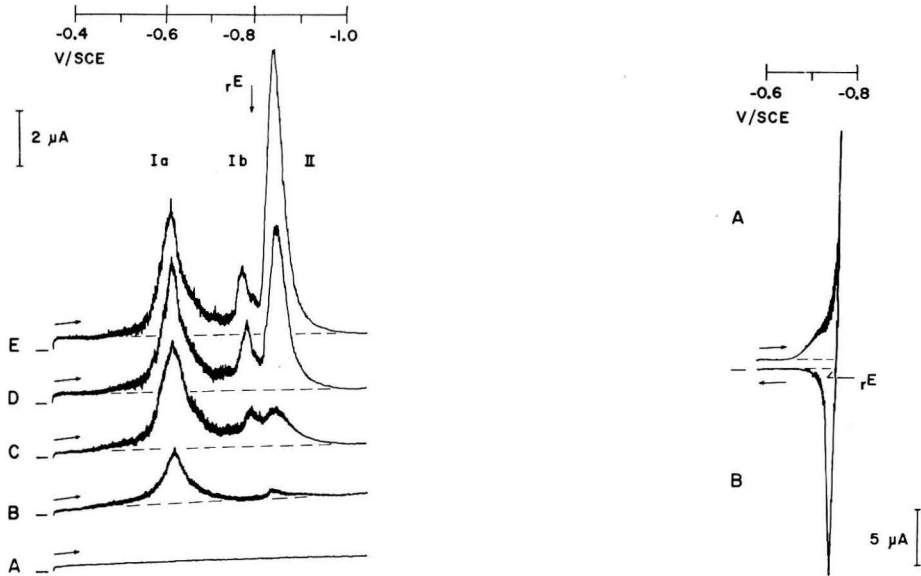


Fig. 8. Strom-Spannungskurven der Abscheidung von Tl an Cu in Abhängigkeit von der Kammerhöhe δ (Potentialvorschub in kathod. Richtung, Vorstufentyp, Nr. 7 Tab. 2). Ia, Ib, Tl-Vorstufen an Cu. II, Tl-Hauptstufe. rE , Ruhepotential einer reinen Tl-Elektrode. A, Grundstrom; B, 0 cm; C, $3.0 \cdot 10^{-3}$ cm; D, $6.0 \cdot 10^{-3}$ cm; E, $9.0 \cdot 10^{-3}$ cm. Bei Kurve B entspricht das Kammervolumen dem Restvolumen V_0 (vgl. Lit. 6). Depolarisator, $6.61 \cdot 10^{-4} M$ TlCl. Leitsalz, 0.5 M KCl, pH = 5. Elektrodenmetall, Cu. Elektrodenfläche, $A = 0.785 \text{ cm}^2$. Durchlaufgeschw., $\beta = 0.1 \text{ V min}^{-1}$. Widerstand im Leitkanal, $R_K = 1000-1200 \Omega$. Bei den angegebenen Potentialen wurde die Ohm'sche Spannungskorrektur nicht berücksichtigt.

Fig. 9. Strom-Spannungskurve der Depolarisatorabscheidung bzw. Auflösung im System Cd-Sn bei offener Kammer (Einzelpeaktyp, Nr. 11 Tab. 2). A, Potentialvorschub in kathodischer Richtung (Abscheidungskurve). B, Potentialvorschub in anodischer Richtung (anodic stripping-Kurve). (—), Grundstrom. rE , Ruhepotential einer reinen Cd-Elektrode. Depolarisator, $2.3 \cdot 10^{-4} M$ CdSO₄. Leitsalz, 0.5 M NH₄ClO₄-HClO₄, pH = 2. Elektrodenmetall, Sn. Elektrodenfläche, $A = 0.785 \text{ cm}^2$. Kammerhöhe, $\delta = \infty$. Durchlaufgeschw., $\beta = 0.1 \text{ V min}^{-1}$. Widerstand, $\sim 30 \Omega$.

cm^{-2} und liegt demnach in der Grössenordnung der vom eingangs definierten Monoschichtmodell geforderten einatomigen Sättigungsbelegung s_y , wenn man Rauheitsfaktoren um 1-2 annimmt und die gemessenen Sättigungsstromintegrale

$$s_q = s_y z F A = \int_0^{t_s} i(t) dt \quad \text{mit } a_{Me} = 1 \text{ bei } t = t_s,$$

mit dem Strombedarf zum Auf- und Abbau der dichtest gepackten Netzebene im

TABELLE 3

SÄTTIGUNGSBEDECKUNGEN DER UNTERSUCHTEN DEPOLARISATORSYSTEME

Depolarisator	Unterlage	Leitelektrolyt (0.5 M)	Stromintegral im Bereich der ungesättigten Bedeckung s_q (mAsec cm^{-2})	Strombedarf zum Aufbau der dichtest gepackten Netzebene im Kristall des Depol. metalls s_q^* (mAsec cm^{-2})	s_q/s_q^* (\triangle Rauigkeitsfaktor)
Bi ³⁺	Ag	HClO ₄	0.68 ± 0.04	~ 0.45 \triangle (0001) im Bi-Kristall bei 25°	~ 1.5
Pb ²⁺	Ag	KCl	0.50 ± 0.04	} 0.305 \triangle (111) im Pb-Kristall bei 25°	1.50-1.77
Pb ²⁺	Cu	KCl	0.45 ± 0.04		1.35-1.60
Tl ⁺	Au	KCl	0.22 ± 0.02	} 0.160 \triangle (0001) im α -Tl-Kristall bei 25°	1.25-1.50
Tl ⁺	Ag	KCl	0.30 ± 0.02		1.75-2.00
Tl ⁺	Cu	KCl	0.38 ± 0.02		2.25-2.50
Tl ⁺	Sn	NH ₄ ClO ₄	0.25 ± 0.02		1.45-1.70
Cd ²⁺	Bi	NH ₄ ClO ₄	0.31-0.34	} 0.416 \triangle (0001) im Cd-Kristall bei 25°	0.74-0.81
Cd ²⁺	Pb	NH ₄ ClO ₄	0.31-0.33		0.74-0.79
Cd ²⁺	Sn	NH ₄ ClO ₄	0.27-0.29		0.65-0.70

kristallinen Depolarisatormetall vergleicht. Die angeführten Messwerte von s_q wurden bei Systemen mit Einzelpaktransienten im Interesse einer sicheren Festlegung der oberen Integrationsgrenze t_s aus Versuchsansätzen mit offener Kammer ermittelt ($\delta \rightarrow \infty$, $0C_{Me} \approx m$), bei denen ein charakteristischer Stromanstieg den Uebergang von der ungesättigten zur gesättigten Bedeckung eindeutig kennzeichnet (Fig. 9). Bei den Kurven vom Vorstufentyp darf s_q in den Grenzen der Auswertefehler mit der Stromsumme der Vorpeaks identifiziert werden.

Man kann mit Hilfe der Kammermethode voraussetzungsfrei zeigen, dass die dem Integral s_q äquivalente Depolarisatormenge im Spannungsintervall $aE > E > rE$ tatsächlich auf der Messelektrode fixiert wird, obgleich ein kompakter Niederschlag mit $a_{Me} = 1$ thermodynamisch nicht existenzfähig ist. Wird die Elektrode nämlich ausserhalb der Kammer in der Nähe des Ruhepotentials ($E > rE$) kathodisch vorpolarisiert, so ist der nach dem Einsetzen in die Kammer und erschöpfender Anodisierung registrierte Stromtransient seiner Peakstruktur und Stromsumme nach identisch mit einer bei erhöhter Depolarisatorkonzentration und gleichem Kammer-volumen, aber ohne Vorpolarisation aufgenommenen Strom-Spannungskurve, wobei die Zunahme des Depolarisatorinhalts der Kammer gerade dem Stromintegral der kathodischen Vorbelastung entspricht (Fig. 10). Der zusätzliche Depolarisatorbetrag kann nach Art der Versuchsdurchführung und unter Berücksichtigung der systembedingten Unlöslichkeit des abgeschiedenen Metalls in der Unterlage (vgl. Tab. 1) nur in Form einer Sorptionsschicht des Reduktionsprodukts Me auf der Elektrodenoberfläche in den Diffusionsraum gelangt sein.

Die durch Messung des Gesamtstromintegrals q_{cath} (vgl. (8)) als Funktion der Kammerhöhe δ bestimmte Ladungsaufnahme pro Ion

$$z_{(q)} = dq_{cath}/mFA d\delta \quad (22)$$

unterscheidet sich bei den meisten Systemen im Monoschicht- wie auch im gesättigten

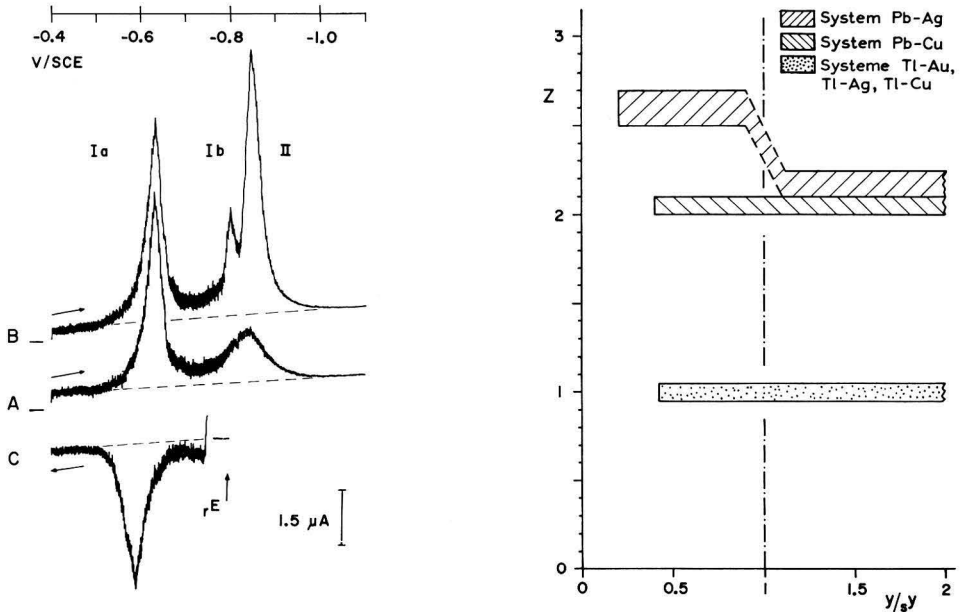


Fig. 10. Einfluss der kathodischen Vorpolarisation im Potentialgebiet der Vorstufen auf das Stromintegral der Abscheidung von Tl auf Ag (Vorstufentyp, Nr. 6 Tab. 2). (—), Grundstrom. rE , Ruhepotential einer reinen Tl-Elektrode. Ia, Ib, Tl-Vorstufen an Ag; II, Tl-Hauptstufe. A, Vergleichspolarogramm einer nach S. 301 behandelten Messelektrode. B, Polarogramm nach Vorpolarisation der Messelektrode bei -750 mV vs. SCE vor dem Einschrauben in die Kammer. C, Anodischer Ablösestrom beim Einstellen des Startpotentials -750 mV vs. SCE nach Einschrauben der vorpolarisierten Messelektrode in die Kammer.

Depolarisator, $5,55 \cdot 10^{-4} M$ TlCl. Leitsalz, $0,5 M$ KCl, pH = 5. Elektrodenmetall, Ag. Elektrodenfläche, $A = 0,785 \text{ cm}^2$. Kammerhöhe (für A, B, C), $\delta = 4,0 \cdot 10^{-3} \text{ cm}$. Durchlaufgeschw., $\beta = 0,1 \text{ V min}^{-1}$. Widerstand im Leitkanal, $R_K = 1100 \Omega$.

Bei den angegebenen Potentialen wurde die Ohm'sche Spannungskorrektur nicht berücksichtigt.

Fig. 11. Effektive Ladungsaufnahme z pro Grammatom Depolarisator als Funktion des Bedeckungsgrades y/sy in $0,5 M$ KCl (Vorstufensysteme). (—), Sättigungsschwelle.

Bedeckungsgebiet um nicht mehr als $\pm 5\%$ von den zur Neutralisation der Kationen Me^{z+} nach (I) erforderlichen Werten z_{wahr} (Fig. 11). Die bemerkenswerte Ueberhöhung von z bei der Abscheidung der Bleimonoschicht auf Silber tritt nur in halogenidhaltigen Leitelektrolyten in Erscheinung und wird auf den gleichzeitigen partiellen Abbau der Halogensorptionsschicht der Silberoberfläche¹⁶ zurückgeführt:



Dabei hängt der auf den gesamten Vorstufenbereich bezogene Ladungsüberschuss

$$\begin{aligned} \Delta q &= sq_{\text{gemessen}} - z_{\text{wahr}} F A s y_{\text{wahr}} \\ &= sq_{\text{gemessen}} - z_{\text{wahr}} F s V m^* \end{aligned} \quad (23)$$

von der Halogenidkonzentration ab und beträgt beispielsweise in $0,5 M$ KCl rund ein

* Die Grösse sV in (23) gibt das Volumen der Elektrodenkammer an, bei dem der Depolarisatorinhalt gerade zur Sättigung der Elektrode ($a_{Me} = 1$) ausreicht, und kann einer Auftragung der experimentellen q -Werte gegen δ entnommen werden. Die Grösse $s y_{\text{wahr}}$ ist als Produkt $s y_{\text{wahr}} = s V m / A$ definiert.

TABELLE 4

STROMBILANZ DER ABSCHIEDUNG VON Pb AN Ag IN GEGENWART VERSCHIEDENER LEITELEKTROLYTE (vgl. Gl. (23))

Leitelektrolyt (0.5 M)	pH	sq_{gemessen} (mAsec cm ⁻²)	Δq (mAsec cm ⁻²)	$z_{\text{wahr}} F s y_{\text{wahr}}$ (mAsec cm ⁻²)	$s y_{\text{wahr}}$ (mM cm ⁻² · 10 ⁻⁴)
NaF	5	0.48 ± 0.02	—	0.48 ± 0.02	2.5
NH ₂ SO ₃ H	0.5	0.47 ± 0.02	—	0.47 ± 0.02	2.2
KCl	5	0.53 ± 0.02	0.10 ± 0.01	0.43 ± 0.02	2.2
KBr	5	0.47 ± 0.02	0.19 ± 0.02	0.28 ± 0.02	1.5
KSCN	5	0.50 ± 0.02	0.12 ± 0.02	0.38 ± 0.02	2.0

TABELLE 5

PEAKDATEN DER BLEIVORSTUFE AN Ag IN VERSCHIEDENEN ELEKTROLYTEN

Leitelektrolyt (0.5 M)	Peakpotentiale der Pb-Vorstufe, bezogen auf rE (mV)		rE (mV vs. SCE)
	cath.	anod.	
KOH	145 ± 5	200 ± 5	-820
NaF	135 ± 5	175 ± 5	-520
NH ₂ SO ₃ H	115 ± 5	125 ± 5	-475
KCl	100 ± 5	115 ± 5	-525
KBr	50 ± 5	80 ± 5	-540
KSCN	40 ± 5	75 ± 5	-520
KI	30 ± 5	30 ± 5	-670

Drittel der von VESELOVSKY¹⁶ angegebenen Chlorsorptionskapazität (0.9 · 10¹⁵ Atome cm⁻²) einer blanken Silberelektrode. In Gegenwart von Rhodanid, Chlorid und vor allem von Bromid erfährt $z_{\text{wahr}} F A s y_{\text{wahr}}$ eine deutliche Verringerung im Vergleich zu in Sulfaminat- und Fluoridlösung ermittelten Vergleichswerten (Tab. 4), was darauf hinweist, dass Halogenadsorbat und Bleimonoschicht um zumindest teilweise identische Adsorptionspositionen konkurrieren²⁶ (ein analoges Verhalten der Silberoberfläche ist bei der simultanen Adsorption von Iodid und Hydroxyd¹⁹ festgestellt worden).

Der Potentialabstand zwischen Vorstufe und Ruhepotential wird durch die Anwesenheit nichtmetallischer Sorptionsschichten (einschliesslich der Sauerstoff- bzw. OH-Bedeckung in stark alkalischem Milieu¹⁶) merklich beeinflusst (Tab. 5), wobei gleichzeitig die Potentiallage des gesamten Stromtransienten bezüglich des Spannungsnullpunkts infolge unterschiedlicher Komplexierung des Depolarisator-kations in den einzelnen Leitlösungen beträchtliche Differenzen aufweisen kann. Ein Ersatz des Leitkations K⁺ durch Na⁺, NH₄⁺, Ba²⁺ oder H⁺ bleibt dagegen ohne erkennbare Auswirkungen auf die Kurvenform.

Zur Ermittlung der Aktivitätsisotherme $a_{\text{Me}(y)}$ aus den experimentellen Strom-Spannungsdaten wird den Bedeckungswerten y eine Funktion

$$a_{(y)}^* = \alpha c_{\text{Me}} \exp \frac{zF}{RT} (\alpha E - E) = \alpha c_{\text{Me}} m^{-1} \exp \frac{zF}{RT} (rE - E) \quad (24)$$

(vgl. (21)) zugeordnet, die sich aus dem gemessenen Elektrodenpotential E und der

jeweiligen Elektrodengrenzenkonzentration $o c_{Me}$ berechnet. $o c_{Me}$ ist über eine numerische Faltungsintegration des gemessenen Stromes $i(t)$ nach Gl. (4) zugänglich.

Sofern der lösungsseitige Depolarisatortransport (3) die Gesamtgeschwindigkeit des Bruttovorgangs (i) bestimmt, ist $a^{*(y)}$ mit der Aktivität $a_{Me(y)}$ identisch, da E dann den durch die Nernst'sche Gleichung (11) vorgeschriebenen reversiblen Wert

$$E_{rev} = oE + \frac{RT}{zF} \ln o c_{Me}/a_{Me}$$

annimmt:

$$a_{Me(y)} = a^{*(y)} \quad \text{für } E = E_{rev(y, o c_{Me})}$$

Wenn dagegen Hemmungen des Ladungsdurchtritts oder des Sorptionsvorgangs die Einstellung des Gleichgewichtspotentials verhindern, definiert Gl. (24) eine Scheinaktivität, die je nach Stromrichtung positiv oder negativ vom wahren Wert $a_{Me(y)}$ abweicht. Bei gegebenem $o c_{Me}$ und y gelten wegen

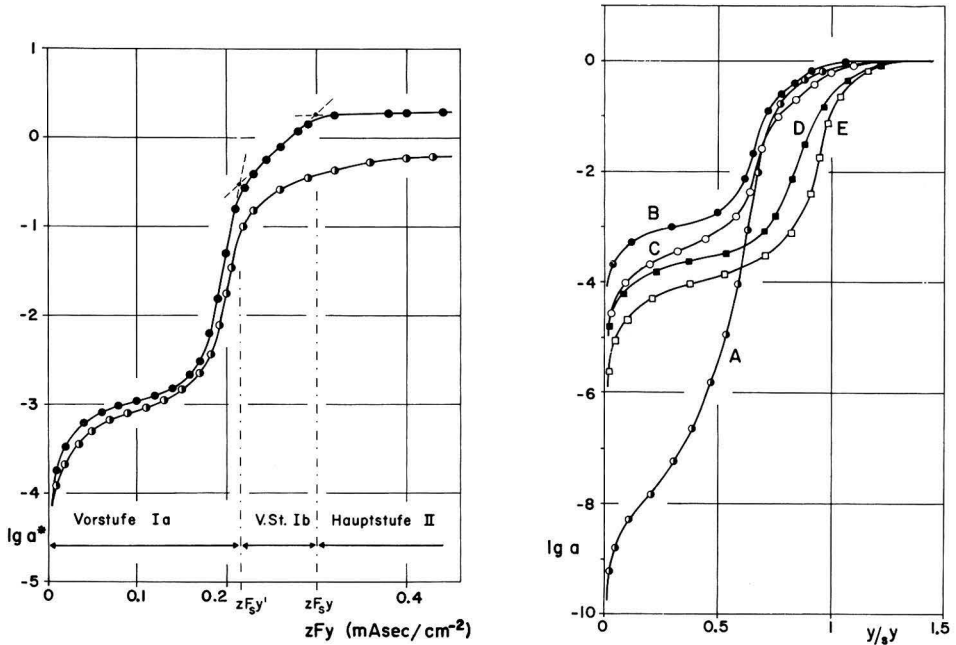


Fig. 12. Scheinaktivitäten a^{*cath} und a^{*an} des Thallium-niederschlags auf einer Ag-Elektrode (Vorstufentyp, vgl. Fig. 10). ●, a^{*cath} ; ○, a^{*an} . Messfehlerspanne, ± 3 mV \triangle 0.1 log. Einheiten. $zF_s y' = 0.215$ mAsec cm^{-2} \triangle $s y' = 2.23 \cdot 10^{-9}$ mole cm^{-2} ; $zF_s y = 0.300$ mAsec cm^{-2} \triangle $s y = 3.11 \cdot 10^{-9}$ mole cm^{-2} (vgl. (25)). Depolarisator, $6.12 \cdot 10^{-4} M$ TlCl. Leitsalz, 0.5 M KCl, pH = 5. Elektrodenmetall, Ag. Elektrodenfläche, A = 0.785 cm^2 . Kammerhöhe, $\delta = 1.0 \cdot 10^{-2}$ cm. Durchlaufgeschw., $\beta = 0.1$ V min^{-1} .

Fig. 13. Aktivitätsisothermen von Depolarisatorniederschlägen des Vorstufentypus. System, Depolarisatorkonz. und Kammerhöhe bei Kurven: (A), Tl-Au, $4.38 \cdot 10^{-4} M$ TlCl, $1.00 \cdot 10^{-2}$ cm; (B), Tl-Ag, $6.12 \cdot 10^{-4} M$ TlCl, $8.0 \cdot 10^{-3}$ cm; (C), Tl-Cu, $6.61 \cdot 10^{-4} M$ TlCl, $8.0 \cdot 10^{-3}$ cm; (D), Pb-Ag, $3.71 \cdot 10^{-4} M$ PbCl₂, $1.00 \cdot 10^{-2}$ cm; (E), Pb-Cu, $3.75 \cdot 10^{-4} M$ PbCl₂, $1.00 \cdot 10^{-2}$ cm. Leitelektrolyt, 0.5 M KCl, pH = 5. Elektrodenfläche, A = 0.785 cm^2 . Durchlaufgeschw., $\beta = 0.1$ V min^{-1} .

$$E_{(y,0^{c_{Me}})} \leq E_{rev(y,0^{c_{Me}})} \quad \text{für } i_{(t)} \geq 0 \text{ (kathod. Strom)}$$

und

$$E_{(y,0^{c_{Me}})} \geq E_{rev(y,0^{c_{Me}})} \quad \text{für } i_{(t)} \leq 0 \text{ (anodischer Strom)}$$

die Ungleichungen $a^*_{cat(y)} \equiv a^*_{(y,i>0)} \geq a_{Me(y)}$ (für kathodische Ströme und $E \neq E_{rev}$) und $a^*_{an(y)} \equiv a^*_{(y,i<0)} \leq a_{Me(y)}$ (für anodische Ströme und $E \neq E_{rev}$) mit deren Hilfe sich ein Intervall

$$a^*_{cath(y)} \geq a_{Me(y)} \geq a^*_{an(y)}$$

abgrenzen lässt, innerhalb dessen der gesuchte Aktivitätswert $a_{Me(y)}$ liegt. Die Größen $a^*_{cath(y)}$ und $a^*_{an(y)}$ können im kathodischen und anodischen Spannungsdurchlauf des gleichen Versuchsansatzes (Fig. 5–7) gemessen werden.

Geeignetes Kurvenmaterial zur Aktivitätsauswertung liegt bislang für die in KCl-Leitlösung untersuchten Systeme Pb–Ag, Pb–Cu, Tl–Ag, Tl–Cu und Tl–Au (Nr. 2, 3, 5, 6, 7 der Tab. 2) vor, deren Strom–Spannungskurven sämtlich zum Vorstufentyp gehören.

Die Werte a^*_{cath} und a^*_{an} differieren im Bereich der Monoschichtbedeckung auf Ag und Au nur um 0.1–0.2 logarithmische Einheiten (Fig. 12), so dass die betreffenden Bruttoreaktionen (I) als polarographisch reversibel angesehen werden

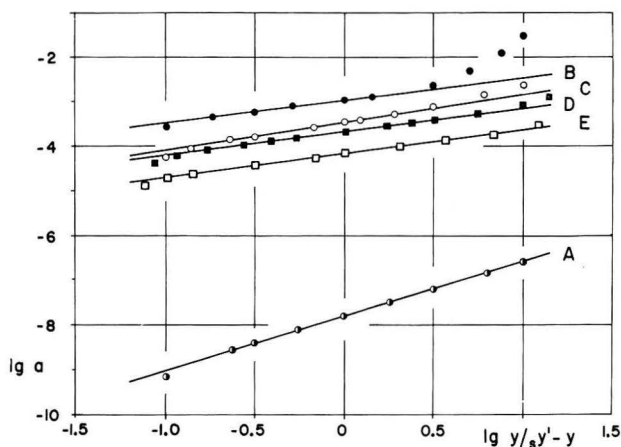


Fig. 14. Darstellung des Mittelwertes $\lg a_{Me(y)}$ als Funktion von $\lg(y/sy' - y)$ für die Vorstufensysteme der Fig. 13. Auswertung vgl. Tab. 6.

dürfen, zumal der Term $|\lg a^*_{cath} - \lg a^*_{an}| RT/zF$ etwa mit der Fehlerbreite der Spannungsmessung (± 3 mV) übereinstimmt. Die Abscheidung der Pb- und Tl-Monoschicht auf Cu ist stärker gehemmt, was eine Zunahme von $|\lg a^*_{cath} - \lg a^*_{an}|$ bis auf ca. 0.5 bedingt. Nahe dem Sättigungspunkt scheint sich das Entladungsgleichgewicht in allen Fällen weniger rasch einzustellen als bei Bedeckungen $y/sy' \ll 1$, da sich der Abstand der kathodischen und anodischen a^* -Kurven in der Umgebung der Ordinate $\lg a^* \approx 0$ generell auf 0.8–1 logarithmische Einheit erhöht; eine eingehende Untersuchung dieser Erscheinung, vor allem im Hinblick auf den Einfluss des koadsorbierten Halogens auf Durchtrittskinetik und Nukleation beim Uebergang

von der Monoschicht zum kompakten Depolarisatormetall, steht jedoch noch aus. Die den errechneten Scheinaktivitäten zugrundeliegenden und durch das geometrische Mittel

$$\lg \bar{a}^*(y) = \frac{1}{2} (\lg a^*_{\text{cath}(y)} + \lg a^*_{\text{an}(y)}) \approx \lg a_{\text{Me}(y)}$$

näherungsweise dargestellten $[\lg a_{\text{Me}}]_{(y)}$ -Isothermen der genannten fünf Systeme zeichnen sich durch deutliche Sigmoidform aus (Fig. 13) und erfüllen demgemäss eine auf die Wendebasis $s_y y$ der Kurve normierte lineare Beziehung (vgl. Fig. 14)

$$\lg a_{\text{Me}} = P + Q \lg \frac{y}{s_y y' - y} \quad \text{mit } s_y y' = 2 s_y y. \quad (25)$$

Der Ordinatenabschnitt P misst die Aktivität bei $y = \frac{1}{2} s_y y'$ und ist daher der Freien Adsorptionenthalpie ΔG_w beim Wendepunkt proportional:

$$\Delta G_w = w \mu_{\text{Me}} - 0 \mu_{\text{Me}} = 2.303 \text{ RTP}.$$

Die Steigungen Q der Geraden in Fig. 14 unterscheiden sich signifikant vom Neigungsquotienten einer im Kurvenverlauf analogen Langmuir-Isothermen

$$\lg a = P + \lg \frac{y}{s_y y - y} \quad \text{mit } d \lg a / d[\lg y(s_y y - y)^{-1}] = 1,$$

die von BYRNE UND ROGERS³ zur Beschreibung der Aktivität von Tracerniederschlägen auf Metallelektroden herangezogen wurde (vgl. Tab. 6). Als Ursache für die bei den vorliegenden Versuchen beobachtete Abweichung vom Langmuir'schen Bedeckungsmodell kommen neben einer energetischen Inhomogenität der polykristallinen Unterlage (d.h. bedeckungsabhängiger Adsorptionswärme) eine Störung durch Halogen- oder andere Anionenadsorption sowie durch Assoziationsvorgänge in der metallischen Monoschicht in Frage. Von NEWMAN²⁰ wurden in submonatomaren Metallaufdampfschichten auf Silberoberflächen Partikelverbände höheren Ordnungsgrades elektronenoptisch nachgewiesen, so dass die Möglichkeit ihres Auftretens auch in elektrolytisch hergestellten Monoschichten und in Gegenwart der Elektrolytphase nicht von der Hand zu weisen ist.

TABELLE 6

PARAMETER DER ISOTHERMENERADEN $\lg a_{\text{Me}} = P + Q \lg y/s_y y' - y$
(vgl. Fig. 14 und Gl. (25))

Nr.	Depolarisator	Grundmetal	Q	P	ΔG_w (kcal/mol)	$s_y y'$ (mM cm ⁻² · 10 ⁻⁶)	$s_y y$ (mM cm ⁻² · 10 ⁻⁶)	$s_y y' / s_y y$
A	Tl ⁺	Au	+ 1.20	- 7.80	- 10.6	1.0	2.3	0.44
B	Tl ⁺	Ag	+ 0.48	- 2.97	- 4.0	2.2	3.0	0.73
C	Tl ⁺	Cu	+ 0.61	- 3.47	- 4.7	2.8	4.1	0.68
D	Pb ²⁺	Ag	+ 0.50	- 3.66	- 5.0	2.0	2.6	0.77
E	Pb ²⁺	Cu	+ 0.50	- 4.15	- 5.6	1.6	2.3	0.70

Die in Gl. (25) verwendeten $s_y y'$ -Werte liegen vor allem beim Tl beträchtlich unter der Sättigungsbedeckung $s_y y$ (Tab. 6). Der Isothermenabschnitt im Intervall $s_y y' < y < s_y y$, der als Gegenstück zur Uebergangsfunktion $g_{1(y)}$ in (18) gelten kann, entspricht dem zweiten Vorstufenpeak der Systeme Tl-Ag, Tl-Cu und Tl-Au.

Die Arbeit wurde mit Unterstützung des Schweizerischen Nationalfonds zur Förderung der wissenschaftlichen Forschung ausgeführt. Wir danken Herrn Prof. Dr. K. HUBER für sein unseren Versuchen entgegengebrachtes Interesse.

ZUSAMMENFASSUNG

Die Reduktion von metallischen Depolarisatoren an Festelektroden aus wässriger Lösung wird auf chronoamperometrischem Wege unter Verwendung von Messelektroden vom Kammertyp auf Monoschichteffekte untersucht, wobei unter einer metallischen Monoschicht eine elektrisch neutrale Fremdmetalbedeckung an der Phasengrenze Elektrode-Elektrolyt von der Grössenordnung einer Atomlage verstanden wird.

Der Verlauf der Strom-Zeit-Kurve ist von der Form der Aktivitätsisotherme im Gebiet der ungesättigten (submonoatomaren) Bedeckung abhängig; die Abscheidung von Tl auf Au, Ag und Cu, Pb auf Ag und Cu sowie Bi auf Ag führt zur Aufspaltung des Stromtransienten in separate Vor- und Hauptpeaks ($a_{Me} < 1$ bzw. $a_{Me} = 1$), während im Falle der Systeme Sn auf Bi, Tl auf Sn sowie Cd auf Bi, Pb und Sn nur ein einziges Strommaximum beobachtet wird.

Die Strombilanz des Elektrodenvorganges wird durch coulometrische Auswertung der Chronoamperogramme geprüft.

SUMMARY

The reduction of metals from aqueous solutions on the surface of solid electrodes is performed chronoamperometrically to study monolayer effects using chamber type indicator electrodes. A metallic monolayer is defined as a layer of electrically neutral foreign metal atoms at the electrode-electrolyte interface, the deposit having the approximate thickness of one atomic diameter.

The shape of current-time curve depends upon the structure of the activity isotherm within the region of unsaturated (submonoatomic) surface coverage of the electrode. A single current peak is observed during the deposition of Sn on Bi, Tl on Sn, and Cd on Bi, Pb and Sn. The reduction of Tl on Au, Ag and Cu, of Pb on Ag and Cu, and of Bi on Ag, however, leads to the splitting of the current transient into a so-called main peak with unit activity of the electrodeposited depolarizer, and a less negative prewave region, within which the activity of the reduced metal is less than unity.

The current balance of the electrode reaction is verified by coulometric evaluation of the chronoamperograms.

RÉSUMÉ

La réduction de dépolarisateurs métalliques dans des solutions aqueuses à la surface des électrodes solides est étudiée au point de vue des effets de couches monoatomiques, par une méthode chronoampérométrique, au moyen d'électrodes indicatrices nommées électrodes de chambre. Le terme "couche monoatomique" indique une couverture de métal étranger, électriquement neutre, à la surface de l'électrode de l'épaisseur d'un atome.

La courbe intensité du courant vs. temps dépend de la forme de l'isotherme d'activité dans la région de la couverture insaturée (submonoatomique). La réduction de Tl sur Au, Ag et Cu, de Pb sur Ag et Cu, de Bi sur Ag mène à la séparation du signal de courant en des peaks primaires (activité du métal déposé moins d'un) et en un peak principal (activité du métal déposé égal un), pendant qu'on trouve dans le cas des systèmes Sn sur Bi, Tl sur Sn, Cd sur Bi, Pb et Sn un seul maximum du courant électrique.

Le bilan de courant du processus à la surface de l'électrode est vérifié par measurement coulométrique des chronoampérogrammes.

LITERATUR

- 1 M. HAISSINSKY, *Experientia*, 8 (1952) 125.
- 2 L. B. ROGERS, *Record Chem. Progr.*, 16 (1955) 197.
- 3 J. T. BYRNE UND L. B. ROGERS, *J. Electrochem. Soc.*, 98 (1951) 457.
- 4 L. B. ROGERS UND A. F. STEHNEY, *J. Electrochem. Soc.*, 95 (1949) 25.
- 5 T. MILLS UND G. M. WILLIS, *J. Electrochem. Soc.*, 100 (1953) 452.
- 6 E. SCHMIDT UND H. R. GYGAX, *Helv. Chim. Acta*, 48 (1965) 1178.
- 7 E. SCHMIDT UND H. R. GYGAX, *Helv. Chim. Acta*, 48 (1965) 1584.
- 8 B. J. BOWLES, *Electrochim. Acta*, 10 (1965) 731.
- 9 M. M. NICHOLSON, *J. Am. Chem. Soc.*, 79 (1957) 7.
- 10 R. PIONTELLI, *J. Chim. Phys.*, 46 (1949) 288.
- 11 P. DELAHAY, G. CHARLOT UND H. A. LAITINEN, *J. Electroanal. Chem.*, 1 (1960) 425.
- 12 G. DOETSCH, *Theorie und Anwendung der Laplace-Transformation*, Springer-Verlag, Berlin, 1937, S. 361.
- 13 G. DOETSCH, *Tabellen zur Laplace-Transformation*, Springer-Verlag, Berlin, 1947, S. 183.
- 14 E. JAHNKE UND F. EMDE, *Funktionentafeln*, Dover Publ., New York, 1945, S. 41.
- 15 K. J. VETTER UND D. BERNDT, *Z. Elektrochem.*, 62 (1958) 378.
- 16 V. J. VESELOVSKY, *Acta Physicochim. URSS*, 11 (1939) 815.
- 17 T. KURASAWA, Japan. Pat. 5619 (1960), *Zit. nach C.A.* 55 (1961) 14.279 a.
- 18 P. BOEHLEN, *Lizentiatsarbeit*, Bern, 1965.
- 19 L. A. MEDVEDYEVA UND YA. M. KOLOTYRKIN, *Dokl. Akad. Nauk. SSSR*, 143 (1962) 1384.
- 20 R. C. NEWMAN, *Phil. Mag.*, [8] 2 (1957) 750.
- 21 F. C. ANSON, *J. Electrochem. Soc.*, 110 (1963) 436.
- 22 C. R. CHRISTENSEN UND F. C. ANSON, *Anal. Chem.*, 35 (1963) 205.
- 23 A. T. HUBBARD UND F. C. ANSON, *Anal. Chem.*, 36 (1964) 723.
- 24 A. T. HUBBARD UND F. C. ANSON, *J. Electroanal. Chem.*, 9 (1965) 163.
- 25 D. M. OGLESBY, S. H. OMANG UND C. N. REILLEY, *Anal. Chem.*, 37 (1965) 1312.
- 26 E. SCHMIDT, H. R. GYGAX UND P. BOEHLEN, *Helv. Chim. Acta*, 49 (1966) 733.
- 27 E. SCHMIDT UND H. R. GYGAX, *Chimia*, 16 (1962) 165.

POTENTIOMETRIC STUDY ON THE INTERACTION OF Ag^+ IONS WITH GELATIN

PIETRO LANZA AND ILEANA MAZZEI

*National Centre for Radiation Chemistry and Radio-elements of CNR, Bologna (Italy)
Chemical Institute "G. Ciamician", University of Bologna, Bologna (Italy)*

(Received November 23rd, 1965)

INTRODUCTION

It is well known that proteins show a considerable tendency to form complexes with metals and especially with heavy metals. Although numerous and detailed works have been carried out, some recently, on the complexes of proteins of biological importance with metals, little is known about the Ag^+ -gelatin interaction. The most important work on this complex was carried out by CARROL AND HUBBARD¹ in 1931 but it is not exhaustive.

Work on macromolecule complexes, and in particular proteins, is generally designed to determine:

- (a) the maximum number of metal ions/mole which can be complexed under different experimental conditions;
- (b) the nature of these complexes, *i.e.*, which ligand group of the macromolecule is involved in the formation of the complex;
- (c) the stability of the complexes.

The problem is especially difficult for proteins, and there is probably no exact solution. Many factors can, in fact, cause complications: simultaneously-active groups of different chemical nature can be found in proteins (such as carboxyl, imidazole, amino, sulfhydryl groups, etc.); each single group can have a complexing activity strongly influenced by its steric position more or less facilitating the formation of chelates; some groups can remain completely inactive because they are internally protected by the proteic mass, but can be activated by denaturation of the protein causing alterations in the molecular structure. It is difficult to evaluate the electrostatic effects and the acid-base strength of the different groups.

Although the true problem does not lend itself to a general mathematical treatment, several authors have undertaken extensive studies to establish a mathematical basis of calculation adaptable to ideal molecular models. Several important reviews on the subject have appeared, among them the work of COHN AND EDSALL², KLOTZ³, GURD⁴, and TANFORD⁵.

The essential idea can be stated thus: a series of stability constants, one for each ligand group, exists for high molecular-weight substances with numerous ligand groups capable of participating in the formation of complexes. Complicated systems, having different types of groups as in the case of proteins, contain an equal number of

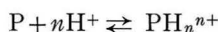
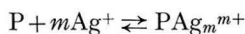
equilibrium systems and types of ligand groups. In this instance, each type of complex has an "intrinsic constant k " which is related to each k_i constant of a series by the expression:

$$k_i = \frac{n-i+1}{i} k$$

where n represents the maximum number of sites that can be associated with the complexing element (Ag⁺) in the macromolecule (P), i is the number of occupied sites and k_i is the equilibrium constant for the process



As the proteic molecule is amphoteric, it often has considerable quantities of both positive and negative electrostatic charges which influence all possible phenomena of ionic dissociation. When acid-base groups are involved in the formation of metal complexes, the possible competition of H⁺ ions must be considered. This happens in the case of the Ag⁺-gelatin complex where the following equilibria take place simultaneously:



If we express the number of Ag⁺ and H⁺ ions combined/mole of gelatin to i -type groups (imidazole, ϵ -amino, carboxyl, etc.) as $\bar{v}_{i\text{Ag}}$ and $\bar{v}_{i\text{H}}$, respectively, the following equations will be valid:

$$\bar{v}_{i\text{H}} = k_{i\text{H}} \Gamma_{\text{H}} a_{\text{H}} (n_i - \bar{v}_{i\text{H}} - \bar{v}_{i\text{Ag}}) \quad (1)$$

$$\bar{v}_{i\text{Ag}} = k_{i\text{Ag}} \Gamma_{\text{Ag}} a_{\text{Ag}} (n_i - \bar{v}_{i\text{H}} - \bar{v}_{i\text{Ag}}) \quad (2)$$

where

$k_{i\text{H}}$ = intrinsic acid association constant of i -type group (inverse to the corresponding constant of acid dissociation),

$k_{i\text{Ag}}$ = intrinsic stability constant of the i -type group complex,

Γ_{H} = $e^{-2w Z_p Z_{\text{H}}}$ } electrostatic factors of the H⁺ and Ag⁺ ions,
 Γ_{Ag} = $e^{-2w Z_p Z_{\text{Ag}}}$ }

a_{H} and a_{Ag} = activity of H⁺ and Ag⁺ ions; when operating at constant ionic strength, the activity is assumed to be equal to the molar concentration $a_{\text{Ag}} = [\text{Ag}^+]$,

n_i = maximum number of i -type group sites present in the mole.

From eqns. (1) and (2) it follows that:

$$k_{i\text{Ag}} = \frac{\bar{v}_{i\text{Ag}} (\Gamma_{\text{H}} + k_{i\text{H}} a_{\text{H}} \Gamma_{\text{H}})}{a_{\text{Ag}} (n_i - \bar{v}_{i\text{Ag}}) \Gamma_{\text{Ag}}} \quad (3)$$

$k_{i\text{Ag}}$ can be obtained from eqn. (3), provided that the $\bar{v}_{i\text{Ag}}$, a_{H} and a_{Ag} values can be obtained experimentally. Γ_{H} and Γ_{Ag} can be calculated by the procedures described in the literature²⁻⁴, and are deducible⁵ from the empirical values of w . $k_{i\text{H}}$ can be obtained from the acid-base titration curve of the protein. Equation (3) can also be expressed as follows:

$$\bar{v}_{iAg} = \frac{n_i k_{iAg} a_{Ag} \Gamma_{Ag}}{1 + k_{iH} a_H \Gamma_H + k_{iAg} a_{Ag} \Gamma_{Ag}} \quad (4)$$

Obviously, this equation is applicable when *i*-type groups only are active. When active groups other than *i*-type groups such as *j*, *y*, etc. are present in the molecule, the expression can be:

$$\begin{aligned} \bar{v}_{Ag} &= \frac{n_i k_{iAg} a_{Ag} \Gamma_{Ag}}{1 + k_{iH} a_H \Gamma_H + k_{iAg} a_{Ag} \Gamma_{Ag}} + \frac{n_j k_{jAg} a_{Ag} \Gamma_{Ag}}{1 + k_{jH} a_H \Gamma_H + k_{jAg} a_{Ag} \Gamma_{Ag}} + \dots \\ \bar{v}_{Ag} &= \sum_i \bar{v}_{iAg} = \sum_i \frac{n_i k_{iAg} a_{Ag} \Gamma_{Ag}}{1 + k_{iH} a_H \Gamma_H + k_{iAg} a_{Ag} \Gamma_{Ag}} \end{aligned} \quad (5)$$

Consideration of the possibility of other generic J-type ions taking part in the formation of the complex besides H⁺ and Ag⁺ ions, leads to the following general equation:

$$\bar{v}_M = \sum_i \bar{v}_{iM} = \sum_i \frac{n_i k_{iM} a_M \Gamma_M}{1 + \sum_j k_{iJ} a_J \Gamma_J} \quad (6)$$

Equation (6) gives the average number of *M*-type ions bonded to all possible ligand groups contained in the molecule. The application of the above equations requires knowledge of the electrostatic term, Γ_J . The necessity of introducing this term into the calculation is due to the presence in the proteic molecule of a number of negative and positive charges the net potential field of which favours or hinders the approach of the complexable ion. This effect, called the electrostatic effect, produces changes in the stability constant of the complex, which has to be determined each time. The electrostatic effect can be calculated on the basis of the Debye-Hückel theory by the equation:

$$\Gamma_J = e^{-2w Z_p Z_j} \quad (7)$$

The electrostatic factor, Γ_J , is thus a function of the net charge of protein Z_p , the charge of ion, Z_j , and the term w which, according to the theory cited, is a constant expressed by the equation:

$$w = \frac{N e^2}{2 D R T} \left(\frac{1}{b} - \frac{\kappa}{1 + \kappa a} \right) \quad (8)$$

where:

- b = radius of the protein,
- a = sum of the radius of protein and complexable ion,
- κ = (Debye function) $(8\pi N \mu \epsilon^2 / 1000 D k T)^{\frac{1}{2}}$.

In practice, eqn (8) often gives useless values for w since b and a are not constant and change with the pH and ionic strength (μ) of the medium.

A critical examination of the limit of applicability of this theory is reported in the recent study of NAGASAWA AND HOLTZER⁶. When w cannot be calculated successfully, it is common practice to treat it as a correction factor and to determine it empirically. It is often possible to calculate w by the acid-base titration curve using the equation:

$$\log \frac{x_i}{1 - x_i} = \text{pH} - \text{p}k_{iH} + 0.868 w Z_p \quad (9)$$

where:

x_i = degree of dissociation of *i*-type groups (*e.g.*, carboxyl),

k_{iH} = intrinsic dissociation constant of the group,

Z_p = net charge of the protein molecule at the chosen pH.

It is not often possible to calculate by means of eqn. (9) the values of w for the whole pH-range, since the equation is valid only when the dissociation process is concerned exclusively with *i*-type groups. Details of the procedure have been described by TANFORD⁵; they were applied by us in the present work.

The value of Z_p in eqns (1) and (6) should be calculated taking into account the variation of the electric charge in the protein molecule due to association of Ag⁺ ions and loss of H⁺ ions. The values of Γ were therefore calculated according to equation:

$$\Gamma = e^{-2w(Z_p + \nu_{Ag} - \nu_H)} \quad (10)$$

In the present work, an attempt was made to apply eqn. (5) to the study of the Ag⁺-gelatin complexes without considering possible interaction of other ions present in the system (K⁺, NO₃⁻) and taking into consideration only the competition of Ag⁺ and H⁺ ions. It should be borne in mind, however, that although eqns (4) and (5) are generally applied to the study of multiple equilibria systems, they are based on assumptions that cannot always find confirmation in such complicated systems as proteins.

The use of eqn. (4) presupposes in fact:

(1) that all *i*-type sites have identical steric structure and therefore can be considered exactly equivalent in statistical treatment, and characterized by the same intrinsic constant;

(2) that all sites are "independent" and do not exert mutual interactions;

(3) that the electrostatic factor is exactly defined;

(4) that each metal ion is bound to only one ligand group and displaces only one H⁺ ion; the equation does not, therefore, take into account the possible formation of chelates in specific sites favourable to chelation, evidently depending on the particular protein structure. In the present study, we have taken into account these important limiting factors which are not always considered.

MATERIALS AND METHODS

Bone gelatin for photographic use was used in all experiments. It was de-ashed by ion-exchange resins (Amberlite IR-120 and IRA-400, B.D.H.). Its active groups content was determined by the acid-base titration curve⁷ and by chromatographic analysis with automatic amino-acid analyzer after complete hydrolysis. The composition, expressed as moles/10⁵ g of gelatin, is as follows:

113 carboxyl groups (aspartic and glutamic acids and terminal —COOH);

5 imidazole groups (histidine), about 3 terminal α -amino groups;

36 ϵ -amino groups (lysine);

44 guanidine groups (arginine).

The gelatin was dissolved in a 0.2 *M* solution of KNO₃ at 40–50° and made up to volume with 0.2 *M* KNO₃ at 25°. The exact quantity of gelatin was weighed, taking into account residual moisture, to obtain solutions containing 1% dry gelatin.

The 0.1 *N* standard volumetric solutions of HNO₃ and KOH were brought to

0.2 ionic strength by the addition of KNO_3 . The 0.1 *N* standard volumetric solution of AgNO_3 at $\mu = 0.2$ was prepared by dissolving an exact quantity of AgNO_3 in KNO_3 in a volumetric flask, to obtain a final solution, 0.1 *N* KNO_3 -0.1 *N* AgNO_3 . The strength of the AgNO_3 solution was checked by potentiometric titration with KCl .

APPARATUS

The pH and pAg measurements were made simultaneously by two separate pH-meters. The pH measurement was made by a precision pH-meter, Electrofact Type 53A, having a sensitivity of ± 0.01 pH in the pH-range 6–8. The high-sensitivity scale was extended by applying externally an adjustable counterpotential. An Ingold 201 NS glass electrode was used. The instrument was calibrated at 25° with the following standard buffer solutions, according to NBS indications:

- 0.05 *M* potassium tetraoxalate (pH = 1.68);
- 0.05 *M* potassium hydrogen phthalate (pH = 4.01);
- 0.025 *M* phosphate buffer (pH = 6.86);
- 0.01 *M* borax (pH = 9.17).

The pAg measurement was made by a Knick Model pH35 precision pH-meter, allowing potential differences of 1400 mV, with an index scale graduated in millivolts. The electrode was a 0.8-mm diam. pure silver wire, coated with insulating varnish except for the dipping end (uncoated length: 20 mm). The calomel reference electrode was the same as that used for the pH measurement. It was connected to the cell by means of a KNO_3 bridge.

The instrument was calibrated with standard volumetric solutions of AgNO_3 at pAg 2, 3 and 4, having constant ionic strength ($\mu = 0.2$).

The determinations were made in a circulating water bath at $25 \pm 0.5^\circ$. Solutions at pH > 8 were measured in an atmosphere of nitrogen.

PROCEDURE

50 ml of 1% gelatin in 0.2 *M* KNO_3 were brought to the desired pH by the addition of KOH or HNO_3 . The time required for attaining apparent equilibrium varies from 1 to 20 h depending on the pH-range. The equilibrium was considered as realised when two measurements of the pH, made at intervals of 1 h, showed a difference of less than 0.01 pH-units. Increasing quantities of 0.01 *N* AgNO_3 solution (in 0.2 *M* KNO_3) were added. After each addition, the pH was brought back to the initial value by the addition of suitable quantities of KOH solution measured with a syringe-microburette. When the pH was stabilized, the potential of the silver electrode was read after at least 5 min of apparent equilibrium. The concentration of free silver, $[\text{Ag}^+]$, was determined by means of a mV/pAg calibration curve. The difference between the concentration of total silver, $[\text{Ag}^+]_0$, and the free silver, $[\text{Ag}^+]$, corresponds to the concentration of combined Ag^+ . \bar{v}_{Ag} is obtained from the following equation:

$$\bar{v}_{\text{Ag}} = \frac{[\text{Ag}^+]_0 - [\text{Ag}^+]}{[\text{gelatin}]}$$

assuming, conventionally, a molecular weight of 100,000 for the gelatin. (\bar{v}_{Ag} is expressed, therefore, as the number of Ag^+ ions bound to 10^5 g of gelatin).

RESULTS

Measurements were made keeping the pH constant at values: 1.5, 2, 2.5, 3, 4, 5, 6, 7, 8, 9, 10. Experimental results obtained at pH 7 and data for subsequent calculations are shown in Table 1, as an example. The values obtained were plotted on graphs which form the basis for the study of this system.

TABLE 1

Initial volume, 52.86 ml; μ , 0.2; [gelatin], $0.946 \cdot 10^{-4}$ M; temp., 25.0°; pH, 7.0.

0.01 N AgNO ₃ (ml)	mV	pAg	[Ag ⁺] · 10 ⁴	\bar{v}_{Ag}	0.10 N KOH (ml)	$-\bar{v}_H$
0.0	86.5	—	—	—	—	—
0.5	181.5	6.08	0.00832	0.99	0.023	0.46
1	228.2	5.28	0.0525	1.94	0.028	0.56
2	278.0	4.44	0.363	3.70	0.049	0.98
3	301.4	4.045	0.9015	5.09	0.083	1.66
4	317.0	3.78	1.66	6.10	0.112	2.24
5	328.6	3.59	2.57	7.01	0.133	2.66
6	337.8	3.43	3.72	7.59	0.148	2.96
8	349.8	3.23	5.89	8.77	0.170	3.40
10	358.0	3.09	8.13	9.68	0.184	3.68
12	364.0	2.98	10.50	10.34	0.193	3.86
14	368.8	2.90	12.60	11.08	0.201	4.02
16	372.5	2.84	14.50	11.93	0.207	4.14
18	375.8	2.79	16.20	12.87	0.213	4.26
20	378.2	2.74	18.20	13.25	0.217	4.34
22	381.0	2.70	20.00	13.97	0.222	4.44
25	393.8	2.65	22.40	14.94	0.228	4.56

TABLE 2

Gelatin active-group	Model	lg k_{iAg}	lg k_{iH}	n_i
—COO ⁻	CH ₃ COO—	0.73 (ref. 15)	4.25 (a)	113 (a)
$\begin{array}{c} \text{—C—NH} \\ \parallel \quad \parallel \\ \text{CH} \quad \text{CH} \\ \diagdown \quad \diagup \\ \text{N} \end{array}$	$\begin{array}{c} \text{CH—NH} \\ \parallel \quad \parallel \\ \text{CH} \quad \text{CH} \\ \diagdown \quad \diagup \\ \text{N} \end{array}$	3.11 (ref. 13)	6.5 (b)	5 (c)
α -NH ₂	NH ₃	3.20 (ref. 14)	7.5 (b)	3 (c)
ϵ -NH ₂	NH ₃	3.20 (ref. 14)	10 (b)	39 (a)

Note: (a) obtained from acid–base titration curve;

(b) mean value of data obtainable from technical literature, TANFORD, l.c.⁵ pp. 73, 112, 113;

(c) obtained from chromatographic analysis.

The formation curves were obtained by plotting the values of \bar{v}_{Ag} and pAg. Formation curves at pH 5, 6, 7, 8, 9, and 10 are shown in Fig. 1. For greater clarity, the curves relating to the pH-range 1.5–5.0 are plotted as $\bar{v}_{Ag}/[Ag^+]$ functions (Fig. 2). Curves which give an immediate schematic representation of the several possible equilibria in the Ag⁺–gelatin system at the experimental conditions under examination, were obtained by plotting pAg-values as functions of the pH, obtainable from

the formation curves at the subsequent values or \bar{v}_{Ag} (Fig. 3). In order to facilitate interpretation of the graph, the functions calculated by eqn. (3) were also plotted, assuming $\bar{v}_{Ag} = 1$ and giving k_{iAg} the values of the stability constants of known Ag-small molecule complexes which function as models for the various active groups of the protein. Data for the calculations are shown in Table 2. The straight line, marked OH^- on the graph, gives the approximate limit below which formation of $AgOH$ and precipitation of oxide is possible. In the graph, the curves indicate (as a function of the pH) the values the pAg must have so that the first active group of a series (*e.g.*, carboxyl, ϵ -amino, etc.) can be complexed.

Higher pAg-values also imply the partial or total dissociation of the first complex. Lower pAg-values imply the subsequent binding of Ag^+ ions with other active groups of the same series. The graph based on eqn. (3) is valid only if:

- (a) each series acts independently;
- (b) sites do not exert mutual interactions;
- (c) chelates do not form.

The displacement of H^+ ions by the Ag^+ complexing is a very important factor in interpreting the experiment.

Figures 4 and 5 show the graphs of $-\bar{v}_H$ as a function of \bar{v}_{Ag} . The \bar{v}_H -values are easily calculated from the volume of the KOH solution used to keep the pH constant.

APPLICATION OF EQN. (5) TO THE CALCULATION OF THE INTRINSIC STABILITY CONSTANTS

On the basis of the data obtained from the experiment, the intrinsic constants were obtained from eqn. (5); a_H , a_{Ag} , as well as I , k_{iH} and n_i , were substituted by the values determined experimentally. The k_{iH^-} and n_i -values of the gelatin are shown in Table 2. The complexing power of the guanidine group of arginine was

TABLE 3

pH	\bar{v}_{Ag}	-COO-	Imidazole	$\alpha-NH_2$	$\epsilon-NH_2$
6-7	1	2.17	5.02	7.07	—
	2	2.17	4.85	5.19	—
	3	2.17	4.66	4.23	—
	5	2.17	3.67	3.37	—
8-9	1	(2.17)	(5.02)	5.73	5.60
	2	(2.17)	(4.85)	5.14	4.84
	3	(2.17)	(4.66)	4.37	5.25
	5	(2.17)	(3.67)	3.37	5.31

Note: the numbers in brackets represent the values calculated at pH 6 and 7 and considered valid at pH 8 and 9.

considered negligible in the pH-range used. The only unknown values remaining after substitution of the known values in eqn. (5), are the four intrinsic constants of the carboxyl, imidazole, α -amino and ϵ -amino group complexes. The equation was applied to the measurement of various \bar{v}_{Ag} -values at pH-values 6, 7, 8 and 9, each time applying hypotheses in order to facilitate calculation. The results expressed as $\log k_{iAg}$ are shown in Table 3.

DISCUSSION ON RESULTS

From a general survey of the data obtained, it can be concluded that gelatin shows a considerable tendency to complex Ag^+ ions in the whole pH-range examined; this tendency, is particularly strong in basic or neutral environment. Although the number of moles of Ag^+ ions bound/mole of gelatin, (conventional mol. wt. = 10^5) reaches the maximum value of 4 (Fig. 2) in decidedly acid solutions ($\text{pH} \leq 3$), for higher pH-values it increases continually without limitation at the concentrations examined (Figs. 1 and 2).

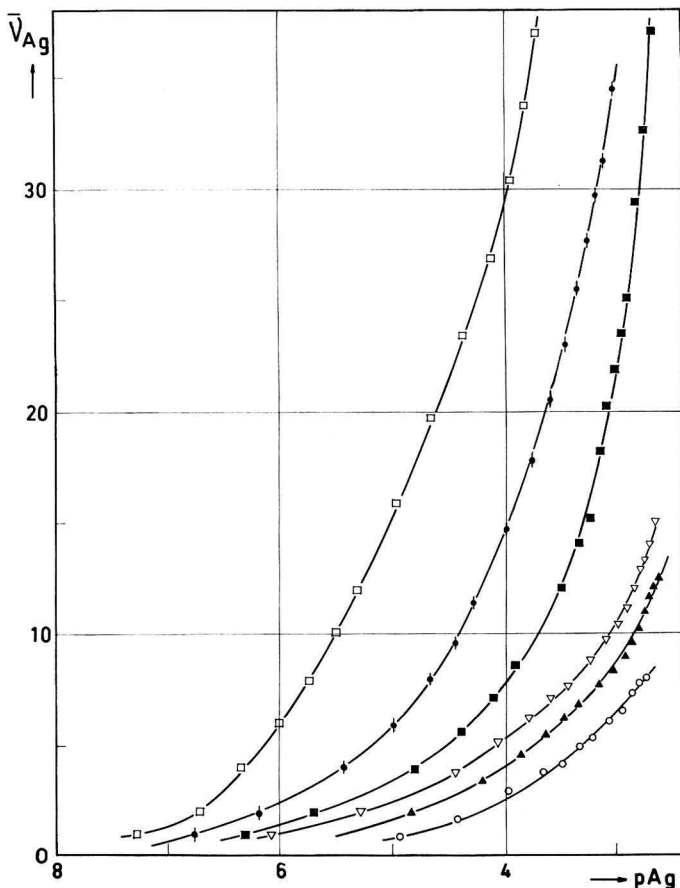


Fig. 1. Binding of Ag^+ ions by gelatin at pH: (\circ), 5; (\blacktriangle), 6; (∇), 7; (\blacksquare), 8; (\blacklozenge), 9; (\square), 10.

Figure 3 shows the trend of functions pAg/pH for different values of \bar{v}_{Ag} . The curves give an immediate indication of the stability of complexes. Given identical conditions, it is obvious that stable complexes are formed at high pH-values. It is also evident from the graph that more stable complexes exist in the Ag^+ -gelatin system than would be expected from the chemical nature of the ligand groups present in the protein. The graph, in fact, extends over an area of high pAg, clearly above the area

of hypothetical model complexes such as Ag-carboxyl, Ag⁺-ε-amino, Ag⁺-imidazole groups, etc. The intrinsic constants calculated by means of eqn. (5), are higher than the constants of the relevant models having the same ligand groups of the type considered (see Tables 3 and 4). Such high values might be justified if we suppose that simple complexes are not formed in the interaction but that we arrive directly at the formation of chelates by more than one ligand group. This would mean a considerable

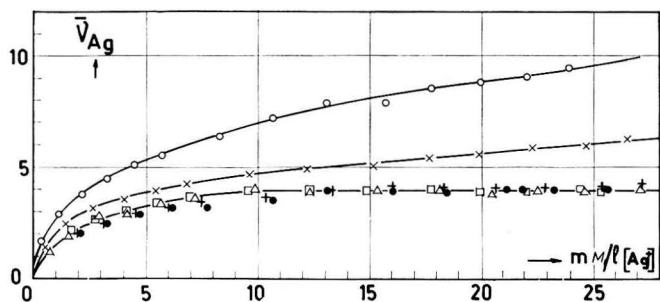


Fig. 2. Binding of Ag⁺ ions by gelatin at pH: (●), 1.5; (+), 2; (Δ), 2.5; (□), 3; (×), 4; (○), 5.

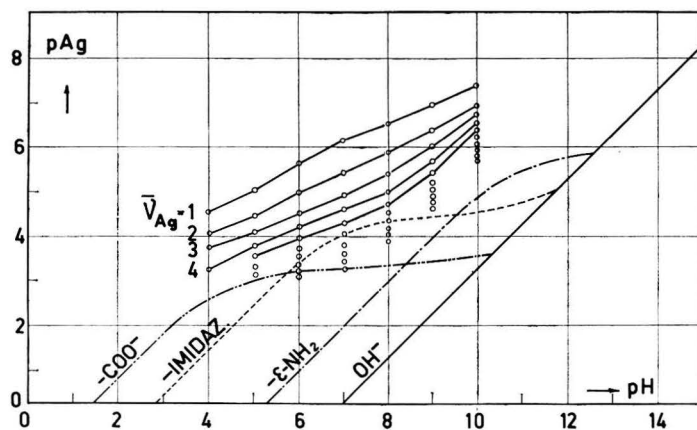


Fig. 3. Variation of pAg as a function of the pH, with subsequent values of \bar{v}_{Ag} . Curves calculated for various model-systems are plotted.

increase in the stability of the complex. This of course, implies the inapplicability of eqns. (1)–(6).

In analogy with better known Ag⁺ complexes, it can reasonably be supposed that chelates are formed by two ligand groups with a formation of linear bi-coordinated complexes relating to the hybrid $5sp$ orbitals of Ag⁺.

Graphs $-\bar{v}_H/\bar{v}_{Ag}$ shown in Figs. 4 and 5 are also significant and give a picture in accordance with the hypothesis of chelate formation. In fact, if we consider the factor of H⁺ ion displacement during the gradual association of Ag⁺ ions with the protein molecule at the different pH-values, useful information can be deduced on the possible nature of the complexing ligand groups. A large H⁺ displacement indicates that highly protonated groups are involved in the interaction. If Ag⁺ is complexed

without displacing H⁺ ions, this means that either the groups involved have no acid-base properties or have completely lost their proton due to dissociation at that pH condition.

For the purpose of discussion, the values of the slope of curves deduced from Figs. 4 and 5 are shown in Table 4. The values correspond to the mean values of H⁺ ions displaced/Ag⁺ ion complexed at different pH conditions and in the indicated \bar{v}_{Ag} interval.

TABLE 4

pH	$(-\Delta\bar{v}_H)/(\Delta\bar{v}_{Ag})$		
	$\bar{v}_{Ag} = 1-4$	$\bar{v}_{Ag} = 4-8$	$\bar{v}_{Ag} > 8$
4	0.4	—	—
5	0.35	0.55	—
6	0.4	0.40	0.18
7	0.15	0.55	0.15
8	0.25	0.50	0.36
9	0.25-0.9	0.9-0.65	1.2-0.6
10	0.8-1.28	1.25	1.50

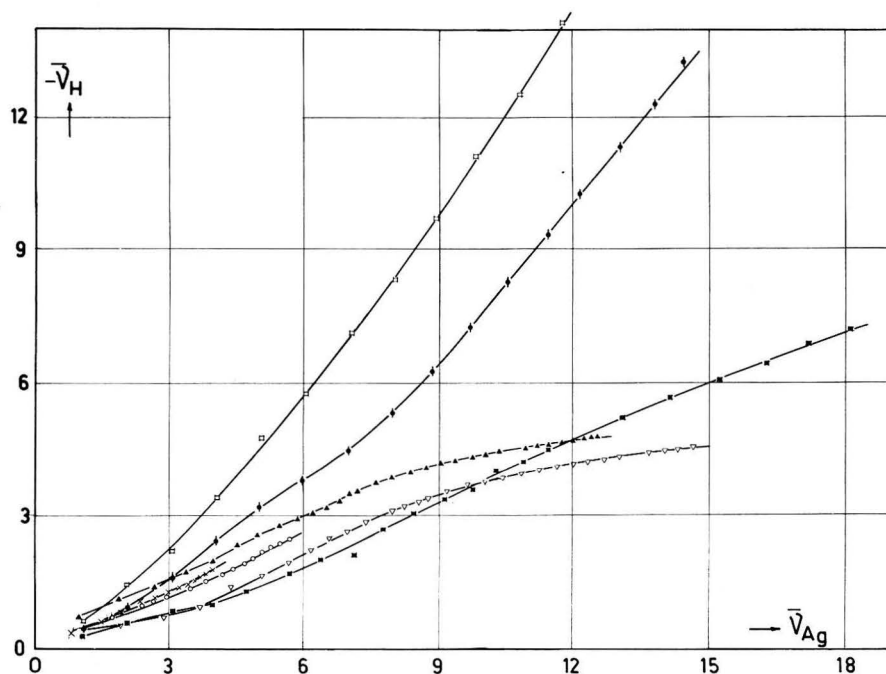


Fig. 4. Displacement of H⁺ ions by binding of Ag⁺ ions, as a function of the pH: (×), 4; (○), 5; (Δ), 6; (∇), 7; (■), 8; (◆), 9; (□), 10.

Displacement of approximately 0.4 H⁺ ion/Ag⁺ ion bound is seen at pH 4. Such a low value excludes the possibility that imidazole- or amino-groups may be involved since, being fully protonated at that pH-value, they would displace a greater quantity of H⁺ ions. Among the various ligand groups present in gelatin, the only groups to be

taken into consideration are the carboxyl groups, preferably those showing more acid properties because of their position in the protein molecule.

The same can be said of the first four Ag^+ ions which are complexable at pH 5. When the pH increases, the quantity of H^+ ions displaced by the first three or four Ag^+ ions complexed, has a tendency to decrease. The succeeding Ag^+ ions displace a higher quantity of H^+ (about 0.55). In this case, the complexing action can be ascribed to the less acid carboxyls (more protonated) or to incipient action of imidazole groups.

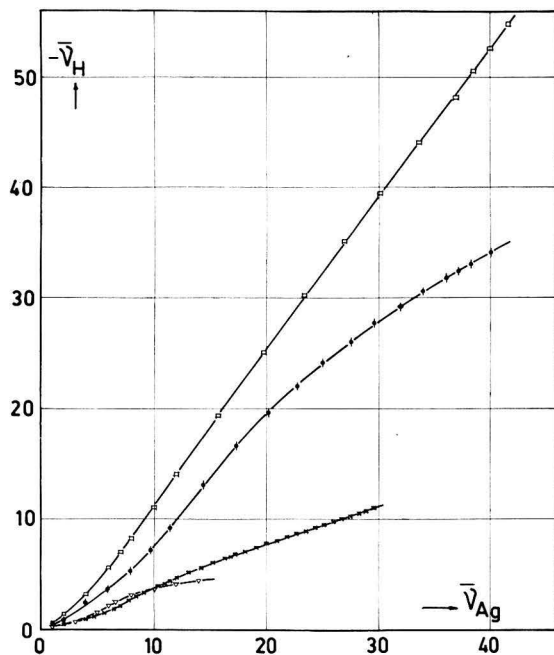


Fig. 5. Displacement of H^+ ions by binding of Ag^+ ions, as a function of the pH: (∇), 7; (\blacksquare), 8; (\blacklozenge), 9; (\circ), 10.

At that pH-value when amino-groups are involved in the formation of chelates, the H^+ displacement should be greater.

At pH 6, the slope of the curve increases for the first few Ag^+ ions. Moreover, there is a decided displacement of H^+ ions caused by the first complexed Ag^+ (about 0.75 H^+ ions) noticeably higher than the one measured at lower pH-values (Fig. 4). An appreciable increase of the pAg can, in fact, be observed in the graph pAg/pH (Fig. 3) at about pH 6 for $\bar{v}_{\text{Ag}} = 1$. This indicates the formation of more stable complexes and therefore requires the presence of groups with different chemical natures. They might be the imidazole- or the α -amino-groups. The ϵ -amino groups would displace a greater quantity of H^+ ions and cannot therefore be considered. Under these conditions, there would be mixed chelates by carboxyl- and imidazole-groups, or carboxyl- and α -amino-groups. Above $\bar{v}_{\text{Ag}} 8$, the slope of the curve descends again to 0.2, approximately. When the imidazole- and α -amino-groups, eight in all, are used

up, the only remaining active groups at this pH are the carboxyls that liberate small quantities of H^+ when they are complexed because they are highly dissociated.

At pH 7, similar reasons support the hypothesis that the first Ag^+ ions are complexed with carboxyl- and imidazole-groups in a mixed chelate and the succeeding groups are bound to carboxyl- and α -amino-groups because of the greater H^+ ion displacement. The succeeding decrease of the slope again indicates that the ligand groups left after $\bar{\nu}_{\text{Ag}}=8$ are the carboxyls.

The reading of the curve at pH 8 is more difficult. While a complexing action can reasonably be ascribed to the imidazole- and α -amino-groups up to $\bar{\nu}_{\text{Ag}}$ 8, the constant, relatively high slope of the curve that is noticeable for $\bar{\nu}_{\text{Ag}}$ 8–30, causes some perplexity as to the identification of the ligand group. Indeed, as the slope of the curve is so high, the action obviously cannot be attributed to the carboxyl groups only and would not explain the increase from 0.15–0.36 going from pH 7–8. On the other hand, the H^+ ion displacement seems to be too small to be caused by ϵ -amino groups which, with their alkaline properties, should not give a slope of a value much lower than 1. The same difficulty can also be encountered in part in reading the curve at pH 9, although the greater slope of the curve seems to indicate a possible intervention of the ϵ -amino groups.

In our opinion the results can be explained if under these conditions, peptide links take part in the chelation. This possibility has rarely been considered in the study of the metal–protein complexes; however, mention should be made of the work of DATTA AND RABIN⁸, RABIN⁹ and KOLTUN, FRIED AND GURD¹⁰ on the chelation of copper by dipeptides, and the recent research by BRESLOW AND GURD¹¹ on Cu^{2+} and Zn^{2+} interaction with sperm-whale myoglobin. The unexpected displacement of H^+ observed by the above-mentioned authors, is therefore connected with the dissociation of hydrogen from the complexed peptide group.

The $-\text{CO}-\text{NH}-$ group has extremely weak acid properties, and consequently its dissociation is generally disregarded at pH-values lower than 13 or 14. Hydrogen can dissociate only when the peptide link takes part in the chelate formation^{9,10}. The gradual dissociation of the peptide hydrogen that increases with the alkalinity of the environment seems to explain the slope of the curve at pH 8 and 9 and in particular the increase of the slope with increase of alkalinity.

At pH 8, the first eight Ag^+ ions would then bind with the imidazole- and α -amino-groups and the succeeding ones would be chelated by the peptide links, due, of course, to the intervention of the carboxyls.

The curve at pH 9 can be similarly interpreted although the slope of the curve which is higher in the initial part indicates that participation of the ϵ -amino groups is probable, as already stated.

At pH 10, the graph assumes a peculiar aspect: when the first six or seven Ag^+ ions are complexed, the curve has a constant slope with a value 1.5, in the whole $\bar{\nu}_{\text{Ag}}$ interval examined, *i.e.*, up to and even more than 40 Ag^+ ions bound. If the ϵ -amino group takes part in the chelate formation together with the peptide group, the value, 1.5, of the slope is fully explained: for each Ag^+ ion bound, one H^+ ion from the peptide link and half a H^+ ion from the ϵ -amino group, are displaced; 50% of the ϵ -amino group should, in fact, be dissociated at pH 10 ($\log k_{\text{H}}=10$).

In regard to the behaviour of the system in a decidedly acid environment (pH 1–3), it can be seen that Ag^+ is fixed by gelatin in the interval considered, independent-

ly of the pH (Fig. 2), reaching a maximum number of 4 Ag^+ ions bound/mole of gelatin, and no measurable H^+ displacement is noted. The difficulty in the interpretation as far as formation of complexes is concerned, is that none of the ligand groups that are generally considered remains in its active (basic) form at these low pH-values. A similar effect was observed by WORMSER¹² in a Ag^+ -serum albumine system. The author, although emphasizing the close analogy with adsorption processes, does not propose any particular interpretation. The subject is still being studied experimentally.

CONCLUSION

The results obtained lead to the conclusion that in gelatin several ligand groups are simultaneously active, with different nature and affinity for Ag^+ . According to the pH, one group prevails over the other and, at a constant pH, Ag^+ progressively occupies sites of lower affinity, going from one class to another as its concentration increases. For instance, at pH 7 we notice first the occupation of the imidazole groups, then of α -amino groups and finally of the carboxyls only. It is practically impossible to isolate the action of one type of ligand group, with the exception, perhaps, of the first few Ag^+ ions at pH 4 and 5 where only carboxyl groups seem to take part in the complexing. Owing to the complexity of the problem, it is inadvisable to propose a deeper interpretation on the basis of the data obtained. Instead, it is of interest to point out certain characteristics that seem a peculiarity of the Ag^+ -gelatin system.

Although, for instance, formation of chelates is considered more an exception than a rule in the metal-protein interaction⁴, in this case it seems to be the prevailing form of interaction if not the only one. This is probably due to the steric form of the Ag^+ ion, which is particularly suitable for intramolecular cross-linking through $5s\bar{p}$ orbitals of linear symmetry.

Although cross-linking of some metal-protein systems, *e.g.*, Hg^{2+} -serum albumine (dimer)¹⁶, Hg^{2+} -papain¹⁷, Zn^{2+} -insulin¹⁸, Fe^{3+} -transferrin¹⁹ and Cr^{3+} -collagen²⁰, are described in the literature, equally clear examples in the Ag^+ -protein systems are not known. This is probably due to a scarcity of work on the subject. We wish to point out, however, that in the Ag^+ -polyvinylimidazole complex the coordination number of 2 was given¹³ to Ag^+ .

In the Ag^+ -gelatin interaction, a large number of sites in the protein molecule is noted; at pH 10, no tendency to saturation can be noted even after complexing more than 40 Ag^+ ions/mole. In most cases, instead, the number of metal ions complexed in the interaction with proteins is relatively small and often corresponds to the number of certain ligand groups present in the molecule.

Serum albumin, for instance, binds 16 Zn^{2+} ions, below 37°, corresponding with the 16 imidazole groups present²¹. In the Zn^{2+} -insulin system, it can be found that each protein molecule binds one Zn^{2+} ion⁴; metmyoglobin binds a maximum of 7 Zn^{2+} or Cu^{2+} ions/mole¹¹.

The Cu^{2+} -serum albumin system, on the other hand, presents a certain analogy with the Ag^+ -gelatin system; in this case, also, saturation at pH 9 is not reached and the maximum value of \bar{v}_M remains undetermined. However, in the case of Cu^{2+} -serum albumine, the investigation is greatly limited by hydrolysis of Cu^{2+} and its precipitation in a more alkaline environment. Ag^+ ion is very suitable for the study of

interaction with proteins in an alkaline environment because its tendency to hydrolysis is negligible²² up to at least pH 10.

Quantitatively, it is evident that the Ag^+ -gelatin interaction has not the simplicity of an ideal model for mathematical treatment. Any tentative application of eqns. (5) and (6) might, at the most, demonstrate once again the difficulty of finding the stability constants of the several types of complexes. This subject might be developed by systematic research on synthetic polymer models or on the gelatin itself, suitably modified by chemical inactivation of the various types of ligand groups. Further work in this direction is in progress.

ACKNOWLEDGEMENT

We wish to thank the Research Department of the company "Ferrania S. p. A.", for their interest in our work and for preparing the samples of de-ionized gelatin.

This research was supported by a financial contribution from the C.N.R.

SUMMARY

From a study of the Ag^+ -gelatin system it can be deduced that complex formation is possible in the whole pH-range examined (1.5-10). The ligand groups of gelatin, carboxyl, α - and ϵ -amino and imidazole groups, can be active simultaneously; the predominant action of one or other group depends on the pH. In alkaline environment (pH > 8) the Ag^+ complex directly affects the peptide link.

From the observed pAg -values and the measurement of the number of H^+ ions displaced/ Ag^+ ion complexed, it can be deduced that the interaction Ag^+ -gelatin leads essentially to the formation of chelate complexes.

REFERENCES

- 1 B. H. CARROLL AND D. HUBBARD, *J. Res. Nat. Bur. Std.*, 7 (1931) 811.
- 2 E. J. COHN AND J. T. EDSALL, *Proteins, Amino Acids and Peptides*, Reinhold, New York, 1943.
- 3 I. M. KLOTZ, *The Proteins*, Vol. I, Part B, edited by H. NEURATH AND K. BAILEY, Academic Press, New York, 1953, p. 727.
- 4 F. R. N. GURD AND P. E. WILCOX, *Advances in Protein Chemistry*, 11 (1956) 311.
- 5 C. TANFORD, *Electrochemistry in Biology and Medicine*, edited by T. SHEDLOVSKY, Wiley, New York, 1955, p. 248.
- 6 M. NAGASAWA AND A. HOLTZER, *J. Am. Chem. Soc.*, 86 (1964) 531.
- 7 P. LANZA AND I. MAZZEI, *Ann. Chim. Rome*, 53 (1963) 1833.
- 8 S. P. DATTA AND B. R. RABIN, *Trans. Faraday Soc.*, 52 (1956) 1123.
- 9 B. R. RABIN, *Trans. Faraday Soc.*, 52 (1956) 1130.
- 10 W. L. KOLTUN, M. FRIED AND F. R. N. GURD, *J. Am. Chem. Soc.*, 82 (1960) 233.
- 11 E. BRESLOW AND F. R. N. GURD, *J. Biol. Chem.*, 238 (1963) 1332.
- 12 W. WORMSER, *J. Chim. Phys.*, 48 (1951) 344.
- 13 D. H. GOLD AND H. F. GREGOR, *J. Phys. Chem.*, 64 (1960) 1461.
- 14 J. BJERRUM, *Metal Amine Formation in Aqueous Solution*, Haase and Sons, Copenhagen, 1941.
- 15 F. H. McDougall AND S. PETERSON, *J. Phys. Colloid Chem.*, 51 (1947) 1346.
- 16 W. L. HUGHES JR., *J. Am. Chem. Soc.*, 69 (1947) 1836.
- 17 E. L. SMITH, I. R. KIMMEL AND D. R. BROWN, *J. Biol. Chem.*, 207 (1954) 533.
- 18 C. TANFORD AND J. EPSTEIN, *J. Am. Chem. Soc.*, 76 (1954) 2163.
- 19 B. A. KOEHLIN, *J. Am. Chem. Soc.*, 74 (1952) 2649.
- 20 K. H. GUSTAVSON, *The Chemistry and Reactivity of Collagen*, Academic Press, New York, 1956.
- 21 F. H. N. GURD AND D. S. GURDMAN, *J. Am. Chem. Soc.*, 74 (1952) 670.
- 22 J. BJERRUM, *Chem. Rev.*, 46 (1950) 381.

POTENTIAL SWEEP CHRONOAMPEROMETRY IN DIMETHYL SULFOXIDE AT THE HANGING MERCURY DROP ELECTRODE

JERRY L. JONES AND HERBERT A. FRITSCHÉ, JR.

Department of Chemistry, Texas A&M University, College Station, Texas (U.S.A.)

(Received November 19th, 1965)

INTRODUCTION

Several workers have carried out electrochemical investigations in dimethyl sulfoxide (DMSO). It has been used in a study of solvent effects on the oxidation of iodide ion¹ and has been considered for possible use in the electrodeposition of cerium and plutonium². Most results reported have been obtained utilizing the dropping mercury electrode (DME)³⁻⁸, the rotating mercury pool electrode⁴ and the rotating platinum electrode⁴. More recently, a method for the determination of carbon dioxide in DMSO at gold, platinum, amalgamated gold, and amalgamated platinum electrodes was published⁹.

This investigation extends existing studies to include the use of chronoamperometry with a single potential sweep at the hanging mercury drop electrode (HMDE).

EXPERIMENTAL

Electrical measurements

The experiments were carried out with a d.c. polarograph (Model FS, E. H. Sargent & Co.) which had calibrated sweep rates of 16.6, 24.9, 33.1, 41.4, and 49.7 mV/sec. The potential of the working electrode was controlled with a potentiostat (E. H. Sargent & Co.) which is similar to the one described by ARTHUR¹⁰. Voltages are reported *vs.* the aqueous saturated calomel electrode (SCE) and are uncorrected for junction potentials. Temperatures were regulated at $25.0 \pm 0.1^\circ$. Bridge voltages were checked with a calibrated digital voltmeter (NLS Model 4312, Non-Linear Systems, Inc.). The solution was not stirred during potential scans.

Half-wave and peak potentials

The peak potentials obtained from the polarograph were converted to half-wave potentials by subtracting $28/n$ mV from the measured peak potential where n is the number of faradays transferred/mole of reactant¹¹.

Cell

The electrochemical cell was a 150-ml chamber with one side arm 5 cm long. The side arm was fabricated so that it accommodated two neoprene "O" rings (13 mm o.d. \times 10 mm i.d.) located about 2 cm apart. This arm received a capillary probe reference electrode chamber.

Electrodes

The working electrode was a hanging mercury drop electrode¹² the usual drop area of which was 0.030 cm². The area was calculated from the weight of a determined number of drops provided by a conventional DME at zero volts applied potential.

The counter electrode was a short length of 22-gauge platinum wire which was inserted directly into the test solution on the side of the working electrode that was opposite the reference electrode probe.

The reference electrode assembly consisted of a commercial fiber-junction SCE which was inserted into a separate chamber. This chamber was made of glass tubing and contained a 90° bend. One portion fitted horizontally into the side arm of the cell through the two "O" ring seals and terminated as a capillary probe with an orifice of about 0.1 mm diam. The tip was plugged with a very small quantity of agar gel of conventional composition. The vertical portion of the chamber was slightly larger and received the SCE. The chamber was filled with an aqueous saturated KCl solution. Horizontal adjustment of the working electrode-reference electrode distance was easily accomplished by manual adjustment of the separate chamber. This distance was never greater than 0.5 mm during measurements with the HMDE.

Reagents

Pre-purified grade nitrogen (minimum purity 99.996%) was used without further purification for de-aeration. It was also used to maintain a protective covering during measurements.

Reagent-grade DMSO (Fisher Scientific Company) or reclaimed DMSO⁴ gave virtually no residual current until a potential of -2.7 V was reached after which a current of about 0.1 μ A was observed.

Tetrabutylammonium perchlorate was synthesized in the following manner. A portion of Eastman White-Label grade tetrabutylammonium iodide was dissolved in a 60% solution of perchloric acid. Water was then added to precipitate the tetrabutylammonium perchlorate. The pale yellow crystals were washed with cold water and filtered. They were recrystallized once from a 50% (v/v) acetone-water solution and the pure, white crystals were dried for 4 h at 60°.

All other chemicals were reagent grade. De-ionized water was used. Depolarizer salts were dried in an oven at 100° or under vacuum with phosphorus pentoxide. Thallium solutions were prepared from the metal using a minimum amount of nitric acid.

Potentiostatic control

TAYLOR AND SMITH¹³ have indicated that in ordinary solutions of low specific resistance the *IR* drop in the immediate vicinity of the working electrode may be large enough to measure. Also, KNECHT AND KOLTHOFF¹⁴ point out that even in a solvent the dielectric constant of which is greater than that of water, as in the case of N-methylacetamide, the resistance of the solution can be at least ten times as great as that of an aqueous solution of comparable electrolyte concentration. Thus, it frequently becomes desirable to introduce into the measurements some means of compensation for the *IR* drop in the solution. This is necessary in order to make measured half-wave or peak potentials as meaningful as possible.

IR drop as a source of measurement error becomes most significant when the

specific conductivity is low or the current density to be used is high. The results of BARNARTT'S¹⁵ study indicate that when electrode polarization is accompanied by a high current density, some type of potentiostatic control could give improved results even in aqueous solutions. The need for such compensation in ordinary d.c. polarographic measurements in water is uncommon since currents usually need not exceed several microamperes in magnitude. However, the use of unusually high depolarizer concentrations with consequently greater currents can give rise to appreciable distortion in the uncompensated polarogram, unless potentiostatic control is utilized.

NEMEC¹⁶ has suggested that *IR* compensation is relatively ineffective for the DME, largely because of the complications involved with the proper location of the Luggin capillary. This arises because of the constantly changing distance between the working electrode surface and the tip of the reference electrode probe. The use of the stationary drop electrode has an obvious advantage over the conventional dropping mercury electrode in this respect.

The stationary HMDE used in these experiments was constructed so that shielding of the working electrode was minimum. Careful attention was given to maintaining the least possible distance between the tip of the reference probe and the HMDE¹⁷.

RESULTS

Carrier electrolytes

Several electrolytes were used to suppress migration currents in the DMSO. As expected, the combination of a tetraalkylammonium cation and the perchlorate anion

TABLE 1
POTENTIAL RANGES OF CARRIER ELECTROLYTES IN DMSO (VOLTAGES MEASURED *vs.* SCE)

<i>Carrier electrolyte</i> ^a	<i>Anodic limit (V)</i>	<i>Cathodic limit (V)</i>	<i>Reference</i> ^b
<i>0.10 M</i>			
KClO ₄	+0.20	-1.84	8
KClO ₄	+0.30	-1.88	
Bu ₄ NClO ₄	+0.31	-3.00	8
Bu ₄ NClO ₄	+0.37	-2.70	
Bu ₄ NI	-0.41	-2.85	
LiCl	-0.21	-2.17	
NaClO ₄	+0.25	-1.90	4
Et ₄ NClO ₄	+0.25	-2.80	4
Et ₄ NNO ₃	-0.20	-2.74	3
<i>0.010 M</i>			
NaNO ₃	+0.31	-1.85	
NaC ₂ H ₃ O ₂	-0.10	-1.96	

^a Bu = *n*-butyl; Et = ethyl

^b Values without refs. are those determined in this investigation.

give the widest possible useful polarization range. This combines a difficultly reduced cation with an anion lending minimum stability to the oxidation product of mercury.

Table 1 gives the cathodic and anodic polarization limits obtained at the HMDE with six electrolytes. Literature values for other salts are included for completeness and permit comparisons in the cases of 0.10 *M* potassium perchlorate and

0.10 *M* tetrabutylammonium perchlorate. Solutions of sodium nitrate and sodium acetate more concentrated than 0.01 *M* were not easily prepared due to solubility limitations. The other salts listed were readily soluble in DMSO.

Oxygen

Two waves of oxygen were observed in 0.10 *M* KClO₄ in DMSO. The first one was well formed and exhibited a peak potential of -0.73 V. The second wave was poorly defined and gave a drawn-out wave the peak of which occurred at approximately -1.5 V. The height of the second wave appeared to be considerably less than that of the first. One of the difficulties of the potential sweep method, however, is the uncertainty involved in measuring the peak currents of waves that have been preceded by earlier ones.

A more thorough investigation of the oxygen waves obtained in DMSO is in progress and the results will be published later.

Tests for diffusion control

If the mass-transfer process is diffusion-controlled, a Randles–Sevčik^{18,19} plot of peak current against the square root of the voltage scan rate should be linear. This is true for both reversible and irreversible electrode reactions. If, however, the plot is non-linear, irreversibility may be indicated, provided that no significant *IR* drop goes uncompensated and that depletion effects are eliminated by stirring after each potential sweep. Both of these requirements were met in this study and a Randles–Sevčik plot was made for each of the depolarizers examined.

The five scan rates used in this study fall within the limits suggested by FRANKENTHAL AND SHAIN²⁰ and DELAHAY²¹. They point out that at slow scan rates, convection can give rise to peak currents which are greater than those predicted from theory. Conversely, very fast or repetitious scans produce a depletion effect and, consequently, smaller peak currents than expected.

TABLE 2
COMPARISON OF HALF-WAVE POTENTIALS IN DMSO
(Voltage measured *vs.* SCE)

Depolarizer	Peak potential	Calculated $E_{\frac{1}{2}}$	Literature
Cd ²⁺	-0.65^a	-0.64	see text
Co ²⁺	-1.44^a	-1.43	$-1.4^{c,4}$
Mn ²⁺	-1.74^a	-1.73	$-1.68^{b,8}$
Ni ²⁺	-1.11^b	-1.10	$-1.14^{b,8}$
Pb ²⁺	-0.51^b	-0.50	$-0.53^{b,8}$
Mg ²⁺	-2.20^a	-2.19	$-2.28^{d,3}$
K ⁺	-2.09^a	-2.06	$-2.11^{d,3}$
Li ⁺	-2.41^a	-2.38	$-2.45^{d,3}$
Tl ⁺	-0.53^a	-0.50	—
O ₂	$-0.73,$ -1.5^b	—	see text

^a 0.10 *M* tetrabutylammonium perchlorate carrier electrolyte

^b 0.10 *M* potassium perchlorate carrier electrolyte

^c 0.10 *M* sodium perchlorate carrier electrolyte

^d 0.10 *M* tetraethylammonium perchlorate carrier electrolyte

Randles-Sevcik plots for $\text{Mg}(\text{NO}_3)_2$, MnCl_2 , $\text{Co}(\text{NO}_3)_2$, LiNO_3 and TlNO_3 were linear, which indicates that the reductions of these salts are describable in terms of semi-infinite linear diffusion. Plots obtained using solutions of $\text{Cd}(\text{NO}_3)_2$, KClO_4 , $\text{Pb}(\text{NO}_3)_2$ and $\text{Ni}(\text{NO}_3)_2$ showed degrees of non-linearity which increased in that order. The peak current due to Ni^{2+} increased much less per unit increase in scan rate than did that of any other depolarizer and the Randles-Sevcik plot exhibited curvature. The curvature observed in the several cases indicate that simple diffusion is not the sole rate-determining process in those instances.

Millimolar solutions of depolarizer in the appropriate carrier electrolyte listed in Table 2 were used for the tests of diffusion control.

Peak potentials

Millimolar solutions were used to obtain peak potentials of nine depolarizers. These were recorded at a scan rate of 33.1 mV sec^{-1} . Scan rates between 16.6 and 49.7 mV sec^{-1} gave few significant differences in peak potentials. Table 2 lists the depolarizers investigated and permits a comparison of calculated half-wave potentials with previously published results. The carrier electrolytes used are designated in the table.

The calculated half-wave potentials of Co^{2+} , Mn^{2+} , Ni^{2+} , Pb^{2+} , Mg^{2+} , K^+ , and Li^+ agree with previously reported values.

No literature value for the half-wave potential of thallium in DMSO could be found. The value of -0.50 V vs. the aqueous SCE obtained in this investigation compares favorably with that found in water²². The value found in N-methylacetamide is reported¹⁴ to be -0.42 V .

Cadmium

Cadmium solutions in KClO_4 were examined in detail. Some of the measurements were made with a conventional DME ($t=5.0 \text{ sec}$ at $E_{\frac{1}{2}}$, $h=54 \text{ cm}$) so that further characterization of the solvent-electrolyte systems would be possible. For these measurements, the Model FS polarograph was modified by exchanging the chart drive and bridge drive motors for others with slower speeds so that the electrical characteristics of the instrument resembled those of a conventional d.c. polarograph.

Half-wave potentials of millimolar cadmium solutions were -0.66 V and -0.63 V at the DME in 1.0 M KClO_4 and 0.10 M KClO_4 , respectively. The polarographic wave plots obtained were linear and had slopes of 0.029 V in 1.0 M KClO_4 and 0.034 V in 0.10 M KClO_4 .

The conventional polarograms were well formed in all cases. No misbehavior by the capillary electrode was noted except for an occasional bad drop or very small maximum in a few of the more concentrated solutions.

A typical cell resistance reading was $0.20 \text{ M}\Omega$ when measured through the capillary probe electrode and the DME. The values obtained with a simple 60-cycle Wheatstone bridge and by calculation using Ohm's law and the displacement of $E_{\frac{1}{2}}$ upon removal of the potentiostat agreed satisfactorily.

Although half-wave potentials changed significantly upon the removal of the potentiostat from the measuring circuit (largely due to uncompensated resistance in the capillary reference probe), the change in limiting diffusion current was negligible ($<0.6\%$) in the case of millimolar cadmium in 0.10 M KClO_4 .

The influence of the depolarizer concentration as well as that of the carrier electrolyte concentration can be seen in Table 3. These data record peak potentials of the carrier electrolyte concentration.

The addition of successive 1-ml aliquots of water (0.10 *M* in KClO_4) to a millimolar cadmium solution in 0.10 *M* KClO_4 in DMSO followed by de-aeration for 2 min caused measurable shifts (10–50 mV) of the peak potential and the conventional half-wave potential. The magnitude, rate, and direction of these shifts varied with the total water content, with time, and with the cross-sectional area of the tip of the

TABLE 3

INFLUENCE OF CARRIER ELECTROLYTE CONCENTRATION ON THE PEAK POTENTIAL OF CADMIUM IN DMSO

<i>Molarity</i> <i>KClO</i> ₄	<i>E</i> _p (<i>V</i>) 1.00 · 10 ⁻³ <i>M Cd</i> ²⁺	<i>E</i> _p (<i>V</i>) 5.00 · 10 ⁻⁴ <i>M Cd</i> ²⁺
10 ⁻³	-0.71	-0.72
10 ⁻²	-0.65	-0.68
10 ⁻¹	-0.65	-0.67
10 ⁰	-0.66	-0.65

capillary reference probe. Final equilibrium values of peak potentials or conventional half-wave potentials were generally more negative than the value obtained in dry DMSO. These shifts are probably due largely to changes in the liquid junction potential across the capillary reference probe tip.

DISCUSSION AND CONCLUSIONS

Although, of all the electrolytes examined, tetrabutylammonium perchlorate permits the widest possible voltage scan, several common salts can function as carrier electrolytes in DMSO. Potassium perchlorate was commonly used in this investigation since synthesis was unnecessary and most common cations are more easily reduced in DMSO than is potassium ion. The solubility behavior of potassium perchlorate is very satisfactory and the salt is recommended for general use in DMSO.

The behavior of oxygen in DMSO resembles that observed in water and several organic solvents^{4,14,23,24}. Two waves are formed. The first, at -0.73 V, is well formed, while the second one, which occurs at about -1.5 V, is poorly defined and is apparently quite irreversible.

The magnesium wave observed at -2.20 V required the use of a tetraalkylammonium salt as the carrier electrolyte. It was well formed in DMSO but would be unobservable in ordinary aqueous solutions because of interference from hydrogen evolution.

Assuming that the reduction of cadmium in DMSO is a two-electron process, the slopes of 0.029 V and 0.034 V obtained from the conventional plots of the polarographic wave equation indicate that the single-step process is almost reversible. That the process may not be completely reversible when using the faster scan rates, is indicated by the small dependence of the peak potential on the depolarizer concentration as shown in Table 3.

The reduction of millimolar cadmium in 0.10 *M* KClO_4 in DMSO is probably

diffusion-controlled at the DME since a series of values of the ratio of the diffusion current to the square root of the height of the mercury column were constant to within $\pm 4\%$ of the mean value. This finding agrees with that of BURRUS⁸.

BURRUS also showed that a plot of wave height *vs.* concentration for several ions in DMSO is linear. The plot shown by BURRUS for cadmium is linear at least up to $1.0 \cdot 10^{-3} M$ in $1 M KClO_4$, $0.1 M KClO_4$, and $0.1 M (n-C_4H_9)_4NClO_4$. Slopes of the plots in these carrier electrolytes were reported as 3.18, 5.36, and $5.56 \mu A/mmole$, respectively.

ACKNOWLEDGEMENT

We are indebted to the Research Council of the Graduate College, Texas A&M University, for partial support of this work.

SUMMARY

Electroanalytical studies in dimethyl sulfoxide have been extended to the hanging mercury drop electrode. Potential sweep chronoamperometry was utilized with potentiostatic control of the working electrode. Several ions have been examined for diffusion control in this system by means of the Randles-Sevcik equation. Half-wave potentials of selected depolarizers and polarization limits of several carrier electrolytes have been measured.

REFERENCES

- 1 R. T. IWAMOTO, *Anal. Chem.*, 31 (1959) 955.
- 2 J. A. PORTER, U. S. Atomic Energy Commission D. P. - 389 (1959) pp. 1-12.
- 3 V. GUTMANN, P. HEILMEYER AND G. SCHOEBER, *Monatsh. Chem.*, 92 (1962) 240.
- 4 I. M. KOLTHOFF AND T. B. REDDY, *J. Electrochem. Soc.*, 108 (1961) 980.
- 5 T. B. REDDY, *Electrochemistry and Acid-Base Studies in Dimethyl Sulfoxide as Solvent*, Ph.D. Thesis, University of Minnesota, 1960.
- 6 V. GUTMANN AND G. SCHOEBER, *Advances in Polarography*, Vol. 3, Pergamon Press, New York, 1960, p. 940.
- 7 V. GUTMANN AND G. SCHOEBER, *Monatsh. Chem.*, 93 (1962) 212.
- 8 R. T. BURRUS, *Polarographic Studies in Dimethyl Sulfoxide*, Ph.D. Thesis, University of Tennessee, 1962.
- 9 J. L. ROBERTS, JR. AND D. T. SAWYER, *J. Electroanal. Chem.*, 9 (1965) 1.
- 10 P. ARTHUR AND R. K. VANDERKAM, *Anal. Chem.*, 33 (1961) 765.
- 11 W. T. DE VRIES AND E. VAN DALEN, *J. Electroanal. Chem.*, 6 (1963) 490.
- 12 E. H. SARGENT & Co., *Instruction Manual for Fast Sweep Polarograph*, pp. 12-13.
- 13 J. K. TAYLOR AND S. W. SMITH, *J. Res. Nat. Bur. Std.*, 56 (1956) 143.
- 14 L. C. KNECHT AND I. M. KOLTHOFF, *Inorg. Chem.*, 1 (1962) 195.
- 15 S. BARNARTT, *J. Electrochem. Soc.*, 108 (1961) 102.
- 16 L. NĚMEC, *J. Electroanal. Chem.*, 8 (1964) 166.
- 17 W. SCHAAP AND P. MCKINNEY, *Anal. Chem.*, 36 (1964) 1251.
- 18 J. E. B. RANDES, *Trans. Faraday Soc.*, 44 (1948) 327.
- 19 A. ŠEVČÍK, *Collection Czech. Chem. Commun.*, 13 (1948) 349.
- 20 R. P. FRANKENTHAL AND I. SHAIN, *J. Am. Chem. Soc.*, 78 (1956) 2969.
- 21 P. DELAHAY, *J. Am. Chem. Soc.*, 75 (1953) 1190.
- 22 L. MEITES, *Polarographic Techniques*, Interscience Publishers, Inc., New York, 1955, p. 285.
- 23 J. COETZEE AND W.-S. SIAO, *Inorg. Chem.*, 2 (1963) 14.
- 24 J. COETZEE AND I. KOLTHOFF, *J. Am. Chem. Soc.*, 79 (1957) 6110.

DETERMINATION POLAROGRAPHIQUE DE LA NITROHYDROXYLAMINE

A. CĂLUȘARU

Institut de polarographie "J. Heyrovský", Prague (Tchécoslovaquie)

(Reçu le 12 novembre, 1965)

INTRODUCTION

Le composé azoté de formule brute $\text{Na}_2\text{N}_2\text{O}_3$ est le plus souvent dénommé nitrohydroxylamine de sodium¹⁻⁴, correspondant au sel de sodium de l'acide hypothétique $\text{H}_2\text{N}_2\text{O}_3$, appelé acide nitrohydroxylaminique⁴ ou nitrohydroxylamine^{2,3}. Dans d'autres travaux⁵ la même substance est dénommée α -oxyhyponitrite de sodium pour pouvoir la différencier de son isomère β -oxyhyponitrite de sodium. L'isomère α peut être obtenu par l'action du nitrate d'éthyle sur l'hydroxylamine, tandis que l'isomère β peut être obtenu par l'action du tétraoxyde d'azote liquide sur l'hyponitrite de sodium⁵.

Ce travail étudie la détermination polarographique de l'ion nitrohydroxylaminique (α -oxyhyponitrite).

La détermination quantitative par titration avec du permanganate de potassium est relativement compliquée et implique un temps assez long d'analyse⁶. En tenant compte du fait que les solutions aqueuses de cette substance ne sont pas stables, il est préférable d'employer une méthode physico-chimique rapide. Dans la littérature, deux méthodes seulement sont décrites: (1) une méthode spectrométrique^{5,7} qui n'est pas utilisable en présence d'autres composés azotés⁶ et (2) une méthode colorimétrique⁸ fondée sur la détermination du complexe $[\text{Ni}(\text{CN})_3\text{NO}]^{2-}$. Ce complexe résulte de la réaction de la nitrohydroxylamine avec le complexe $[\text{Ni}(\text{CN})_4]^{2-}$. La méthode n'est pas applicable en présence de l'hydroxylamine.

On a constaté auparavant⁸ que la nitrohydroxylamine forme en présence du cobalt un complexe nitrohydroxylamine qui donne une vague catalytique en polarographie. Dans le travail présent, on étudie une méthode polarographique quantitative, à partir de cette vague catalytique.

RÉACTIFS ET APPAREILLAGE

Afin d'effectuer les courbes d'étalonnage, il est nécessaire d'utiliser la nitrohydroxylamine de sodium à l'état très pur. On a effectué la synthèse de cette substance d'après la méthode d'ANGELI¹, utilisée aussi dans d'autres travaux^{3,5,8,9,10}.

Puisque la détermination polarographique nécessite l'utilisation de solutions faiblement ammoniacales, on a travaillé avec des solutions fraîchement préparées. On a constaté que ces solutions sont stables pendant 1 h à la température ambiante et 4 h à 2°. On a utilisé un polarographe type LP 55, avec une cellule de Kalousek dont l'anode est une électrode saturée de calomel. Le capillaire a les caractéristiques

* Adresse permanente: Institut de Physique Atomique, Bucarest, Roumanie.

suivantes: $m = 2.73 \text{ mg sec}^{-1}$ et $t_1 = 3 \text{ sec}$, en circuit ouvert, $h = 85 \text{ cm}$ et dans la solution suivante: NH_4Cl , 0.1 M ; NH_4OH , 0.07 M ; CoCl_2 , 0.001 M ; gélatine, 0.01% . Sensibilité du galvanomètre, $1.82 \times 10^{-9} \text{ A/mm}$.

RÉSULTATS EXPÉRIMENTAUX

Influence de quelques facteurs physico-chimiques

Cobalt. A une concentration constante en nitrohydroxylamine, la hauteur de la vague croît lorsque la concentration en cobalt augmente. La Fig. 1 montre la variation de la hauteur de la vague catalytique en fonction de la concentration en cobalt. La courbe a la forme d'une parabole avec un exposant inférieur à l'unité (0.75). Toutefois le rapport entre la vague catalytique et la vague du cobalt diminue avec la croissance de la concentration en cobalt^{9,10}. C'est la raison pour laquelle il est nécessaire d'utiliser des petites concentrations en cobalt lorsque l'on désire travailler à des sensibilités plus grandes.

Solution tampon et pouvoir tampon. La vague de la nitrohydroxylamine en présence du cobalt peut être obtenue soit en solutions tamponées, soit en solutions non tamponées⁸⁻¹⁰. La vague est mieux définie dans le premier cas et, par conséquent, on

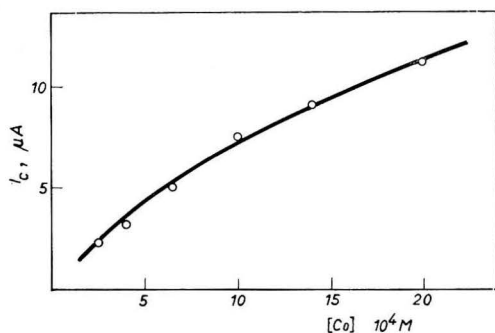


Fig. 1. Influence de la concn. en Co sur la hauteur de la vague catalytique pour une concn. en $\text{Na}_2\text{N}_2\text{O}_3$ de $4 \cdot 10^{-4} \text{ M}$; Soln: NH_4Cl , 0.1 M ; NH_4OH , 0.07 M ; gélatine, 0.01% .

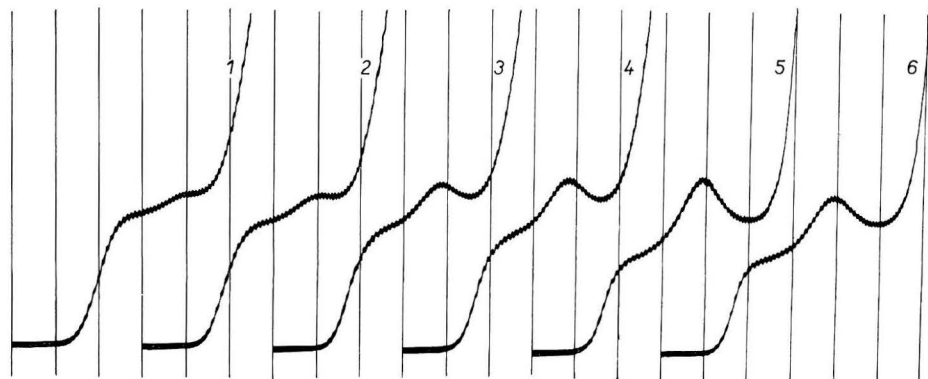


Fig. 2. Influence du pH sur la vague catalytique de la nitrohydroxylamine $4 \cdot 10^{-4} \text{ M}$ en soln. tampon véronal-acétate + Co^{2+} , 10^{-3} M + gélatine, 0.01% ; sensibilité $1/100$; potentiel de départ -0.8 V ; -200 mV/absc. ; anode E.S.C.; pH: (1), 6.12; (2), 6.99; (3), 7.42; (4), 7.66; (5), 8.55; (6), 8.68.

utilisera des solutions tamponées à des fins analytiques. On peut utiliser le système chlorure d'ammonium-hydroxyde d'ammonium ou véronal-acétate. En présence du premier système, la vague catalytique est plus haute qu'en présence du second.

Le pouvoir tampon a aussi une influence marquée sur la vague catalytique. Dans le cas de la nitrohydroxylamine, la vague catalytique diminue lorsque le pouvoir tampon augmente, puisque les équilibres de complexation au sein de la solution sont modifiés¹⁰.

Influence du pH. En présence de tampon ammoniacal, la vague catalytique diminue avec le croissence de la concentration en ammonium¹⁰. Puisque les milieux ammoniacaux ne sont utilisables qu'aux pH alcalins, on a utilisé le système véronal-acétate afin d'étudier l'influence du pH. Sur la Fig. 2 on peut voir que le pH influence en même temps la forme et la hauteur de la vague catalytique. Les conditions expérimentales les plus favorables se situent dans l'intervalle de pH=7.6-8.6. Aux pH plus acides que 4.9, il y a une décomposition brusque de la nitrohydroxylamine.

Concentration saline. Avec la croissence de la concentration en sel de fond, la vague du cobalt est déplacée vers les potentiels négatifs, tandis que la vague catalytique est peu déplacée. C'est la raison pour laquelle les vagues sont mal séparées dans les solutions concentrées en électrolyte indifférent. Dans le système véronal-acétate, il n'est plus possible de distinguer la vague catalytique de la vague du cobalt pour une concentration en KCl de 1.2 M. Pour des buts analytiques, il faut donc travailler à des faibles concentrations salines.

Courbe d'étalonnage

Puisqu'on utilise la vague catalytique du complexe cobalt-nitrohydroxylamine, la variation de la hauteur de la vague en fonction de la concentration en nitrohydroxylamine, est celle qui est caractéristique aux courants catalytiques (Fig. 3). On

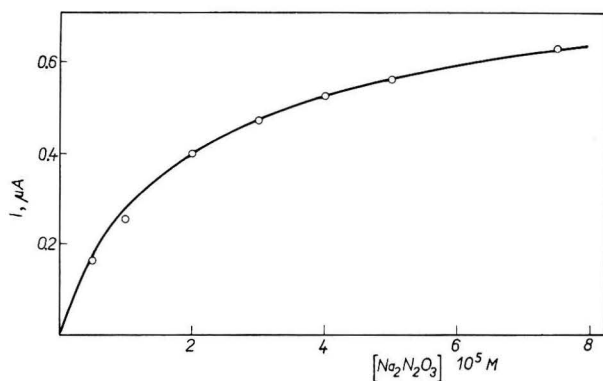


Fig. 3. Courbe d'étalonnage de Na₂N₂O₃. Intervalle des concns., 10⁻⁶-10⁻⁵ M. Soln: Co²⁺, 25·10⁻⁶ M; NH₄Cl, 0.05 M; NH₄OH, 0.025 M; gélatine, 0.02%.

a trouvé auparavant¹⁰ que, dans le cas de la nitrohydroxylamine, la vague catalytique varie linéairement avec $\sqrt{h_c}$ (h_c étant la hauteur corrigée). Il est donc nécessaire de contrôler la hauteur du réservoir et en général d'utiliser de grandes valeurs pour cette hauteur. Une concentration en cobalt de 10⁻³ M est favorable pour un domaine de concentrations en nitrohydroxylamine de l'ordre de grandeur de 10⁻⁴-10⁻³ M.

Dans le cas des solutions diluées en nitrohydroxylamine, il est nécessaire d'utiliser des sensibilités plus grandes du galvanomètre et par conséquent de concentrations plus faibles en cobalt. Pour l'intervalle de 10^{-6} – 10^{-5} *M* de la concentration en nitrohydroxylamine, on peut utiliser une concentration en cobalt de $2,5 \times 10^{-5}$ *M* (Fig. 3).

Influence d'autres composés de l'azote

Il est intéressant d'étudier l'influence d'autres composés de l'azote spécialement: NO_3^- , NO_2^- , NH_2OH , N_2O_2^- et NO_2NH_2 sur la vague catalytique de la nitrohydroxylamine.

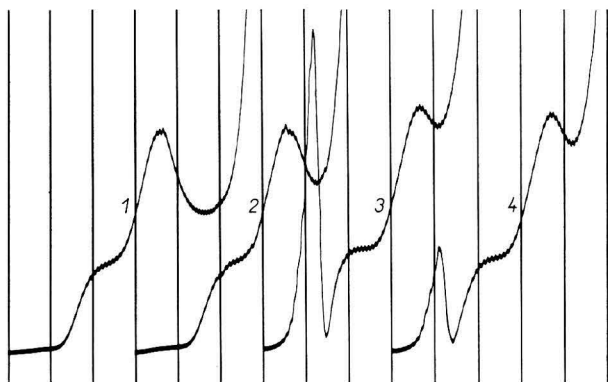


Fig. 4. Influence de l'azotate et de l'azotite sur la vague catalytique de la nitrohydroxylamine. Soln.: Co^{2+} , 10^{-3} *M*; $\text{Na}_2\text{N}_2\text{O}_3$, *M*; NH_4Cl , 0.05 *M*; NH_4OH , 0.025 *M*; gélatine, 0.02%. Temp., 22°, sensibilité, 1/100; potentiel de départ, -0.8 V; -200 mV/absc. (1), NaCl 0.05 *M*; (2), NaNO_3 0.05 *M*; (3), NaNO_2 0.05 *M*; (4), $\text{NaNO}_3 + \text{NaNO}_2$, 0.025 *M*.

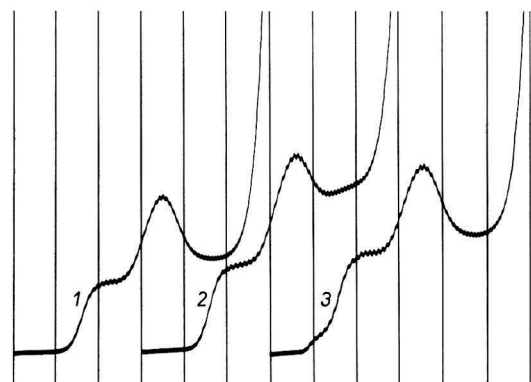


Fig. 5. Influence de la nitramide et de l'hypoazotite sur la vague catalytique de la nitrohydroxylamine. Même soln. et mêmes conditions qu'en Fig. 4. Temp. 2°; $\text{Na}_2\text{N}_2\text{O}_3$, $5 \cdot 10^{-4}$ *M*. (1), Soln. seule; (2), soln. + NH_2NO_2 , $5 \cdot 10^{-4}$ *M*; (3), soln. + $\text{Na}_2\text{N}_2\text{O}_2$, $5 \cdot 10^{-4}$ *M*.

On a représenté (Fig. 4) les polarogrammes en présence de NO_3^- , NO_2^- et $\text{NO}_3^- + \text{NO}_2^-$ à une température de 22° et (Fig. 5) les polarogrammes en présence de $\text{N}_2\text{O}_2^{2-}$ et NO_2NH_2 à 2°. On a toujours maintenu constants la force ionique et le pouvoir tampon.

Azotate. La présence de l'ion azotate ($0.05 M$) ne produit pas une influence visible sur la hauteur de la vague. On constate seulement que la décharge des composants de la solution de base a lieu à des potentiels plus anodiques.

Azotite. Dans le cas de l'azotite ($0.05 M$) il y a un processus électrochimique supplémentaire qui se produit avant la décharge du cobalt. Celui-ci est aussi observable en absence de cobalt. Ce processus est caractérisé par un maximum très haut, qui disparaît partiellement par apport de gélatine. La vague catalytique est peu modifiée: sa hauteur augmente seulement de 5%.

Azotate plus azotite. En présence du mélange azotate ($0.025 M$) et azotite ($0.025 M$), seul l'azotite exerce son influence.

Nitramide. De la Fig. 5, il résulte que la nitramide, même pour une concentration de $5 \cdot 10^{-4} M$, produit une augmentation de la vague catalytique. En pratique il est peu probable d'avoir des mélanges de nitrohydroxylamine et nitramide parce que ces deux substances ne peuvent être préparées et ne sont stables que dans des conditions opposées: la nitrohydroxylamine est stable dans les milieux fortement alcalins et la nitramide dans les milieux acides. De plus, dans les conditions de pH utilisées pour observer la vague de la nitrohydroxylamine, il y a une décomposition très rapide de la nitramide à 20° .

Hyponitrite. La présence de l'hyponitrite se manifeste par l'apparition d'un processus qui précède la décharge du cobalt. Elle n'a aucune influence sur la vague catalytique.

Hydroxylamine. L'hydroxylamine pour des concentrations supérieures à $5 \cdot 10^{-4} M$ produit des effets supplémentaires plus importants et plus complexes que les azotites; la vague catalytique interfère avec les vagues cathodiques de l'hydroxylamine.

Ces résultats montrent que la détermination polarographique des nitrohydroxylaminates (α -oxyhyponitrites) est possible en présence de la plupart des composés de l'azote. En présence des nitrites il est nécessaire d'enregistrer rapidement les solutions fraîchement préparées. Seule la présence de l'hydroxylamine à une concentration supérieure à $5 \cdot 10^{-4} M$ empêche la détermination polarographique de la nitrohydroxylamine, comme dans les autres méthodes^{5,6}.

Précision des déterminations

A des concentrations molaires égales en nitrohydroxylamine et en cobalt, la hauteur de la vague catalytique est 1.44 fois celle de la vague du cobalt. La précision dans la mesure est pratiquement égale pour les deux vagues et elle est de l'ordre de celle que l'on obtient généralement en polarographie. Compte tenu des erreurs d'étalement, l'erreur maximale est de 3% et l'erreur moyenne 1%.

CONCLUSION

Pour la détermination polarographique des nitrohydroxylaminates il est possible d'utiliser les systèmes tampon chlorure d'ammonium-hydroxyde d'ammonium, ou véronal-acétate. En général, il est nécessaire d'employer des concentrations faibles en électrolyte indifférent. Les meilleurs résultats ont été obtenus pour les conditions suivantes: NH_4Cl , $5 \cdot 10^{-2} M$; NH_4OH , $2.5 \times 10^{-2} M$; la concentration du cobalt doit être de $10^{-3} M$ pour des concentrations en $\text{N}_2\text{O}_3^{2-}$ de 10^{-4} – $10^{-5} M$ et de

$2.5 \times 10^{-5} M$ pour des concentrations en $N_2O_3^{2-}$ de 10^{-6} – $10^{-5} M$. En présence d'hydroxylamine, la détermination polarographique n'est pas possible, mais elle l'est en présence de nombreux autres composés de l'azote.

RÉSUMÉ

La vague catalytique de la nitrohydroxylamine en présence de cobalt divalent peut être utilisée pour la détermination polarographique de cette substance. Les vagues catalytiques sont bien développées dans l'électrolyte suivant: NH_4Cl , $0.05 M$; NH_4OH , $0.025 M$; gélatine, 0.02% . La concentration en cobalt doit être environ de $10^{-3} M$ pour 10^{-4} – $10^{-5} M$ en $N_2O_3^{2-}$ et de $2.5 \times 10^{-5} M$ pour 10^{-6} – $10^{-5} M$ en $N_2O_3^{2-}$. D'autres composés de l'azote comme: l'azotate, l'azotite, l'hypoazotite et la nitramide ont peu ou pas du tout d'influence sur la vague catalytique de la nitrohydroxylamine. La présence de l'hydroxylamine seule empêche la détermination.

SUMMARY

The catalytic wave of nitrohydroxylamine in the presence of divalent cobalt can be used for the polarographic determination of this substance. The catalytic waves are well-developed in the following supporting electrolyte solution: NH_4Cl , $0.05 M$; NH_4OH , $0.025 M$; gelatine, 0.02% . The cobalt concentration should be about $10^{-3} M$ for 10^{-4} – $10^{-5} M$ $N_2O_3^{2-}$ and $2.5 \times 10^{-5} M$ for 10^{-6} – $10^{-5} M$ $N_2O_3^{2-}$. The other nitrogen-containing compounds present such as nitrate, nitrite, hyponitrite and nitramide have little or no effect on the catalytic wave of nitrohydroxylamine. Only hydroxylamine interferes with the determination.

BIBLIOGRAPHIE

- 1 A. ANGELI, *Gazz. Chim. Ital.*, 26 II (1896) 17; 27 II (1897) 357; *Atti Accad. Lincei*, 5 (1896) 120.
- 2 P. PASCAL, *Nouveau Traité de Chimie Minérale*, Masson et Cie, Paris, 1956, p. 578.
- 3 J. VEPŘEK-ŠIŠKA, V. PLIŠKA, F. ŠMIROUS ET F. VESELÝ, *Collection Czech. Chem. Commun.*, 24 (1959) 687.
- 4 J. W. MELLOR, *Inorganic and Theoretical Chemistry*, Longman, Green and Co. Ltd., London, 1928, p. 305.
- 5 C. C. ADDISON, G. A. GAMLEN ET R. THOMPSON, *J. Chem. Soc.*, (1952) 338; (1952) 346.
- 6 J. VEPŘEK-ŠIŠKA, F. ŠMIROUS ET V. PLIŠKA, *Collection Czech. Chem. Commun.*, 24 (1959) 1175.
- 7 G. KORTÜM ET B. FINKH, *Z. Physik. Chem.*, B 48 (1941) 42.
- 8 A. CĂLUȘARU ET J. KŮTA, *Nature*, 207 (1965) 750.
- 9 A. CĂLUȘARU ET J. KŮTA, *Elektrochemische Meth. Prinz. Molekular-Biologie, Symposium, Jena, Mai, 1956*.
- 10 A. CĂLUȘARU ET J. KŮTA, *Collection Czech. Chem. Commun.*, 31 (1966) 814.

J. Electroanal. Chem., 12 (1966) 341–346

CORROSION POTENTIOMETRY AND POTENTIOMETRIC TITRATION
WITH DROPPING AMALGAM ELECTRODE

A. R. DESPIĆ AND K. I. POPOV-SINDJELIĆ

Faculty of Technology, University of Belgrade, Belgrade (Yugoslavia)

(Received November 17th, 1965)

INTRODUCTION

Potentiometry and potentiometric end-point indication have found wide application in acid-base and redox titrations, where reversible electrodes give good reproducibility of potential measurements. They have proved much less suitable for determining the concentration in solution of ionic species the other valency state of which is zero, since most metals require special precautions and treatment to get reproducible, reversible electrode potentials.

It is the purpose of this paper to show that in such cases, corrosion potentials (mixed potentials), as characteristics of corroding systems, can have analytical applications if certain conditions are established at the metal-solution interface.

Corrosion potential, which appears whenever a solid is immersed in a solution containing non-corresponding ionic species undergoing electroreduction at more positive potentials, is a property easily measurable with standard potentiometric equipment. It is, in general, a function of time and of the concentrations of all the species involved in the process. However, if the time is fixed, for a fixed concentration of the oxidizable component the corrosion potential becomes a function of the concentration of the reducible species only, provided all other characteristics of the system are kept constant. Obviously, the latter condition can be satisfied with reproducibility of the conditions of the electrode process, such as is obtained, for example, with the dropping mercury electrode at potentials at which diffusion controls the rate. The potential of the electrode is then a good indicator of the concentration of the reducible species and as such can be used for analysis even where potentiometry of reversible processes fails. The dropping mercury electrode itself, however, cannot have a wide application of this kind, because of the relatively high positive standard electrode potential of the mercury dissolution process. However, amalgams of some metals such as zinc and cadmium have negative standard potentials and therefore can be corroded at a fixed, diffusion-controlled rate dependent solely on the concentration of any species the polarographic half-wave potentials of which are more positive than the potential of the dropping amalgam. This versatility gives dropping amalgam electrodes attractive possibilities. Their use as indicators in the potentiometric titration of copper ions is demonstrated below.

EXPERIMENTAL

The experimental set-up for corrosion potentiometry with a dropping amalgam electrode is shown in Fig. 1. For observing the change of corrosion potential with time, the cell was isolated from the atmosphere with a ground-glass lid and purified hydrogen introduced before measurements. Potentiometric titrations were done in open beakers, the dissolved oxygen being removed by adding sodium sulphite to the titrated solution. All the experiments were carried out at room temperature, which was $25 \pm 3^\circ$.

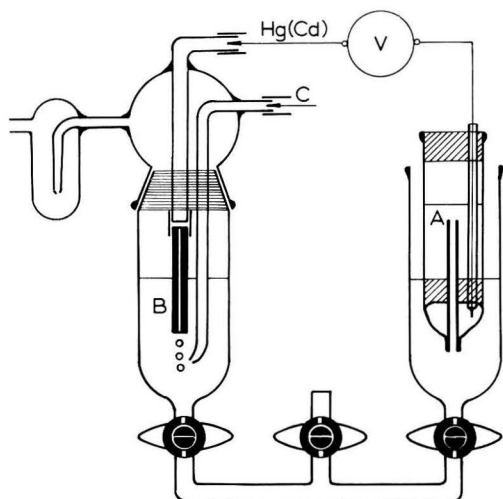


Fig. 1. Apparatus for corrosion potentiometry and corrosion titration. (A), standard electrode; (B), dropping amalgam electrode; (C), inlet for hydrogen.

The time-dependence of the corrosion potential was recorded on a "Tektronix 551" oscilloscope. The e.m.f. between the corroding electrode and the reference electrode were measured on a Hewlett-Packard type 412A precision voltmeter. To increase the precision of the readings in some experiments, a standard cell was introduced into the circuit in opposition so that a higher sensitivity of the instrument could be used.

Cadmium amalgam was made by dissolving a weighed amount of the metal in mercury. The concentration of amalgam was about 2%.

Solutions to be titrated were prepared by taking known amounts of a more concentrated ($10^{-1} M$) copper sulphate solution and diluting with $1 M$ ammonium chloride solution as supporting electrolyte to an approximately constant volume, to make the concentration about $10^{-2} M$ in copper ions. The titrant was a $1 \cdot 10^{-1} M$ solution of EDTA "Chelaton" 3 G.R. (Chemapol).

RESULTS AND DISCUSSION

For convenience, the potentiometry investigated here is called corrosion potentiometry and the corresponding titrations corrosion potentiometric titrations.

A typical time-dependence of the corrosion potential is given in Fig. 2. The corrosion potential may be seen to be virtually independent of time. This can be explained theoretically by the following reasoning:

The corrosion process taking place at the interface is



(a) and (s) denoting the amalgam and the solution phase, respectively. If the concentration of cupric ions is sufficiently low that conditions of pure diffusion control are established at the interface, the electrode behaves as totally polarized with respect to

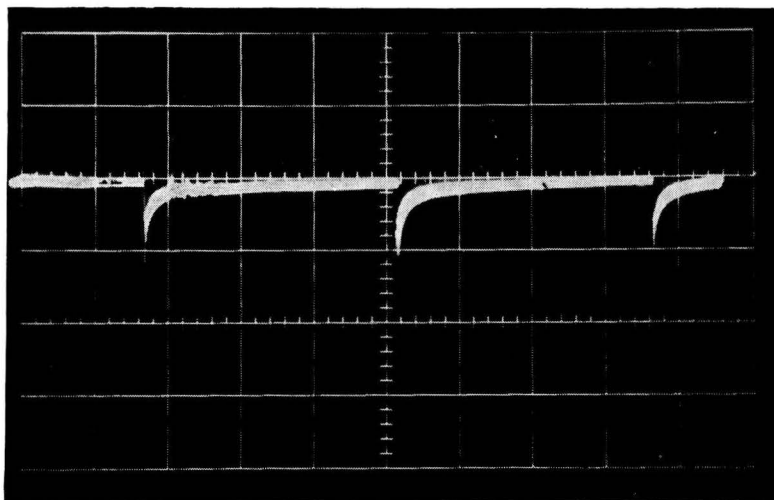


Fig. 2. Time-dependence of the corrosion potential at the dropping cadmium-amalgam electrode. Time scale 0.5 sec/cm, voltage scale 5 mV/cm.

cupric ions and its potential is determined solely by the electrochemical oxidation of cadmium. This is known to be fast enough for an equilibrium between cadmium and cadmium ions to be maintained at the interface at corrosion current densities equal to cupric ion diffusion currents. Hence, the corrosion potential can be considered near enough equal to the reversible potential of the cadmium-amalgam electrode. The latter is determined by the concentrations of cadmium and cadmium ions on the amalgam and solution sides of the interface, respectively, as given by the Nernst equation

$$E(t) = E_{\text{Cd}/\text{Cd}^{2+}}^{\circ} + \frac{RT}{2F} \ln \frac{C_{\text{Cd}^{2+}}(0,t)}{C_{\text{Cd}}(0,t)} \quad (2)$$

These concentrations can be found by an approach similar to that of MCGILLAVRY AND RIDEAL¹, VON STACKELBERG² or KOUTECKY³ for evaluating instantaneous current at a dropping mercury electrode.

Any depletion of cadmium ions in the reaction layer at the interface, caused by any type of anodic current that is large enough to cause concentration polarization

effects, must satisfy the differential equation

$$\frac{\partial C_{\text{Cd}}}{\partial t} = D_{\text{Cd}} \frac{\partial^2 C_{\text{Cd}}}{\partial x^2} + \frac{2x}{3t} \frac{\partial C_{\text{Cd}}}{\partial x} \quad (3)$$

and

$$\frac{\partial C_{\text{Cd}^{2+}}}{\partial t} = D_{\text{Cd}^{2+}} \frac{\partial^2 C_{\text{Cd}^{2+}}}{\partial x^2} + \frac{2x}{3t} \frac{\partial C_{\text{Cd}^{2+}}}{\partial x} \quad (4)$$

These are the 2nd Fick's law equations corrected for linear expansion and compression of diffusion layers, respectively.

To solve this set of equations, the following initial and boundary conditions can be assumed:

$$C_{\text{Cd}}(x, 0)_{x < 0} = (C_{\text{Cd}})_0; \quad C_{\text{Cd}^{2+}}(x, 0)_{x > 0} = 0 \quad (5, 6)$$

$$C_{\text{Cd}}(\infty, t) = (C_{\text{Cd}})_0; \quad C_{\text{Cd}^{2+}}(\infty, t) = 0 \quad (7, 8)$$

Stoichiometry of the anodic oxidation of cadmium requires that the fluxes of the two species are equal, *i.e.*,

$$+ D_{\text{Cd}} \left(\frac{\partial C_{\text{Cd}}(x, t)}{\partial x} \right)_{-x \rightarrow 0} = D_{\text{Cd}^{2+}} \left(\frac{\partial C_{\text{Cd}^{2+}}(x, t)}{\partial x} \right)_{+x \rightarrow 0} \quad (9)$$

Both these fluxes are caused by the corrosion current, which is related to the flux of cupric ions at the electrode. Since all the stoichiometric factors in eqn. (1) are unity, this relation is such that the equality (9) extends to the flux of cupric ions as well. This is (*cf.* ref. 4)

$$+ D_{\text{Cu}^{2+}} \left(\frac{\partial C_{\text{Cu}^{2+}}}{\partial x} \right)_{x=0} = - (C_{\text{Cu}^{2+}})_0 \sqrt{\frac{7}{3}} \frac{D_{\text{Cu}^{2+}}}{\pi t} = \alpha t^{-\frac{1}{2}} \quad (10)$$

With all these conditions the following solutions are obtained

$$C_{\text{Cd}}(x, t) = (C_{\text{Cd}})_0 - (C_{\text{Cu}^{2+}})_0 \sqrt{\frac{D_{\text{Cu}^{2+}}}{D_{\text{Cd}}}} \operatorname{erfc} \frac{x}{2\sqrt{\frac{3}{7}} D_{\text{Cd}} t} \quad (11)$$

$$C_{\text{Cd}^{2+}}(x, t) = (C_{\text{Cu}^{2+}})_0 \sqrt{\frac{D_{\text{Cu}^{2+}}}{D_{\text{Cd}^{2+}}}} \operatorname{erfc} \frac{x}{2\sqrt{\frac{3}{7}} D_{\text{Cd}^{2+}} t} \quad (12)$$

Substituting the relevant concentrations at $x=0$ into eqn. (2) we get

$$E(t) = E_{\text{Cd}/\text{Cd}^{2+}} + \frac{RT}{2F} \ln \sqrt{\frac{D_{\text{Cu}^{2+}}}{D_{\text{Cd}^{2+}}}} + \frac{RT}{2F} \ln \frac{(C_{\text{Cu}^{2+}})_0}{(C_{\text{Cd}})_0 - (C_{\text{Cu}^{2+}})_0 \sqrt{\frac{D_{\text{Cu}^{2+}}}{D_{\text{Cd}}}}} \quad (13)$$

for the time- and concentration-dependence of the instantaneous corrosion potential at the electrode drop. The sum of the first two terms represents a standard quantity for this process and has a similar form to the polarographic half-wave potential. Function (13) has all the shortcomings of the simple Ilkovič equation, but can nevertheless be considered a good-enough approximation.

The peak of a few millivolt in Fig. 2 obtained immediately after the fall of each drop is due to deviation of the real systems from idealities assumed in the initial and boundary conditions (discharge of Cu^{2+} ions existing in the layer at $x \rightarrow 0, t = 0$). The peaks are smaller the greater the concentration of cupric ions, and around $10^{-2} M$ they can hardly be recorded.

Although the initial potential is undefined because of the initial boundary conditions, the value from very soon after the beginning of formation of the drop un-

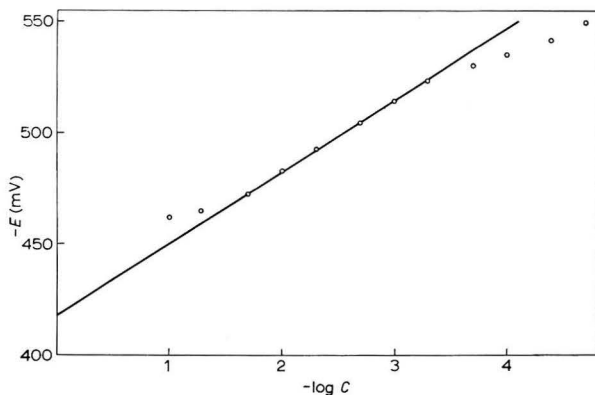


Fig. 3. Corrosion potential of dropping cadmium-amalgam as a function of the concn. of cupric ions in soln.

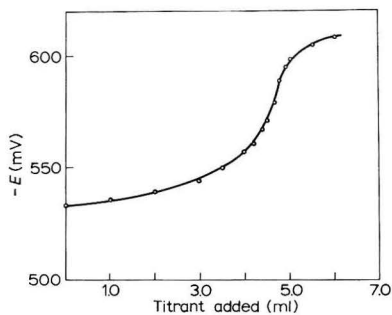


Fig. 4. Corrosimetric titration curve for $5 \cdot 10^{-4}$ moles of CuSO_4 in $0.01 M$ soln. with $0.1 M$ EDTA as titrant.

til drop fall is a simple logarithmic function of the concentration of cupric ions when $(C_{\text{Cd}})_0 \gg (C_{\text{Cu}^{2+}})_0$, since the ratio of the two diffusion coefficients is close to unity. This quality makes the electrode usable in corrosionmetry.

Results for the corrosion potential at various concentrations of cupric ions are shown in Fig. 3. They lie on a straight line in the concentration range 10^{-2} – $5 \cdot 10^{-5} M$ in Cu^{2+} ions. According to eqn. (13) the slope of the straight line in a log-linear plot should be

$$\frac{dE_{\text{max}}}{d \log(C_{\text{Cu}^{2+}})_0} = \frac{2.3 RT}{2F} = 0.0296 \quad (14)$$

at 25° .

This is in accordance with experiment since the slope of the straight line obtained by least squares is 0.033.

After these relations had been established, two series of corrosimetric titrations were performed. A typical titration curve is shown in Fig. 4. The first part, before the end-point is indicated by inflection, reflects the logarithmic dependence of the potential on concentration. The inflection and the second part, which does not conform to the theoretically predicted tendency to infinity, is due to the background corrosion current of some very low concentration impurities that are not titrated with EDTA.

In the first series, the reproducibility of the results was tested by titrating $5 \cdot 10^{-4}$ moles of cupric ions in an approximately 10^{-2} M solution. The results are shown in Table 1. It can be seen that the reproducibility is within the limits of error usually obtained in potentiometric titrations with EDTA.

TABLE 1

CORROSIMETRIC TITRATION OF 0.5 MMOL OF COPPER IONS WITH EDTA AT THE DROPPING CADMIUM-AMALGAM ELECTRODE (CONCENTRATION OF THE TITRANT 0.104 M)

<i>Titration no.</i>	<i>Titrant used (ml)</i>	<i>CuSO₄ found (mmole × 10)</i>	<i>Error (%)</i>
1	4.75	4.95	-1
2	4.75	4.95	-1
3	4.75	4.95	-1
4	4.65	4.85	-3
5	4.75	4.95	-1
6	4.70	4.90	-2
7	4.75	4.95	-1
8	4.75	4.95	-1
9	4.80	5.00	0
10	4.70	4.89	-2
11	4.85	5.05	+1
12	4.85	5.05	+1
13	4.80	5.00	0
14	4.75	4.95	-1
15	4.82	5.02	+0.5
			Average 1.1

TABLE 2

THE EFFECT OF DILUTION UPON THE ACCURACY OF TITRATION OF COPPER IONS WITH EDTA AT DROPPING CADMIUM-AMALGAM ELECTRODE

<i>Concn. test soln. (M)</i>	<i>CuSO₄ taken (mmole)</i>	<i>No. of titration</i>	<i>Av. titrant used (ml)</i>	<i>Av. CuSO₄ found (mmole)</i>	<i>Av. error (%)</i>	<i>Max. error (%)</i>
10^{-2}	0.5	15	4.76	$4.95 \cdot 10^{-1}$	1.1	-3
10^{-3}	0.05	6	4.70	$4.90 \cdot 10^{-2}$	2.8	-6
10^{-4}	0.005	5	4.85	$5.05 \cdot 10^{-3}$	4.7	+9.5

In the second series, the effect of dilution on the accuracy of titration was investigated. The results are shown in Table 2. They show that the dropping amalgam electrode can be used as an indicator electrode for corrosimetric titration of cupric ions down to concentrations of about 10^{-4} M with errors within 5%.

These results indicate that the dropping amalgam electrode can be used for corrosimetric analysis. Because of the lack of selectivity, however, it can only be used for (i) the titration of pure solutions of one ionic species, or (ii) the titration of the total ionic content of all the species that either have a half-wave potential more positive than the potential of the dropping amalgam or are more readily complexed by the titrant than other species that corrode the electrode.

Some separations can be done, *i.e.*, some selectivity obtained, by using different amalgams with considerable differences in standard potentials. This will be discussed in a later publication.

ACKNOWLEDGEMENT

We are indebted to Dr. S. P. BINGULAC for his contribution to the mathematics of the problem.

SUMMARY

Corrosion potential in direct corrosion of a dropping amalgam electrode in contact with a solution of more electropositive ionic species has been studied. It is shown to be a function of the concentrations of these species when a diffusion-controlled rate of corrosion is established at the surface.

Because of this, the dropping amalgam electrode can provide a versatile electrode for potentiometric titration of dilute solutions, especially when amalgams of electronegative metals such as zinc and cadmium are used, since most systems of practical interest have more positive standard electrode potentials and thus are able to initiate the corrosion process. As an example of the application of this principle "corrosimetric" titration of copper ions with EDTA has been investigated. The error is within the usual limits for this type of analysis.

REFERENCES

- 1 D. MCGILLAVRY AND E. K. RIDEAL, *Rec. Trav. Chim.*, 56 (1937) 1013.
- 2 M. VON STACKELBERG, *Polarographische Arbeitsmethoden*, p. 284, Walter de Gruyter, Berlin, 1950.
- 3 J. KOUTECKY, *Collection Czech. Chem. Commun.*, 18 (1953) 597.
- 4 K. J. VETTER, *Elektrochemische Kinetik*, Springer-Verlag, Berlin, p. 196, 1961.

J. Electroanal. Chem., 12 (1966) 347-353

SHORT COMMUNICATIONS

Theory of programmed-current derivative chronopotentiometry*

A discussion of the basic concepts of derivative chronopotentiometry has been given recently by PETERS AND BURDEN¹. These workers presented equations pertinent to the derivative chronopotentiometric technique as applied to both reversible and irreversible electrode processes, and they verified their equations experimentally by studying several electrochemical systems. Their treatment was restricted to the condition most frequently utilized in experimental chronopotentiometry, *i.e.*, electrolysis with constant impressed current density. Of interest also is derivative chronopotentiometry when the impressed current density is programmed as some other function of time. The theoretical equations that are pertinent to this latter method of derivative chronopotentiometry are presented in this communication.

Theory

MURRAY AND REILLEY² have given an excellent treatment of chronopotentiometry with the general current program

$$i_0 = \frac{i}{A} = \beta t^r, \quad (1)$$

in which a current i at an electrode of area A gives an impressed current density i_0 ($A \text{ cm}^{-2}$); β is a current-time proportionality constant ($A \text{ cm}^{-2} \text{ sec}^{-r}$), and r is any number greater than -1 . We adopt their results and symbology with only one exception: we prefer to use C^b to denote the bulk concentration of the electroactive species rather than A^0 .

The relationships pertinent to programmed-current derivative chronopotentiometry are presented in Table 1. Derivation of those expressions is straightforward, albeit laborious, and will only be outlined here. Note that the equations in Table 1 refer to chronopotentiometric reduction processes. For oxidation processes, the signs of derivative equations should be positive and the signs before the second terms on the right-hand sides of eqns. (5-R) and (5-I) in Table 1 should be negative. In agreement with PETERS AND BURDEN¹, we refer to the inflection point in the normal chronopotentiogram as the *minimum* value of the derivative chronopotentiogram, because that is the point at which the rate of change of potential with time is minimal.

Reversible processes involving soluble reactants and products

Equation (1-R) in Table 1 (*i.e.*, eqn. (34) of ref. 2) describes the programmed-current chronopotentiometric wave for simple, reversible processes involving soluble reactants and products that occur under the condition of semi-infinite linear diffusion.

* Research sponsored by the U. S. Atomic Energy Commission under contract with the Union Carbide Corporation.

Equation (2-R) in Table 1 is the first time-derivative of expression (1-R), r being constant. Hence, eqn. (2-R) describes the programmed current derivative chronopotentiogram for processes obeying eqn. (1-R). The minimum value of the derivative chronopotentiogram corresponds to the inflection point in the normal chronopotentiogram. The derivative minimum occurs at a time, t_{\min} , given by eqn. (3-R) and has a value, $(dE/dt)_{\min}$, given by eqn. (4-R). Equation (3-R) is derived by differentiating eqn. (2-R) with respect to time, equating the resulting expression to zero, and solving for t . Equation (4-R) is then obtained by substituting the value of t_{\min} given by eqn. (3-R) for t in eqn. (2-R) and simplifying the resulting expression. Similarly, eqn. (5-R) is obtained by substituting the value of t_{\min} given by eqn. (3-R) for t in eqn. (1-R) and simplifying the resulting expression to obtain E_{\min} . This is the potential at which the inflection point occurs on the normal chronopotentiogram and corresponds to $(dE/dt)_{\min}$ on the derivative chronopotentiogram.

Both t_{\min} and $(dE/dt)_{\min}$ are related explicitly to the transition time through eqns. (3-R) and (4-R), respectively. These parameters may be related to the concentration of the electroactive species of interest by invoking the general relationship between transition time and concentration. This latter relationship, according to MURRAY AND REILLEY (eqn. (24) of ref. 2), is

$$\tau^{r+1/2} = \frac{nFD^{1/2}C^b \Gamma(r+3/2)}{\beta \Gamma(r+1)} \quad (1-G)$$

Thus, combination of eqns. (1-G) and (4-R) and simplification yields the relationship between concentration and the minimum value of the first derivative, eqn. (6-R). Similarly, combination of eqns. (1-G) and (3-R) and simplification yields the relationship between concentration and the time at which the first derivative attains its minimum value, eqn. (7-R). The lumped constants, N_r^{rev} and M_r^{rev} , are defined in the legend of Table 1.

Totally irreversible processes involving soluble reactants and products

Equation (1-I) in Table 1 (*i.e.*, eqn. (38) of ref. 2) describes the programmed-current chronopotentiometric wave for totally irreversible processes involving soluble reactants and products that occur under the condition of semi-infinite linear diffusion. Equations (2-I)–(7-I) in Table 1 can be derived from eqn. (1-I) in the same manner that eqns. (2-R)–(7-R) were derived from eqn. (1-R). Derivation of t_{\min} in this case requires the solution of a quadratic equation; the positive root yields a real and finite solution. The rather cumbersome result has been simplified by using the r -function, ϕ , that is defined in the foot-note of Table 1. The lumped constants, N_r^{irrev} and M_r^{irrev} , in eqns. (6-I) and (7-I), respectively, are also defined in the legend to Table 1.

The values of these constants were computed (a FORTRAN-63 program is available) and are tabulated in Tables 2 and 3 for reversible and totally irreversible processes, respectively, along with other pertinent information. The selected r -values are those used by MURRAY AND REILLEY². A temperature of 298°K was assumed for computation of the defined constants. Note that these defined constants assume different values (for a fixed r) in eqns. (1-R)–(7-R) from those in eqns. (1-I)–(7-I), and the differences change as r is changed.

Table I
EXPRESSIONS FOR PROGRAMMED-CURRENT DERIVATIVE CHRONOPOTENTIOMETRY

Reversible		Totally Irreversible	
No.	No.	No.	
1-R	1-I	$E = \frac{RT}{\alpha n_0 F} \ln \frac{k_f \Gamma(r+1)}{D^{\frac{1}{2}} \Gamma(r+\frac{3}{2})} + \frac{RT}{\alpha n_0 F} \ln \frac{\tau^{r+\frac{1}{2}} - t^{r+\frac{1}{2}}}{t}$	
2-R	2-I	$\frac{dE}{dt} = \frac{-RT}{nF} \frac{(r+\frac{1}{2}) \tau^{r+\frac{1}{2}}}{t(\tau^{r+\frac{1}{2}} - t^{r+\frac{1}{2}})}$	
3-R	3-I	$t_{\min} = \tau \left[\frac{1}{r+\frac{3}{2}} \right]^{r+\frac{1}{2}}$	
4-R	4-I	$\left(\frac{dE}{dt} \right)_{\min} = \frac{-RT}{nF\tau} \left[r+\frac{3}{2} \right]^{r+\frac{3}{2}}$	
5-R	5-I	$E_{\min} = E_{\frac{1}{2}} + \frac{RT}{nF} \ln \left(r+\frac{1}{2} \right)$	
6-R	6-I	$C^b = \frac{N_r^{\text{rev}} \beta}{n^{r+\frac{3}{2}} D^{\frac{1}{2}}} \left[\frac{1}{(dE/dt)_{\min}} \right]^{r+\frac{1}{2}}$	
7-R	7-I	$C^b = \frac{M_r^{\text{rev}} \beta}{n D^{\frac{1}{2}}} \left[t_{\min} \right]^{r+\frac{1}{2}}$	
		$\left(\frac{dE}{dt} \right)_{\min} = \frac{-RT}{2\alpha n_0 F \tau} \left[\frac{\phi + 2r}{\phi^{r+\frac{1}{2}} - \phi^{r+\frac{3}{2}}} \right]$	
		$E_{\min} = \frac{RT}{\alpha n_0 F} \ln \left[\frac{nFC^b k_1}{\beta \tau r} \right] + \frac{RT}{\alpha n_0 F} \ln \left[\phi^{r+\frac{1}{2}} - \phi^{r+\frac{3}{2}} \right]^{1/2}$	
		$C^b = \frac{N_r^{\text{irrev}} \beta}{(\alpha n_0)^{r+\frac{1}{2}} n D^{\frac{1}{2}}} \left[\frac{1}{(dE/dt)_{\min}} \right]^{r+\frac{1}{2}}$	
		$C^b = \frac{M_r^{\text{irrev}} \beta}{n D^{\frac{1}{2}}} \left[t_{\min} \right]^{r+\frac{1}{2}}$	

Legend

$$N_r^{\text{irrev}} \equiv \left[\frac{1}{F} \right]^{r+\frac{3}{2}} \left[\frac{RT}{2} \left(\frac{\phi + 2r}{\phi^{r+\frac{1}{2}} - \phi^{r+\frac{3}{2}}} \right) \right]^{r+\frac{1}{2}} \left[\frac{\Gamma(r+1)}{\Gamma(r+\frac{3}{2})} \right]$$

$$\phi \equiv \left[\left(r^4 + 4r^3 + \frac{7}{2}r^2 + r + \frac{1}{16} \right)^{\frac{1}{2}} - r^2 - 2r + \frac{1}{4} \right]$$

$$N_r^{\text{rev}} \equiv \left[\frac{r+\frac{3}{2}}{F} \right]^{r+\frac{3}{2}} \left[RT \right]^{r+\frac{1}{2}} \left[\frac{\Gamma(r+1)}{\Gamma(r+\frac{3}{2})} \right]$$

$$M_r^{\text{rev}} \equiv \frac{(r+\frac{3}{2})}{F} \left[\frac{\Gamma(r+1)}{\Gamma(r+\frac{3}{2})} \right]$$

$$M_r^{\text{irrev}} \equiv \frac{1}{\phi F} \left[\frac{\Gamma(r+1)}{\Gamma(r+\frac{3}{2})} \right]$$

TABLE 2

COMPUTED VALUES OF PARAMETERS, REVERSIBLE CASE

r	t_{min}/τ	$n(E_{min} - E_{1/2})$ (mV)	$n\tau(dE/dt)_{min}$ (V)	$N_r^{rev} \cdot 10^6$	$M_r^{rev} \cdot 10^4$
0	0.444	-17.8	-0.0867	3.444	0.1754
1/2	0.500	0.0	-0.1028	0.9439	0.1837
1	0.543	+10.4	-0.1183	0.3173	0.1949
3/2	0.577	+17.8	-0.1335	0.1228	0.2067
2	0.606	+23.5	-0.1484	0.05294	0.2183
5/2	0.630	+28.2	-0.1631	0.02492	0.2296

TABLE 3

COMPUTED VALUES OF PARAMETERS, IRREVERSIBLE CASE

r	t_{min}/τ	$E_{min} - \frac{RT}{\alpha n_a F} \ln \frac{nFC^b}{\beta \tau r} k_f^0$ (mV)	$\alpha n_a \tau \left(\frac{dE}{dt} \right)_{min}$ (V)	ϕ_r	$N_r^{irrev} \cdot 10^6$	$M_r^{irrev} \cdot 10^4$
0	0.250	-17.8/ αn_a	-0.0514	0.500	2.651	0.2339
1/2	0.414	-2.4/ αn_a	-0.0749	0.414	0.6877	0.2217
1	0.489	+7.6/ αn_a	-0.0949	0.342	0.2229	0.2278
3/2	0.540	+14.9/ αn_a	-0.1105	0.292	0.08417	0.2363
2	0.578	+20.6/ αn_a	-0.1267	0.254	0.03567	0.2457
5/2	0.608	+25.4/ αn_a	-0.1424	0.225	0.01657	0.2551

Discussion

Inspection of the information in Tables 1-3 reveals several pertinent points. First, the equations in Table 1 for reversible processes are similar in form to the corresponding equations for irreversible processes. Secondly, the expressions for E , (dE/dt) , t_{min} , and $(dE/dt)_{min}$ reduce to those given by PETERS AND BURDEN¹ when r is zero. This is to be expected because an r -value of zero corresponds to conventional chronopotentiometry at constant impressed current density. PETERS AND BURDEN do not present expressions for E_{min} or C^b *per se*, but it can be easily shown that their treatment produces E_{min} and C^b expressions that are analogous to those in Table 1 with $r = 0$. Thirdly, when r is one-half, the equations pertaining to reversible processes indicate that t_{min} occurs at $\tau/2$, $E_{min} = E_{1/2}$, and there is a linear relationship between $(dE/dt)_{min}$ (or τ) and C^b . Again, this behavior is to be expected because the chronopotentiogram corresponding to a reversible electrode reaction is identical in shape to a polarogram, if the impressed current is programmed to increase in proportion to the square root of time³. Fourthly, the difference between the derivative chronopotentiograms for reversible and for totally irreversible processes, as indicated by the value of t_{min} or E_{min} or $(dE/dt)_{min}$, is greatest at small values of r . As r increases, the shape of the derivative chronopotentiogram corresponding to a totally irreversible reaction approaches that of a reversible reaction. This too, is to be expected since the shape of a normal chronopotentiogram for an irreversible process approaches that of a reversible process at increasing values of r . In general, the information in Tables 2 and 3 indicates that with increasing r , t_{min} approaches τ , E_{min} becomes increasingly positive for a reduction process (or increasingly negative for an oxidation process), and the proportionality constant between $(dE/dt)_{min}$ and $1/\tau$ increases.

It is to be emphasized that eqns. (1-R) and (1 I), and hence all equations derived from them, are based upon a fundamental assumption of 100% current efficiency for the faradaic process of interest. PETERS AND BURDEN¹ suggested that derivative chronopotentiometry offers a means for increasing the accuracy with which transition times can be measured. This results from the fact that the loss in current efficiency due to the non-faradaic (charging) process is less during the portion of the electrolysis between $t = 0$ and $t = t_{\min}$ than it is during the entire electrolysis from $t = 0$ to $t = \tau$. The chronopotentiometer with compensation for extraneous currents⁴ also affords increased accuracy in the evaluation of transition times. With this instrument, losses in current efficiency due to the charging process can be effectively nullified electronically so that the chronopotentiogram approaches ideality in shape and the transition time can be measured with good accuracy. Because compensated chronopotentiograms exhibit nearly ideal shapes, their derivatives should be excellent tests of the validity of the equations given in Table 1. We intend to explore the utility of programmed-current derivative chronopotentiometry as part of our evaluative investigation of the chronopotentiometer that incorporates compensation for extraneous currents⁴.

We feel that the real value of derivative chronopotentiometry may lie in its capability for obtaining a measure of the transition time early in the electrolysis. Hence, when it is desirable to minimize the effect of convective disturbances about the electrode surface due to thermal gradients or when it is desirable to limit the potential excursion to prevent unwanted reactions or degradation of the electrode itself, then derivative chronopotentiometry should be preferable to conventional chronopotentiometry. Electroanalytical studies in molten-salt media is a specific application where the derivative technique may be utilized to minimize convective disturbances. A zero (or small) r -value should be selected for such studies so that the measure of τ is obtained early in the electrolysis (*cf.* t_{\min}/τ values in Tables 2 and 3).

On the other hand, the derivative technique may be conjoined advantageously with higher-order current-time programs for kinetic or mechanistic studies or when there is convective disturbance about the electrode surface due to density gradients. In these situations, it may be desirable to obtain a measure of τ under conditions that require minimal total electricity in order to minimize unwanted alterations of the system. The expression for total charge during a programmed-current electrolysis, obtained by integration of eqn. 1, is

$$Q_t = \left[\frac{\beta}{r+1} \right] t^{r+1}. \quad (2)$$

With this expression, it can be readily shown that

$$\frac{Q_t/t_{\min}}{Q_\tau/\tau} = \left[\frac{t_{\min}}{\tau} \right]^r \quad (3)$$

which relates the total electricity required to attain t_{\min} with the total electricity required to attain τ , as a function of r . For reversible processes,

$$\left[\frac{t_{\min}}{\tau} \right]^r = \left[\frac{1}{r+3/2} \right]^{r/(r+1/2)}, \quad (4)$$

TABLE 4

COMPUTED VALUES OF $(t_{\min}/\tau)^r$

r	Reversible Process	Irreversible Process	r	Reversible Process	Irreversible Process
0	1.0	1.0	3/2	0.439	0.397
1/2	0.707	0.643	2	0.368	0.334
1	0.545	0.488	5/2	0.315	0.288

whereas for totally irreversible processes,

$$\left[\frac{t_{\min}}{\tau}\right]^r = [\phi]^{r/(r+\frac{1}{2})} \quad (5)$$

Some values of the right-hand sides of eqns. (4) and (5) are tabulated in Table 4. It is seen that the value of the ratio in eqn. (3) decreases rapidly with increasing r . This means that, as r increases, relatively less electricity is required to attain t_{\min} than to attain τ . Hence a non-zero r -value (e.g., $r = 1$ or 2) should be selected when it is desirable to minimize the accumulation of reaction products about the electrode surface, and the derivative technique should be utilized.

It is interesting to note finally that n and αn_a can be expressed in terms of $(dE/dt)_{\min}$ and t_{\min} . For the reversible case, combination of eqns. (6-R) and (7-R) of Table 1 and simplification yields

$$n = \left[\frac{N_{r,\text{rev}}}{M_{r,\text{rev}}}\right]^{1/(r+\frac{1}{2})} \left[\frac{1}{(dE/dt)_{\min}}\right] \left[\frac{1}{t_{\min}}\right].$$

Similarly, combination of eqns. (6-I) and (7-I) of Table 1 yields, for totally irreversible processes,

$$\alpha n_a = \left[\frac{N_{r,\text{irrev}}}{M_{r,\text{irrev}}}\right]^{1/(r+\frac{1}{2})} \left[\frac{1}{(dE/dt)_{\min}}\right] \left[\frac{1}{t_{\min}}\right].$$

The practical utility of these latter expressions will be limited by the accuracy with which t_{\min} can be determined. It is likely that the PETERS AND BURDEN¹ method—in which n or αn_a is evaluated from $(dE/dt)_{\min}$ and an independently-determined τ —gives superior results in actual practice.

Analytical Instrumentation Group,
Analytical Chemistry Division,
Oak Ridge National Laboratory,
Oak Ridge, Tennessee (U.S.A.)

W. D. SHULTS
T. R. MUELLER

1 D. G. PETERS AND S. L. BURDEN, *Anal. Chem.*, 38 (1966) 530.

2 R. W. MURRAY AND C. N. REILLEY, *J. Electroanal. Chem.*, 3 (1962) 64.

3 H. HURWITZ AND L. GIERST, *J. Electroanal. Chem.*, 2 (1961) 128.

4 W. D. SHULTS, F. E. HAGA, T. R. MUELLER AND H. C. JONES, *Anal. Chem.*, 37 (1965) 1415.

Received February 28th, 1966

Conductometric study on the quantitative precipitation of lanthanum and neodymium as normal tellurites

Introduction

Various methods for the determination of lanthanum and neodymium have been reported¹⁻⁴. Lanthanum has been estimated (i) volumetrically⁵ by titration against citric acid solution in the presence of the indicator arsenazo; (ii) gravimetrically⁶ by precipitation with potassium ferrocyanide; (iii) potentiometrically by titration against ammonium and sodium oxalate⁷ and potassium ferrocyanide⁸; (iv) amperometrically with potassium ferrocyanide⁹ and (v) conductometrically by titration against selenious acid¹⁰. Spectrophotometric¹¹⁻¹³ procedures have been developed for the estimation of neodymium in trace quantities.

Recently, tellurite ion has been used successfully in the electrometric determination of cobalt¹⁴, thorium¹⁵, samarium¹⁶ and praseodymium¹⁷.

The present communication deals with the conductometric titrations of lanthanum and neodymium nitrate with sodium tellurite and has been undertaken to investigate the process as a possible analytical method for the determination of lanthanum and neodymium as the normal tellurites.

Experimental and results

Reagents. Sodium tellurite (B.D.H.), lanthanum nitrate and neodymium nitrate (Atomic Energy Establishment, Trombay) were dissolved separately in conductivity water. The tellurium content was determined as metallic tellurium¹⁸ and lanthanum and neodymium as their respective oxides¹⁹.

Apparatus and procedure. The conductometric titrations of lanthanum nitrate and neodymium nitrate with sodium tellurite were carried out at $25 \pm 0.5^\circ$ in a 100-ml pyrex beaker with a dip cell of the type P.R. 9510 having a cell constant of 1.46. The resistance in ohms was recorded at an output frequency of 50 cycles/sec by a Philips conductivity bridge type P.R. 9500.

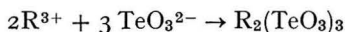
Low results were obtained in purely aqueous medium; these, however, improved on the addition of ethanol. A number of titrations were carried out at various ethanol concentrations; 15-20% ethanol in the case of lanthanum and 20-25% ethanol in the case of neodymium, gave the best results. The final concentrations chosen for the direct and reverse titrations were 15% ethanol by volume for lanthanum and 25% for neodymium. Other procedures are reported in an earlier communication¹⁰.

Lanthanum nitrate solutions in the concentration range $0.8478 \cdot 10^{-4}$ - $2.332 \cdot 10^{-4}$ M were titrated with sodium tellurite solution ($2.193 \cdot 10^{-2}$ M). Neodymium nitrate solution at concentrations between $2.601 \cdot 10^{-4}$ and $13.01 \cdot 10^{-4}$ M were titrated with sodium tellurite (0.1316 M). For reverse titrations, sodium tellurite solution in the concentration ranges $7.31 \cdot 10^{-5}$ - $11.69 \cdot 10^{-5}$ M and $8.77 \cdot 10^{-4}$ - $26.31 \cdot 10^{-4}$ M were successfully titrated with lanthanum nitrate ($6.363 \cdot 10^{-3}$ M) and neodymium nitrate (0.1561 M), respectively. The method is reproducible within 1%.

Discussion

It is evident from the conductometric titration curves that one sharp end point

is obtained corresponding to the formation of lanthanum and neodymium normal tellurites; the reaction involved may be represented as:



where R = La or Nd.

In the case of direct titrations, as sodium tellurite solution is added, the conductance decreases up to the equivalence point owing to the removal of La^{3+} or Nd^{3+} ions as $La_2(TeO_3)_3$ or $Nd_2(TeO_3)_3$ (Fig. 1, Curves A_1 and A_2). After the equivalence point, a rapid increase in conductance is due to the sodium tellurite added in excess. In the case of reverse titrations, there is a slight increase in conductance in the pre-equivalence region due to the substitution of TeO_3^{2-} ions by the more mobile NO_3^- ions (Fig. 1, Curves B_1 and B_2). The presence of ethanol slightly improves the result because it reduces the solubility of the precipitate.

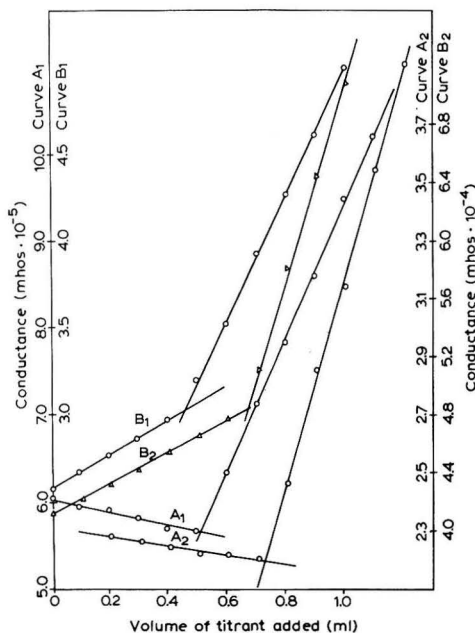


Fig. 1. (A_1), Direct conductometric titration of lanthanum nitrate; (A_2), direct conductometric titration of neodymium nitrate; (B_1), reverse conductometric titration of lanthanum nitrate; (B_2), reverse conductometric titration of neodymium nitrate.

The present investigation thus confirms the conductometric formation of lanthanum and neodymium normal tellurites. The reproducibility and accuracy of the titrations are excellent even at low concentrations. Cations that precipitate with sodium tellurite *e.g.*, cerium, thorium, zirconium, cobalt, nickel, samarium, praseodymium and the anions selenite, vanadate, tungstate, chromate and molybdate, interfere and must be absent.

Acknowledgements

We thank the authorities of the Banaras Hindu University for providing the

necessary facilities. Financial assistance from the Council of Scientific and Industrial Research, New Delhi, to one of us (K.C.P.) is gratefully acknowledged.

*Chemical Laboratories,
Banaras Hindu University,
Varanasi-5 (India)*

SARJU PRASAD
K. C. PATHAK

- 1 I. A. ATANASIU, *Z. Anal. Chem.*, 113 (1938) 276.
- 2 G. SPACU AND P. SPACU, *Z. Anal. Chem.*, 128 (1948) 226.
- 3 H. FLASCHKA, A. J. BARNER, JR. AND W. C. BROAD, *Chemist-Analyst*, 47 (1958) 78.
- 4 B. M. MARYANOV AND V. V. SEREBRENNIKOV, *Zh. Analit. Khim.*, 18 (1963) 58.
- 5 V. I. KUZNETSOV AND L. A. OKHANVA, *Zavodsk. Lab.*, 25 (1959) 1162.
- 6 J. N. GAUR, *Z. Anal. Chem.*, 193 (1963) 86.
- 7 I. A. ATANASIU, *Z. Anal. Chem.*, 112 (1938) 15.
- 8 F. M. SHEMYAKIN AND V. A. VOLKOVA, *J. Gen. Chem. U.S.S.R. Eng. Transl.*, 7 (1937) 1328.
- 9 J. N. GAUR AND K. ZUTSHI, *J. Electroanal. Chem.*, 5 (1963) 208.
- 10 S. PRASAD AND V. N. GARG, *J. Electroanal. Chem.*, 11 (1966) 72.
- 11 C. V. BANKS, J. L. SPOONER AND J. W. O'LAUGHLIN, *Anal. Chem.*, 30 (1958) 458.
- 12 T. M. MALYUTINA, B. M. DOBKINA AND YU. A. CHERNIKOV, *Zavodsk. Lab.*, 27 (1961) 653.
- 13 W. T. CARNALL, *Anal. Chem.*, 34 (1962) 786.
- 14 G. S. DESHMUKH, V. D. ANAND AND A. JOSEPH, *Z. Anal. Chem.*, 180 (1961) 174.
- 15 S. PRASAD AND S. KUMAR, *J. Indian. Chem. Soc.*, 40 (1963) 534.
- 16 S. PRASAD AND K. C. PATHAK, *Indian J. Chem.*, 3 (1965) 341.
- 17 S. PRASAD AND K. C. PATHAK, *J. Indian Chem. Soc.*, in press.
- 18 V. LENHER AND A. W. HOMBERGER, *J. Am. Chem. Soc.*, 30 (1908) 387.
- 19 P. SPACU, M. MAVRODIN, S. SERBAN AND E. ANTONESCU, *Acad. Rep. Populare Romine, Studii Cercetari Chim.*, 11(2) (1963) 247.

Received February 7th, 1966.

J. Electroanal. Chem., 12 (1966) 360-362

BOOK REVIEW

Advances in Analytical Chemistry and Instrumentation, Vol. 3, edited by CHARLES N. REILLEY, Interscience Publishers, John Wiley and Sons, Inc., New York, 1964, pages vii + 523, price £5-13-0.

This volume contains eight specialist chapters written by experts on the following topics: *Atomic Absorption Spectroscopy* by R. TUCKYER; *Photometric Titrations* by A. L. UNDERWOOD; *Analytical Applications of Enzyme-Catalysed Reactions* by W. J. BLAEDEL AND G. P. HICKS; *Ion Sources and Detectors for the Mass Spectroscopic Study of Solids* by L. F. HERZOG, D. J. MARSHALL, B. R. F. KENDALL AND L. A. CAMBEY; *Galvanic Analysis* by P. HERSCH; *Linear Elution Adsorption Chromatography* by LLOYD R. SNYDER; *Concepts and Column Parameters in Gas Chromatography* by J. CALVIN GIDDINGS and *Thin Layer Chromatography* by RENE MAIER AND HELMUT K. MANGOLD.

The concepts are thus wide-ranging and vary from purely practical considerations, such as the chapters on Ion Sources and T. L. C., to the largely theoretical considerations of L.E.A.C. and G.L.C. All chapters are up to date and well referenced and the style is clear, readable and informative.

The theory of *Atomic Adsorption Spectroscopy* is clearly presented and a competent discussion of instrumentation (including sources, atomisers, burners and detectors) is given; this section, however, could have been improved by diagrams since the descriptions are lengthy. There is a useful table of applications to metals but

J. Electroanal. Chem., 12 (1966) 362-364

a discussion on the advantages and disadvantages of the technique compared with others would have been a valuable addition to a section that is already somewhat compressed.

An excellent account of the theory of titrations, involving acid-base, redox and chelatometric types, with and without indicators, is given in *Photometric Titrations*. A careful consideration of the limitations of the method and the treatment of the data and technique of plotting curves, make this a useful contribution to other analytical techniques. A description of the instruments adopted—usually spectrophotometers—is included, but the author puts the matter in perspective and shows that adaptations are often far too elaborate, and titrations can often be done with equal facility and accuracy using much simpler equipment. Titrations carried out by photometric methods are compared with other methods (especially potentiometric and coulometric) and are of considerable value to the analyst.

Enzyme-Catalysed Reactions are dealt with in chapter 3; this gives a clear outline of the methods for following the reaction kinetics involved, and indicates the importance of analyses in the initial stages of reaction. Methods of determining substrates, enzymes, activators and inhibitors are described and the value of enzyme-coupled reactions and enzyme cycling, for the determination of quantities of material in the nanogram region, illustrated. Automated methods based on variable-time and fixed-time procedures and their advantages and disadvantages are discussed. The direct reproduction of recorder tracings, however, is not aesthetically pleasing.

Ion Sources and Detectors form a purely technical section and include new devices such as d.c. hot spark, exploding wire, laser and field emission sources which are compared with the more established R.F. and electron bombardment methods. Photographic plates including nuclear track plates are considered useful integrating devices but not so versatile as electron multipliers, scintillation, P.M. and semi-conductor devices. The sensitivity and usefulness of the various methods are considered and a useful summary is included.

Galvanic Analysis gives a full and well referenced account of a practical aspect of electrical-cell measurements applied specifically to the analysis of industrial gas streams. Principles of transport and activation control are developed. Conditions under which a cell can act, coulometrically at low electrolyte flow rate, and flow insensitive at high flow rate, are explained, and gas-electrolyte-solid interactions are considered. Working electrodes, especially emerging electrodes, are discussed as also are methods of calibration. A large part (perhaps too much) is directed to the analysis of oxygen with the result that the sections on hydrogen, halogens, oxides of nitrogen, water vapour and organic compounds tend to be rather compressed.

The principles underlying *Linear Elution Adsorption Chromatography* are competently dealt with. The author has helped to establish a unifying theory in this rather difficult field. The part played by the adsorbent, particularly alumina, silica and florasil and also the eluent, are discussed and equations are developed in terms of retention volume and eluent adsorption energy. From these, adsorption areas per molecule are determined for aromatic compounds. More advanced considerations of types of adsorption and adsorption sites makes this section of value in the separation of mixtures.

Concepts and Column Parameters in Gas Chromatography are considered very largely with reference to G.L.C. although the final sections deal with gas-solid, capillary columns and programmed-temperature gas chromatography (P.T.G.C.). The basis of the separation of constituents is considered in relation to their diffusion coefficients, which are related to plate heights, and also to retention times. A careful study of column length and radius, flow velocity, pressure and properties of the solid support, liquid phase and temperature, indicate the optimum conditions for obtaining quick and effective separations. Gas chromatography, capillary and P.T.G.C. are shown to follow similar considerations and useful summaries of the effects of various factors make for completeness in the examination of these related techniques.

Thin Layer Chromatography is a somewhat long section, devoted largely to practical applications to the separation of organic substances. Adsorption, ion exchange, partition, and reverse-phase partition methods of application are considered. Plate applicators and coating materials are discussed exhaustively, as are also the techniques of the preparation of plates and application of the sample. The quantitative aspects and micro-preparative uses are also dealt with. Applications to essential oils, vitamins, alkaloids, and other compounds of biological importance, illustrate the use of the various types of technique, although little is said of inorganic systems. A list of suppliers of equipment and a comprehensive list of references (340), and details of procedure within the text, almost converts the article into a laboratory handbook.

Overall, the format and printing are good and there are very few errors. The book forms a useful library reference book for analysts but is likely, in view of its wide-ranging nature and price (113/-), to find its way to Universities, Colleges and large industrial concerns rather than the smaller laboratories with restricted interests.

J. V. WESTWOOD,
Sir John Cass College, London

J. Electroanal. Chem., 12 (1966) 362-364

ANNOUNCEMENT

18th MEETING OF THE COMITÉ INTERNATIONAL DE THERMODYNAMIQUE ET DE CINÉTIQUE ELECTROCHIMIQUES, SCHLOSS ELMAU, BAVARIA (WEST GERMANY), APRIL, 1967

The 18th Meeting of CITCE will be held at Schloss Elmau, near Garmisch-Partenkirchen, Bavaria (West Germany) in the period 24th to 29th April, 1967 in co-operation with the German Bunsen Society for Physical Chemistry. The Meeting will be restricted to the theme *Electrochemical Processes and the Energy States of Electrons*. The topics covered will include: *Electron Exchange and Redox Reactions in Solution, Redox Reactions at Metals and Semiconductors, Semiconductor Electrode Reactions, Electrode Reactions under Illumination, Correlations between Absorption Spectra and Electrode Reactions*.

Attendance at this Meeting will be restricted to 180 participants.

Correspondence regarding attendance or presentation of papers should be addressed to Professor Dr. H. GERISCHER, Physikalisch-Chemisches und Elektrochemisches Institut der Technischen Hochschule München, Arcisstr. 21, 8 München 2, (West Germany) or to Dr. M. FLEISCHMANN, Department of Physical Chemistry, University of Newcastle upon Tyne, Newcastle upon Tyne 1 (England).

Abstracts should be received by October 1st, 1966 and extended abstracts by December 1st, 1966.

J. Electroanal. Chem., 12 (1966) 364

COORDINATION CHEMISTRY REVIEWS

AN INTERNATIONAL JOURNAL

EDITOR A. B. P. LEVER

ELSEVIER PUBLISHING COMPANY AMSTERDAM

PUBLICATION Four issues per (approximately) yearly volume. Publication to start in the course of 1966.

SUBSCRIPTIONS £7.0.0, US\$19.50, Dfl. 70.00 per volume plus 5s., US\$0.70, Dfl. 2.40 postage. Subscription orders may be placed with your usual supplier or directly with the publisher: Elsevier Publishing Company, P.O. Box 211, Amsterdam, The Netherlands.

MANUSCRIPTS Manuscripts should be submitted to: Dr. A. B. P. Lever, Department of Chemistry, University of Manchester Institute of Science and Technology, Manchester 1, Great Britain.

ILLUSTRATIONS Line drawings should preferably be in a form suitable for reproduction, drawn in Indian ink on drawing paper or tracing paper, with lettering, etc. in pencil. Photographs should be submitted as clear black-and-white prints on glossy paper. Legends to the illustrations should be typed on a separate page of the manuscript, and not underneath the drawings or on the reverse of photographs. All illustrations should be numbered consecutively throughout the paper.

LANGUAGES Reviews will be published preferably in English, but French or German texts are also acceptable.

PROOFS Authors should keep a carbon copy of their manuscripts, as the original will not be sent to them with the proofs. It is particularly requested that corrections should be restricted to the absolute minimum required.

COORDINATION CHEMISTRY REVIEWS

With the expansion of the chemical literature proceeding at an ever increasing rate, it is becoming more and more difficult for a chemist to keep up with current work. Review articles provide one way by which it is possible to keep abreast of rapidly developing fields. However even these often have the disadvantage of being several years out of date when they are published, and all too often there is no recent review of a field of particular interest.

Coordination Chemistry Reviews has been initiated as a means by which relatively short review articles may be published quickly. Each issue will contain some 4–8 review articles, and each article is expected to be about 15–25 pages long. The content of these articles should fall within the general area of coordination chemistry and may deal with the theory or practice of the coordination chemistry of transition or non-transition metals. Articles dealing with the application of physical techniques will be especially welcomed. The term "Coordination Chemistry" may be interpreted broadly but should not include Organometallic Chemistry.

Reviews should fall into one of the following general categories: —

- (a) a survey of the developments in a particular area during the last few years;
- (b) a survey, and/or discussion, of the results obtained with a particular technique during the last few years;
- (c) a general or philosophical discussion of some aspect of coordination chemistry.

The articles should be relatively short with the emphasis on recent developments and ideas. In this way it is hoped that **Coordination Chemistry Reviews** will become a useful Journal for both the established expert and the new research student.

Manuscripts will be solicited from authors prominent in the field of coordination chemistry, but unsolicited reviews will be welcomed both from established experts and from younger research workers. It is requested that intending authors should, in the first instance, contact the Editor (Dr. A. B. P. Lever, Department of Chemistry, University of Manchester Institute of Science and Technology, Manchester 1, Great Britain) with a résumé of the proposed review so that its suitability for publication can be judged and duplication can be avoided. Authors will receive payment for reviews on a rate-per-page basis.

Some Forthcoming Papers in CCR

- K. W. Bagnall (Harwell), Coordination Chemistry of Actinide Halides
- L. Belford and R. G. Denning (Urbana, Ill.), Magneto-Circular Dichroism
- D. C. Bradley (London), Metal Oxide Alkoxide Polymers
- G. R. Choppin (Tallahassee, Fla.), Lanthanide Chemistry
- N. F. Curtis (Wellington, New Zealand), Tetradentate Heterocyclic Metal Complexes
- A. J. Edwards (Birmingham), Second and Third Row Transition Metal Halides
- J. E. Fergusson (Christchurch, New Zealand), Rhenium Chemistry
- W. P. Griffith (London), Metal Oxygen Bonding
- R. E. Hester (York), Raman Studies in Coordination Chemistry
- R. J. Irving (London), Thermochemistry of Coordination Complexes
- B. R. James (Vancouver, B.C.), Rhodium Chemistry
- L. H. Jones (Los Alamos, N. Mex.), The Significance of Force Constants of a General Quadratic valence force field. Applications to $\text{Au}(\text{CN})_2^-$, PtCl_4^{2-} , AuCl_4^- , AuBr_4^- and $\text{Au}(\text{CN})_2\text{Cl}_2^-$
- G. B. Kauffman (Fresno, Calif.), Separation of Isomers
- S. Kirschner (Detroit, Mich.), Optical Rotatory Dispersion and Circular Dichroism
- J. A. McCleverty (Sheffield), Transition Metal Dithiolate Chemistry
- P. C. H. Mitchell (Reading), Coordination Compounds of Molybdenum
- D. Nicholls (Liverpool), Coordination Chemistry of Vanadium
- R. V. Parish (Manchester), Eight-Coordinate Complexes
- J. Selbin (Baton Rouge, La.), Vanadyl Complexes
- L. M. Venanzi (Oxford), Group V Ligand Complexes
- J. Wood (Southampton), Recent X-Ray Studies
- S. Yamada (Osaka), Schiff Base Complexes

CONTENTS

Application of mercury-plated graphite electrodes to voltammetry and chronopotentiometry S. P. PERONE AND K. K. DAVENPORT (Lafayette, Ind., U.S.A.)	269
Utilisation de l'impédance opérationnelle pour la détermination des coefficients de diffusion E. LEVART ET E. POIRIER D'ANGÉ D'ORSAY (Bellevue, France)	277
New indicating system: twin electrodes, at zero current. I. Proposed mechanism E. KIROWA-EISNER AND M. ARIEL (Haifa, Israel)	286
Diffusion-limited adsorption at spherical electrodes S. L. PHILLIPS (Poughkeepsie, N.Y., U.S.A.)	294
Chronoamperometrische Untersuchung metallischer Monoschichten E. SCHMIDT UND H. R. GYGAX (Bern, Schweiz)	300
Potentiometric study on the interaction of Ag ⁺ ions with gelatin P. LANZA AND I. MAZZEI (Bologna, Italy)	320
Potential sweep chronoamperometry in dimethyl sulfoxide at the hanging mercury drop electrode J. L. JONES AND H. A. FRITSCH, JR. (College Station, Tex., U.S.A.)	334
Détermination polarographique de la nitrohydroxylamine A. CALUŞARU (Prague, Tchécoslovaquie)	341
Corrosion potentiometry and potentiometric titration with dropping amalgam electrode A. R. DESPIĆ AND K. I. POPOV-SINDJELIĆ (Belgrade, Yugoslavia)	347
<i>Short communications</i>	
Theory of programmed-current derivative chronopotentiometry W. D. SHULTS AND T. R. MUELLER (Oak Ridge, Tenn., U.S.A.)	354
Conductometric study on the quantitative precipitation of lanthanum and neodymium as normal tellurites S. PRASAD AND K. C. PATHAK (Varanasi, India)	360
<i>Book review</i>	362
<i>Announcement</i>	364

DIFFRACTION OF X-RAYS BY CHAIN MOLECULES

by B. K. VAINSHEIN

Foreword by M. F. PERUTZ

6 x 9", xiii + 414 pages, 3 tables, 258 illus., 256 lit.refs.,
Dfl. 65.00, £6.10.0, \$23.50

Contents: 1. Principles of the theory of X-ray diffraction. 2. Structures of chain molecules and assemblies. 3. Diffraction by an isolated chain molecule. 4. Scattering intensity and structure of object. 5. Properties of the distribution and interference functions. 6. Diffraction by assemblies of parallel chain molecules. 7. Diffraction by assemblies with nonparallel packing of chain molecules and by amorphous polymers. Subject index.

INFRA RED INSTRUMENTATION AND TECHNIQUES

by A. E. MARTIN

5½ x 8½", x + 180 pages, 13 tables, 94 illus., 86 lit.refs., 1966,
Dfl. 32.50, 65s., \$12.00

Contents: 1. Historical. 2. Modern infra-red spectrometers. 3. Miscellaneous instruments. 4. Interferometric spectrometers. 5. Accessories. 6. Experimental methods and techniques. Index.

ENERGY TRANSFER IN RADIATION PROCESSES

Chemical, Physical and Biological Aspects

Proceedings of the International Symposium held in Cardiff, 1965

edited by G. O. PHILLIPS

5½ x 8½", xvi + 182 pages, 10 tables, 81 illus., 273 lit.refs., 1966,
Dfl. 32.50, 65s., \$12.00

Contents: Introductions to the sections by F. S. Dainton, G. F. J. Garlick and Tikvah Alper. Invited papers by E. J. Bowen, Jett C. Arthur, N. Riehl, R. Mason. Contributed papers.

MASS SPECTROMETRIC ANALYSIS OF SOLIDS

edited by A. J. AHEARN

5½ x 8½", viii + 167 pages, 13 tables, 46 illus., 242 lit.refs., 1966,
Dfl. 30.00, 60s., \$10.75

Contents: 1. Introductory survey. 2. The production of ions from solids. 3. Photographic emulsions as ion detectors in quantitative mass spectrography. 4. Analysis of special samples. 5. Mass spectrographic microprobe analysis. Subject index.

RADIOCHEMICAL SURVEY OF THE ELEMENTS

Principal characteristics and applications of the elements and their isotopes

by M. HAISSINSKY

and

J.-P. ADLOFF

6 x 9", ix + 177 pages, 1965, Dfl. 32.50, 65s., \$12.00

Contents: Introduction. The elements in alphabetical order. Element 102. Element 104.



ELSEVIER PUBLISHING COMPANY

AMSTERDAM

LONDON

NEW YORK